9-26-2013 12:00 AM

Investigating the Effects of Radiation on Phosphonium-Based Ionic Liquids

Susan Howett
The University of Western Ontario

Supervisor
Dr. J. Clara Wren
The University of Western Ontario

Graduate Program in Chemistry
A thesis submitted in partial fulfillment of the requirements for the degree in Doctor of Philosophy

INVESTIGATING THE EFFECTS OF RADIATION ON PHOSPHONIUM-BASED IONIC LIQUIDS

(Thesis format: Integrated-Article)

by

Susan E. Howett

Graduate Program In Chemistry

A thesis submitted in partial fulfillment
of the requirements for the degree of
Doctor of Philosophy

The School of Graduate and Postdoctoral Studies
The University of Western Ontario
London, Ontario, Canada

Abstract

This thesis presents work on the understanding of the effects of ionizing radiation on phosphonium-based ionic liquids (ILs). The capability of ILs to dissolve a wide range of molecules, and the potential of ILs to be highly resilient in energy-intensive environments makes them particularly promising media for the separation and sequestration of metal ion contaminants from radioactive waste effluents in nuclear fuel cycles. For this application, a water/IL system will be exposed to a continuous stream of ionizing radiation. The radiation environment will strongly influence the chemical state of the water phase in the system and the chemical parameters affecting the separation efficiency of the system. This work examines irradiation of gas/IL and water/IL biphasic systems containing phosphonium-based ionic liquids.

When exposed to ionizing radiation, ionic liquids undergo radiolysis, resulting in the formation of ionic liquid excited species and radiolytic fragments. As well, when exposed to ionizing radiation, water decomposes into a range of reducing ($\bullet e_{aq}^-$, $\bullet O_2^-$, $\bullet H$) and oxidizing (O_2, $\bullet OH$, $HO_2\bullet$, H_2O_2) species. To develop a better understanding of the biphasic water/IL systems when exposed to radiation, small samples of the biphasic systems were exposed to continuous radiation in a γ-cell for periods of time up to several days. A number of surface, spectroscopic, and electrochemical techniques were employed to follow the evolution of the systems. This combination of analytical techniques allowed for the study of changes in the ionic liquid phase, the water phase, and the gas phase in the systems.

Results indicate that even long-term continuous doses of γ-radiation induce a negligible chemical change in phosphonium-based ILs when they are in contact with a

gas phase. In the case of the water/IL system, ion transfer occurs across the water/IL interface, even with the most immiscible phosphonium-based ILs. Irradiation produces surfactants that can accumulate at the interface and accelerate mixing of the IL and water phases by emulsification and the formation of micelles. Despite the micelle formation and emulsification, studies concluded that the phosphonium-based ILs studied undergo very little radiolytic degradation in steady-state γ-radiation fields.

Keywords:

ionic liquid, gamma-radiolysis, interfacial stability, phase mixing, micelles, reverse micelles, emulsion, pulse radiolysis

Co-Authorship Statement

This thesis includes published data (Chapters 4 and 5). For the published results I was the experimental investigator and writer.

Acknowledgments

I would first like to thank my supervisor, Dr. J. Clara Wren, for offering her input, direction, and interpretation of my project throughout my years of study. Clara has provided a fulfilling graduate experience with her dedication to her students. Under her guidance I have learned countless things both personally and professionally. I have travelled to international conferences in North America and Europe, and was given the opportunity to perform experiments at Atomic Energy of Canada (AECL) and at Brookhaven National Lab (BNL). The opportunity to perform unique research in national laboratory settings is an experience that taught me a great deal, and I will not soon forget.

A number of people have assisted me over my time as a graduate student. I have learned a tremendous amount from Dr. Jamie Noël. He has provided countless discussions and assistance in the laboratory and in data collection, for which I am very grateful. His sense of humor was always welcome, especially when experiments are failing and no data collection is occurring. Dr. Jiju Joseph has been of great assistance in experimental aspects and discussions, and her calm demeanor was greatly appreciated in the office and the lab. Dr. Dave Wren has been of great assistance in the writing process, and has given helpful professional advice, especially when transitioning from an academic setting to an industrial environment.

I owe a great deal of thanks to all of the students in the Wren lab, both past and present. They are an excellent group of people to work with and a fun group outside of the lab; I have thoroughly enjoyed my time at Western because of them.

For his love, encouragement, and witty banter, I would like to thank Matt Asmussen.

Most importantly, I would like to thank my parents and sister for their endless support in all aspects of my life. Their encouragement has helped me to get to where I am today.

Finally, I dedicate this thesis to my grandparents, Jack and Betty Howett.

Table of Contents

Symbols, Acronyms, and Ionic Liquids

Symbols

A	electrode area
b	coherent scattering length
C	capacitance
cP	centipoise
D_h	hydrodynamic diameter
D_t	diffusion coefficient
e	electron charge
E	potential
E_{amp}	amplitude of electrochemical impedance spectroscopy sinusoidal potential
ΔE	potential change
$\Delta E_{vibration}$	vibrational energy gap
h	Plank constant
I	current
I_o	incident neutron intensity
I_t	absorption intensities at time t
I_z	absorption intensities at time zero
I_{amp}	EIS current amplitude
$I_{bgd}(q)$	background neutron flux
$I_{emp}(q)$	scattered neutron intensity of an empty cell
$I_{raw}(q)$	raw scattering intensity
$I_{red}(q)$	reduced intensity
j	imaginary unit
k	decay rate constants
k_B	Boltzmann constant
k_i	incident wave vector
k_s	scattered wave vector
ℓ	distance between two electrodes
n	index of refraction
q	momentum transfer
Q	charge
R	resistance
R_s	Onsager Radius
T	absolute temperature (K)
$T_{emp}(\lambda)$	transmitted intensity of an empty cell
$T_{sam}(\lambda)$	transmission of a sample
V	sample scattering volume

Z	impedance
Z_{im}	imaginary impedance
Z_r	real impedance
$\frac{d\Sigma}{d\Omega}(q)$	differential scattering cross section per unit volume
$\Delta\Omega$	sample-to-detector intensity
ε_o	dielectric constant of permittivity in a vacuum
ε_r	dielectric permittivity of a medium
η	viscosity
η_e	detector efficiency
θ	phase shift
θ_{sa}	scattering angle
λ	wavelength
ν_i	incident photon
ν_f	scattered photon
ρ	density
σ	conductivity of a system
ω	angular frequency

Acronyms

AECL	Atomic Energy of Canada Limited
AIL	Ammonium-Based Ionic Liquid
CAC	Critical Aggregation Concentration
CMC	Critical Micelle Concentration
CNBC	Canadian Neutron Bean Centre
CPE	Constant Phase Element
CSC	Confocal Soller Collimator
DLS	Dynamic Light Scattering
DSC	Differential Scanning Calorimetry
EIS	Electrochemical Impedance Spectroscopy
ESI-MS	Electrospray Ionization-Mass Spectrometry
FTIR	Fourier Transform Infrared Spectroscopy
GC/MS	Gas Chromatography-Mass Spectrometry
HSC	Horizontal Soller Collimator
IL	Ionic Liquid
ICT	Integrating Current Transformer
LEAF	Laser-Electron Accelerator Facility
LET	Linear Energy Transfer
MD	Molecular Dynamic

MSD	Mean Square Displacement
NMR	Nuclear Magnetic Resonance
NRU	National Research Universal
NVT	Number Volume Temperature
PG	Pyrolytic Graphite
PTFE	Polytetrafluoroethylene
RDF	Radial Distribution Function
SANS	Small Angle Neutron Scattering
SDC	Self Diffusion Coefficient
SLD	Scattering Length Density
TEM	Transmission Electron Microscopy
TOF	Time-Of-Flight

Ionic Liquids

amide-IL	Trihexyltetradecylphosphonium bis(trifluoromethylsulfonyl)amide
bromide-IL	Trihexyltetradecylphosphonium bromide
dicyanamide-IL	Trihexyltetradecylphosphonium dicyanamide
tosylate-IL	Triisobutylmethylphosphonium tosylate

List of Tables

List of Figures

Chapter 1. Introduction

1.1 THESIS GOAL AND ORGANIZATION

The goal of the work presented in this thesis was to develop an understanding of the effects of ionizing radiation on the biphasic and interfacial reactions of ionic liquids (ILs) in contact with water or a gas. Exposed to ionizing radiation, water decomposes to a range of reducing ($\bullet e_{aq}^-$, $\bullet O_2^-$, $\bullet H$) and oxidizing (O_2, $\bullet OH$, $HO_2\bullet$, H_2O_2) species. Likewise, when exposed to ionizing radiation, ILs undergo radiolysis, forming excited species and radiolytic fragments. Thus, the reactions at the interface of a water/IL system, when exposed to radiation, can be influenced by the decomposition products of both the water and the IL phase, and the interactions between these products.

While some studies have been performed on the radiolysis of a variety of ILs, most of these studies used short pulses of radiation, and looked only at pure-IL systems rather than biphasic systems. In practical uses of ILs, they are more likely to be exposed to a continuous dose of radiation. Hence there is particular interest in the effect of continuous, long term inputs of ionizing radiation to water/IL systems. One special application that has been proposed for ILs is nuclear fuel reprocessing and heavy metal waste separation. Here the effect of ionizing radiation on both water and IL phases are of utmost importance.

Ionic liquids chosen for this type of application must possess a variety of characteristics in order to carry out an efficient and economic separations process. These properties include: (1) a high intrinsic specificity for complexing with trans-uranic actinides over lanthanides and other fission products (the mix of isotopes contained in

spent nuclear fuel), (2) a synthetic route with a high yield, (3) thermal, radiation and chemical stability, (4) an efficient switching mechanism for binding and releasing target elements (in terms of complexation and decomplexation), and (5) a high immiscibility with aqueous solutions. There are an enormous number of possible ILs, based on the range of both cation and anionic components that they can contain. One class of ILs that contain phosphonium cations (phosphonium-based ILs) have been shown to have a number of the desired characteristics. They have high thermal stability, high immiscibility with water, and four substitution locations on the cation that allow for tailoring of their complexation abilities. However, little is known about the radiation stability of this class of ILs, and less is known about their radiation stability when in contact with an aqueous phase. This work is intended to fill this knowledge gap.

To achieve this goal, a number of different experiments were conducted on water/IL systems. Four ILs which possess various physical and chemical properties were investigated: triisobutylmethylphosphonium tosylate, trihexyltetradecylphosphonium bis(trifluoromethylsulfonyl)amide, trihexyltetradecylphosphonium bromide, and trihexyltetradecylphosphonium dicyanamide. The groups of experiments that were performed and analyzed are listed below in the order in which they are presented in this thesis.

- The effect of ionizing radiation on the decomposition of ILs was examined. Studies were conducted with the ILs in contact with a gas phase that was air (with pre-aerated ILs) or Ar (deaerated ILs).
- The biphasic reactions and interfacial stability of water/IL systems was examined and compared using two phosphonium-based ILs with very different properties.

Contact between the ILs and water leads to the formation of an emulsion layer. Micelle formation as a consequence of biphasic mixing and interfacial interactions was studied using light scattering and microscopy techniques.

- The radiation stability of water/IL systems was studied by following the time evolution of the properties of both the water and the IL phases using electrochemical, spectroscopic, and chromatographic techniques.
- The ionizing radiation impacts (energy transfer and absorption) within the interior water droplets contained within reverse micelles formed in phosphonium-ILs was examined. Studies were carried out to follow emulsion layer formation using pulse radiolysis techniques at the Laser-Electron Accelerator Facility (LEAF) at Brookhaven National Laboratory in Brookhaven, NY.
- The composition of the micelles formed in water/IL samples was studied in further detail at the Canadian Institute for Neutron Scattering at the National Research Universal (NRU) reactor in Chalk River, ON. Neutron scattering techniques were used to attempt to characterize the micelles and reverse micelles formed in biphasic samples.

Chapter 2. Technical Background and Literature Review

2.1 MATERIALS BACKGROUND

2.1.1 Structure of Ionic Liquids

Ionic liquids (ILs) are made up of distinct ion pairs; they are "salts". These materials are composed of a large, usually asymmetric, organic cation and a variable organic or inorganic anion. They remain liquid at, or near, room temperature ($\leq 100°C$), and have negligible vapor pressure and high thermal stability [1-3]. They are often referred to as "designer" solvents because they can be easily tuned to have certain desired properties. By altering the cation or the anion, their hydrophobicity, miscibility with other solvents, polarity, density, viscosity, and ability to dissolve metal ions can be varied [4-11]. These and other properties make ionic liquids solvents of choice for use in place of conventional organic solvents in many applications [8, 10, 12, 13].

It is the structure of the ILs that makes them so interesting and useful in a multitude of applications [1]. According to Plechkova *et al.* [14], if all known anion and cation combinations were paired, 10^6 different ILs could be made. Furthermore, if all possible ternary structures were to be included, this number could rise to 10^{18} [1, 14]. The structure of the cation and anion in a given IL dictate the properties that the particular IL possesses. The large sizes of the IL components as well as the asymmetric nature of the cations lower the melting point in the IL [14]. Long alkyl chains in the cations influence the polarity of the ILs and determine their solubility in less polar fluids [3]. Anion choices tend to make an IL more or less water miscible [14]. Much variation

exists between ILs for these reasons. Even ILs containing the same cation and different anions can possess dramatically different physical and chemical properties [15].

Despite the myriad of IL cations and anions available, most research thus far has focused on a few commonly used IL types. The cations largely studied are: imidazolium, pyridinium, piperidinium, ammonium, phosphonium, pyrrolidinium, pyrazolium, thiazolium, and sulfonium. Figure 2.1 illustrates these cation structures [14]. Common anions (including bromide, tosylate, and hexafluorophosphate) are not shown here because the anion possibilities are far more diverse than the commonly used cation types.

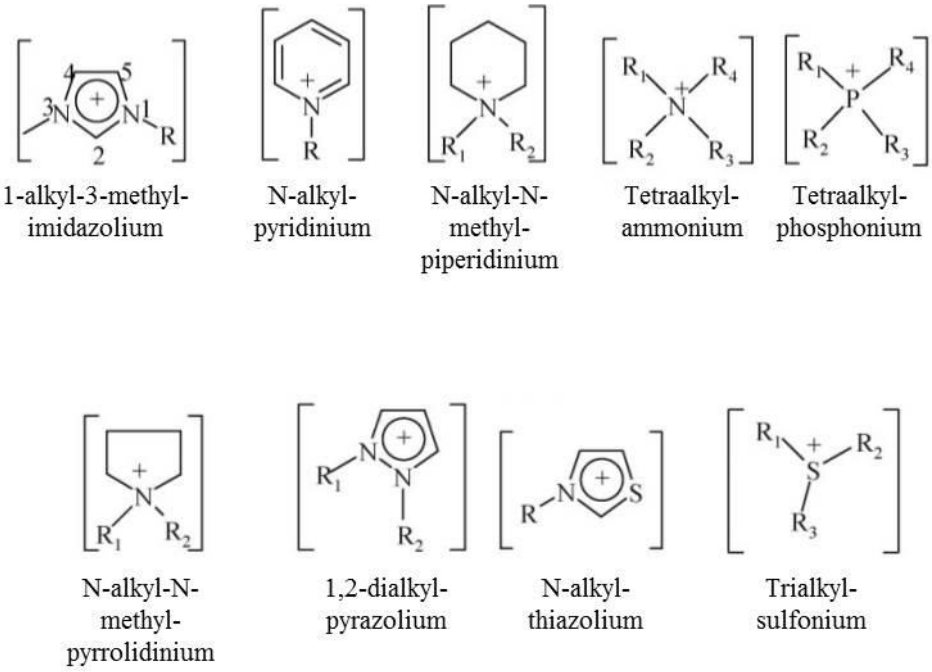

Figure 2.1 Common cations used in ILs [14].

2.1.2 Physical Properties of Ionic Liquids

Generalizations with regards to the influence of cation and anion combinations on IL physical properties are difficult to formulate. For example, studies by various authors

have revealed no correlation between an IL structure and its melting point, and generalities on trends in IL properties can only sometimes be made for related ILs, where related ILs, or ILs in a series, contain the same cation type [16-18]. For example, small alkyl chain length changes can either increase or decrease the IL melting point and the degree of such a change differs between different ILs. The melting points of many ILs are also uncertain as they can undergo supercooling [3]. However, it can be agreed the asymmetry of the ions in the IL, the internal charge distribution, and van der Waals interactions influence the melting points [3, 16].

Anion and cation combinations are specifically chosen to maintain weakly bound crystalline forms; the packing efficiency can be disrupted by reducing the Coulombic attraction, allowing for the melting points to occur at room temperatures [1, 16]. Studies performed by Katritzsky *et al.* [19] corroborate this as they found that melting point predictions could be made using quantitative structure-property relationships. They found that some of the most important parameters were the electrostatic intermolecular interactions and the coordination ability of the cation (determined by its molecular shape and symmetry) [3, 19]. However, while the intermolecular attractions and forces strongly influence the melting point, no generalities can be made between various cation and anion combinations out of a related series of ILs.

Ionic liquids are generally more viscous than conventional solvents, with viscosities ranging from 10 centipoise (cP) to well above 500 cP [16]. Compared to molecular solvents, the viscosity of an IL is closer to that of oil [3, 16]. As a point of reference, at room temperature the viscosities of water, ethylene glycol, and glycerol are 0.890 cP, 16.1 cP, and 934 cP respectively [20]. Although generalities can be found for

the trend in viscosity of ILs in a given series, these generalities are not applicable to other combinations of cation and anion. One of the largest problems plaguing viscosity measurements of ILs is the presence of variable amounts of contaminants in an IL. Small amounts of impurities are known to dramatically influence the viscosity of a given IL [16, 21, 22]. Even with considerable purification efforts, small amounts of impurities are normally present. Thus, for example, although the IL glass transition temperature is known to be related to the IL viscosity, the results from various studies have shown that generalities in this relationship between different series do not exist [3].

The majority of ILs have a density that is higher than that of water [3]. Generally, longer alkyl chains on the IL result in a decrease in its density. Though impurities strongly affect many physical properties, the density is the least affected by their presence [23]. Since the densities of ILs are not particularly sensitive to temperature variations, density is one of the more reliable properties that can be measured.

Conductivity values of the ILs give insight into the charge carriers and the mobility of ions in the IL. As a whole, ILs generally have good conductivities, but their conductivities are lower than would be expected [16]. This lower conductivity is largely attributed to the large sizes of the cations typically used in ILs, as the large size tends to reduce ion mobility [16]. There is no clear relationship between the anion size and conductivity in ILs, with some ILs containing large anions having higher conductivity than related ILs with smaller anions. This has been attributed to strong ion pairing which can decrease the ionicity of an IL, in turn decreasing its conductivity [24]. As with viscosity, the conductivity of ILs can be heavily influenced by the presence of

contaminants and impurities. The impurities can often both decrease the viscosity of the IL and increase the mobility of ions through the IL [16].

2.1.3 Phosphonium-Based Ionic Liquids

Although nitrogen-based ILs account for a large part of research today (seven of the nine most common cation structures, Figure 2.1), the less toxic phosphonium-based ILs feature many advantages over the nitrogen-based species [25]. The slow rise of interest in phosphonium ILs may be, in part, attributed to the difficulty in synthesizing the starting materials; following commercial availability phosphonium ILs have become increasingly popular [15].

Phosphonium ILs are available on a commercial scale and, in comparison to nitrogen-based ILs, they have a lower cost and higher availability [15]. Beyond this phosphonium ILs also possess many physical properties making them attractive. The phosphonium cation has four locations for substitution, giving many opportunities for "tuning" a particular IL. Perhaps due partially to the larger cation, in comparison to nitrogen-based counterparts, the viscosity of phosphonium ILs is higher at room temperature [26]. The consequences of this can be positive or negative, depending on the application of the IL. Relatively higher electrochemical and thermal stability are observed in phosphonium ILs [3, 26]. Finally, many nitrogen-based ILs contain acidic protons and ring structures. These acidic protons and rings are able to interact with solutes through the aromatic rings or by hydrogen bonding [26]. These interactions make such ILs not entirely inert and this can be an issue for many desired applications. This problem does not exist for phosphonium-based ILs.

2.2 GAS/IONIC LIQUID INTERFACIAL CHEMISTRY

In many applications chemistry will occur at interfaces, whether this is at gas/IL, water/IL, or solid/IL interfaces. For this reason the orientation of the IL at the interface is a very important aid in the prediction of the IL macroscopic surface and interface properties. Currently the majority of gas/IL interfacial studies have focused on the imadazolium IL series [27]. As was the case with the physical properties, generalities in the interfacial chemistry of ILs are difficult to make. However, although much is unknown about this emergent interfacial chemistry, great strides are being made, both experimentally and theoretically.

In contact with a gas phase, ILs become highly ordered at the interface [27-30]. Various studies have shown that the ordered ILs have a density that is higher at the surface than in the bulk phase and that the high density decreases going further into the bulk phase [29]. At the interface those IL species that contain alkyl chains orient themselves so that the alkyl chain extends into the gas phase from the surface [1, 28, 31]. The alkyl chain acts as a surfactant in the IL and longer chain lengths induce aggregation of IL species [28, 32]. Due to the aggregation nature and the ordering that occurs a hydrocarbon monolayer can form that covers the cation and anion polar moieties [28, 30].

2.3 WATER/IONIC LIQUID INTERFACIAL CHEMISTRY

Though there are some similarities, the chemistry and interfacial ordering that occur at a water/IL interface is far more complex than that that occurs at a gas/IL interface. The ordering and aggregation that occurs at the gas/IL interface also occurs at a water/IL interface, but it leads to different consequences. Research in the area of

water/IL interfacial chemistry is still very new. As was the case with other IL properties, generalizations cannot be made for IL behaviour in contact with an aqueous phase. Currently, published data on the aggregation characteristics of ILs also does not allow for predictions to be made regarding the formation of micelles and emulsions in IL systems; there is no observable correlation between the structural features of ILs and their molecular characteristics [33].

There is a slowly growing number of publications devoted to the study of the chemistry occurring at water/IL interfaces [34]. Recent work has found the development of micelles, reverse micelles, nanoemulsions, microemulsions, and vesicles [35-39]. The surfactant activity of ILs in contact with an aqueous phase causes aggregation at the interface. This ultimately can lead to micelle formation due to the increased concentration of ions at the interfacial region [38, 40-43]. Water is able to interact with IL molecules through intermolecular interactions (including hydrogen bonding) which can sometimes result in the formation of useful assemblies [34]. Micelles and resulting emulsion systems can develop as has been observed in both hydrophobic and hydrophilic IL and water systems [44]. Aggregation and micelle formation has not been observed for all ILs in contact with water due to the varied nature from their cation and anion combinations. Those ILs that form micelles and aggregates normally have bulky cations with long alkyl chains, as the alkyl chains act as surfactants that can promote micelle formation [42, 45].

At this time the microscopic structure of micelles and aggregates in ILs have not been examined in depth and many questions remain [46]. Techniques for the characterization of micelles and emulsion systems vary. Scattering methods are currently

the most common techniques used for the purpose of characterization [47]. Dynamic light scattering (DLS) and small angle neutron scattering (SANS) are two of the most popular techniques as they can detect the size of features, such as micelles and reverse micelles, in emulsion systems. In the case of SANS, curve fitting and data analysis techniques can also reveal the shape and structural form of the micelles [47]. Other techniques such as viscosity measurements, conductivity measurements, and nuclear magnetic resonance (NMR) spectroscopy have been used for the study of micelles and emulsions as well. However, these techniques are not as sensitive as the scattering methods and should be used with other supporting techniques [47, 48].

2.4 RADIATION AND WATER RADIOLYSIS

2.4.1 Ionizing Radiation

2.4.1.1 *Radiation from Radioactive Nuclides*

Many fission products and neutron activation products present in nuclear reactor environments are radioactive. These radioactive nuclides decay to stable isotopes by emitting α- or β-particles with each particle emission accompanying the emission of high-energy electromagnetic radiation (*x*- and γ-ray). These are high-energy particles (in the range of 10 keV to 10 MeV) and are referred to as ionizing radiation. An alpha particle is a high energy (or fast) helium nucleus $^{4}_{2}\mathrm{He}^{2+}$ [49]. Alpha particles emitted from a decaying radionuclide have a discrete energy that is characteristic of the originating nuclide. For example, α-particles emitted from polonium-210 all have an energy of 5.304 MeV, while α-particles from radon-222 have an energy of 5.49 MeV [49]. Beta

particles are fast moving electrons emitted from decaying radionuclides [49]. Rather than having a discrete energy, the energy of β-particles ranges from zero to a maximum energy that is characteristic of the radionuclide. Typically, the maximum energy ranges from a few hundred keV to several MeV. Monoenergetic fast electrons can be produced from electron accelerators. The energy of a γ-photon emitted from a decaying radionuclide is discreet. However, radionuclide decay can release multiple photons with different energies. As an example, the γ-rays emitted during the β-decay of cobalt-60 have energies of 1.332 MeV or 1.173 MeV [49].

2.4.1.2 *Energy Transfer from Radiation to the Interacting Medium*

Radiation particles or photons interact with matter mainly via classical particle-particle collisions. The collisions of high energy particles or photons are mainly with the electrons in the medium. The rate of energy transfer per penetration length through a medium is referred to as the linear energy transfer (LET) rate. In a given medium, the LET is highest for α-particles, followed by β-particles, and it is the lowest for γ-photons [49]. Accordingly, the penetration depths of 20 – 25 μm are typical for α-particles, 0.5–1.0 cm for β-particles, and tens of cm for γ-rays in water at room temperature. Due to a larger collisional cross section with electrons, the heavier and highly charged α-particle loses its energy at a faster rate than the lighter β-particle. High energy photons lose their energy by Compton scattering and the photoelectric effect. In this work, we are only concerned with electron or photon radiation and further discussion will be restricted to this type of radiation.

Due to their high energy, each fast electron or photon undergoes many collisions while it loses its energy and eventually becomes "thermalized" (with a velocity dictated by the temperature of the interacting matter). The consequence of this behaviour is that the multiple interactions are not selective (dependent on the atomic nature of the target matter) and instead depend only on the relative abundance of electrons in the matter [49]. As electron density is nearly proportional to the mass of an atom (except for H), the energy transfer from the radiation to matter is nearly the same per unit mass for all types of matter. Hence, the probability of an incident electron or photon interacting with impurities in the matter is very small compared to the probability of interacting with the bulk matter. Thus, chemical processes induced by low LET ionizing radiation are often referred to as solvent-oriented processes as opposed to solute-oriented processes. (A contrasting solute-oriented process is UV photolysis where incident photons can match the excitation energies of target solute molecules [49].)

The amount of energy absorbed by the medium, rather than radiation source strength is the controlling parameter in determining the consequences of its exposure to radiation. The absorbed dose (or the total energy absorbed) by the interacting matter is expressed in units of Gray (Gy), where 1 Gy = 1 $J \bullet kg^{-1}$. The rate of energy transfer from radiation to the medium and the radiation source strength dictates the absorbed dose rate. The rate of energy transfer from radiation to matter depends on the type of radiation as well as the density of electrons (or mass) of the interacting matter as described above.

2.4.2 Radiation-Induced Chemistry

A fraction of the energy absorbed by the medium is used to create ions and excited species along the track of the radiation, while the rest of the energy is dissipated as kinetic energy (i.e., heat) or photons with lower energy. The latter forms of energy are less effective in inducing chemical changes. How densely these ions and excited species are initially formed along the radiation track is an important parameter in determining chemical speciation that drives bulk phase reactions at longer times. The ion density along the track depends mainly on the LET rate and hence, the type of radiation and the density of the interacting medium. The chemical speciation that arises from absorption of radiation depends on the initial ion track density and also the electrochemical properties (such as the dielectric constant) of the interacting medium. My thesis project involves two mediums, water and ionic liquids. To interpret our results, we need to consider the interactions of ionizing radiation on both mediums; processes have been well described by various authors [49-56].

2.4.2.1 *Water Radiolysis*

When exposed to ionizing radiation, water will break down into a number of chemically reactive species [57]. The initial interactions of a water molecule with ionizing radiation result in either ionization or excitation of the water molecule. This creates ion pairs ($H_2O\bullet^+$ and e^-_{hot}) or electronically excited water molecules (H_2O^*) along the radiation track. The energetic ("hot") electron (e^-_{hot}) may have sufficient energy to ionize a neighbouring solvent molecule to produce a secondary ion pair or excited water molecule. Because the energy of the 'hot' electron will be much lower than that of the

incident radiation, such secondary ionization will be located near the main ionization track and result in a cluster of 2-3 groups of ionized or excited species. This cluster is referred to as a "spur" along the ionizing radiation track.

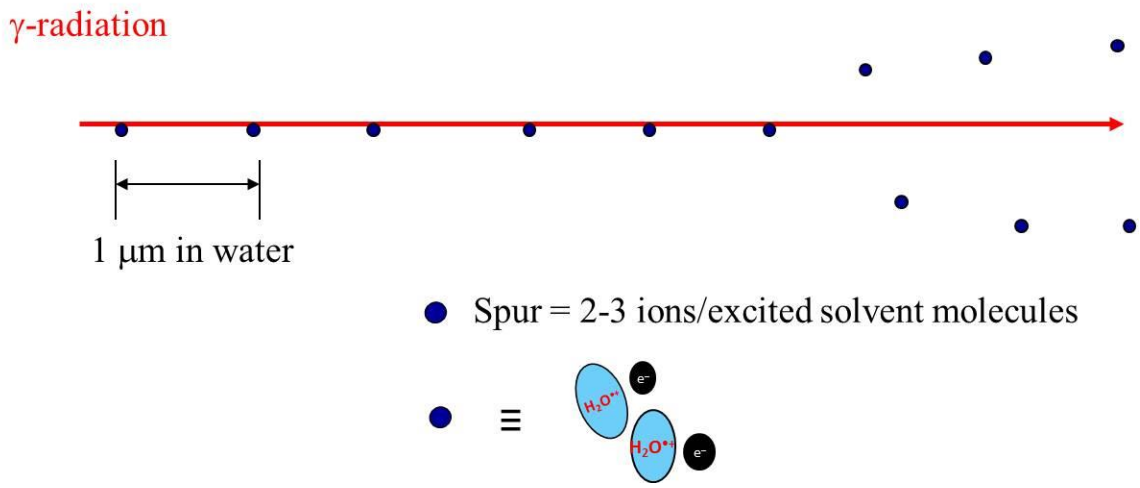

Figure 2.2 The radiation track resulting from a γ-photon [49].

In aqueous solutions the energy transferred from radiation to water molecules quickly dissipates by inter- and intra-molecular collisions of the initially-formed ions and electronically excited molecules on a time scale typically less than 1 μs. The yields of the radiation impact at the end of this time period are ions, molecular fragments (radicals) and molecular recombinant species. These have a density distribution that is uniform along the tracks created by the incident radiation particle/photon. If the incident radiation dose rate is sufficiently high, diffusion of these species from multiple tracks into the bulk phase creates a homogeneous distribution of radiation impact products (or radiolysis products) throughout the water on the time scale of about 1 μs, and hence this time period is designated the homogeneous stage. For the aqueous phase chemical reactions that

follow this deposition of energy, the concentrations of the radiolysis product species that are present at this homogeneous stage can be taken as the initial reactant concentrations. Thus, the species formed at this stage are referred to as the primary radiolysis products, even though they are not the first species formed by the interaction of a radiation particle/photon with a water molecule [49, 53]. Figure 2.3 illustrates in detail the breakdown of water into radiolysis products in the presence on ionizing radiation and subsequent reactions. In a constant radiation field where a continuous flux of incoming radiation produces primary radiolysis products, the radiolysis products will reach steady-state concentrations at low levels.

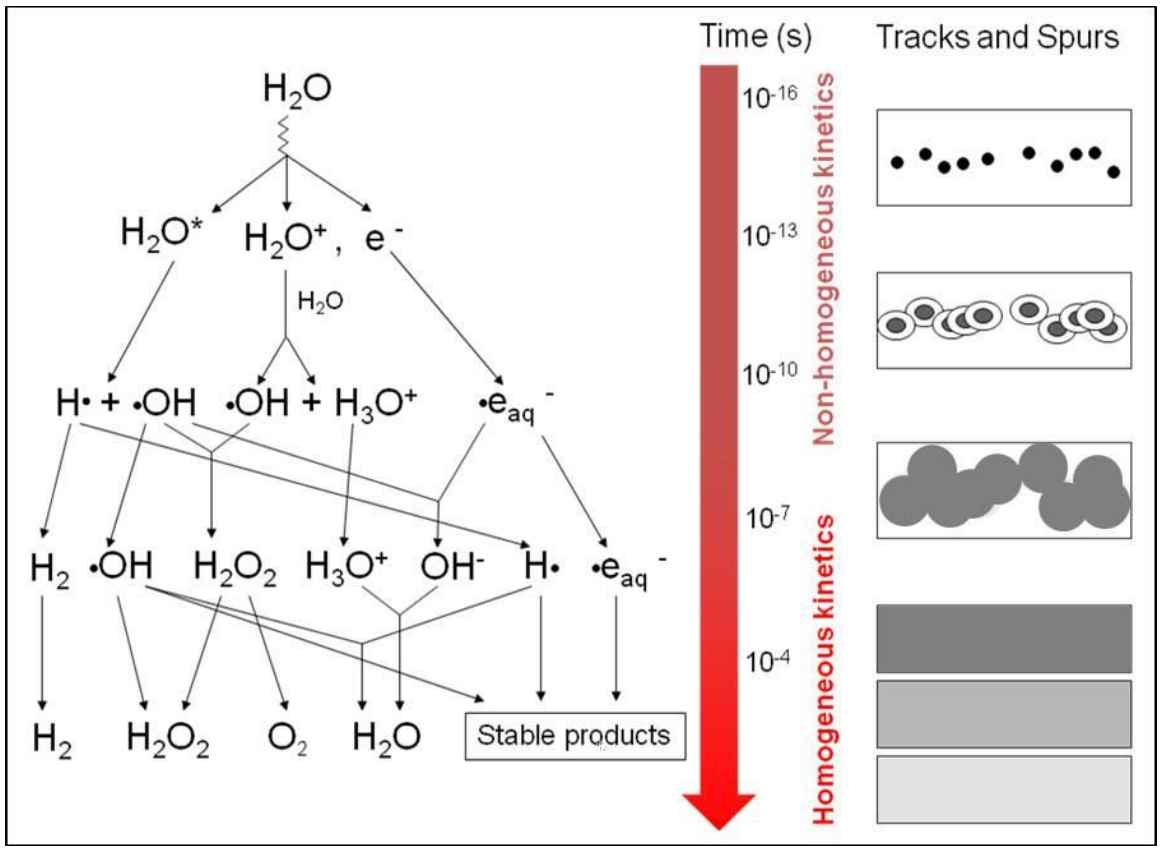

Figure 2.3 The effect of ionizing radiation on water [58].

The homogenous distribution stage along the radiation track is achieved in a short time scale (e.g., ~ 100 ns in water at 25°C). For a given type of radiation, the chemical yields at the initial homogenous distribution stage depends primarily on the absorbed energy and are expressed using G-values. The standard units of G-values are $\mu mol \bullet J^{-1}$ (older units of G-values use number of species produced per 100 eV of absorbed energy). Since the LET rate determines the spur density along the track, the G-value is a function of the LET rate of the ionizing radiation in a given medium. For example, the G-values for the α-radiolysis of water differs from those of γ-radiolysis [49]:

G-values for α-radiolysis (in brackets):

$$H_2O\ (-0.27) \rightarrow \bullet OH\ (0.021),\ \bullet e_{aq}^{-}\ (0.021),\ H\bullet\ (0.010),\ H_2\ (0.12),$$

$$H_2O_2\ (0.12),\ H^+\ (0.28),\ HO_2\bullet\ (0.0040) \qquad (2.1)$$

G-values for γ-radiolysis (in brackets)

$$H_2O\ (-0.43) \rightarrow \bullet OH\ (0.28),\ \bullet e_{aq}^{-}\ (0.28),\ H\bullet\ (0.062),\ H_2\ (0.047),$$

$$H_2O_2\ (0.073),\ H^+\ (0.28) \qquad (2.2)$$

The G-values are given for the primary radiolysis products. These primary products undergo further chemical reactions with each other and with any other chemical species in solution. Other species, such as $HO_2\bullet$, O_2, $\bullet O_2^-$ and $\bullet O_3^-$, that are formed by reactions of primary radiolysis products with water molecules or themselves are termed secondary radiolysis products. Primary radiolysis yields are not the species first formed following the absorption of radiation energy, but they are the set of 'stable' species that first will undergo bulk phase chemistry. Within the bulk aqueous phase these primary

products will continually react with each other, or, if present, with solute species as well. With a continuous radiation source, primary radiolysis products are continuously formed so that steady-state chemistry will eventually arise [2, 57].

2.4.3 Pulse and Steady-State Radiolysis

Radiation is typically applied to a system in two different formats. In the case of pulse radiolysis, a short (typically < 1 μs duration) intense burst of radiation is input into a system. The result is the rapid creation of primary and secondary radiolysis products. The more reactive of these species (the radicals and ions) quickly react with each other and any other species present. The concentrations of reactive species decay continuously with time until they are all consumed. The rate of decay is used to track the kinetics of a reaction with any species in the system. In the case of steady-state (or continuous) radiolysis, radiation is input into a system continuously over a much longer time period (up to days). With continuous radiation there is a constant rate of production of primary radiolysis products. As the radiolysis products accumulate, the rates of reaction with each other and other species that are present also increase (their loss or removal rate). The removal rates of individual species eventually match their radiolytic production rates and a continuously irradiated system will reach a dynamic steady-state [53, 57, 59]. This may be achieved rapidly. At this point with reactive primary and secondary radiolysis products at steady-state concentrations slower reactions become important and a system slowly changes over time to reach a true steady-state. The pseudo-steady-state concentrations of reactive species determine the effect of long-term continuous

irradiation on slow processes such as solid-liquid interfacial reactions, mass transfer, and corrosion [53, 57, 59].

The fast reactions of ions and radicals are studied on a very short time scale (nanoseconds and smaller) using pulse radiolysis [60]. However, in this work we are not interested in reactions occurring on a short time scale and want to focus on the slower processes that occur in a system under long-term continuous irradiation. This is the case for many practical situations where a radiation source is the natural decay of radionuclides that are present. For example, if an IL is used as a solvent for reprocessing spent nuclear fuel, the IL will be in an energy intensive environment caused by the continuous decay of the radioactive spent fuel. Figure 2.4 illustrates the situation where a continuous source of γ-radiation impacts a system with both IL and water phases present.

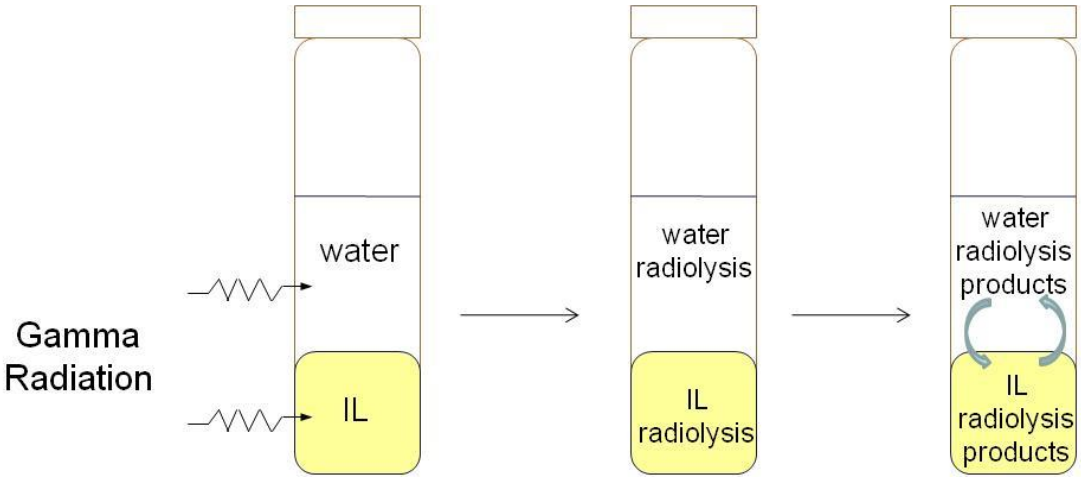

Figure 2.4 Steady-state γ-radiation of a water/IL sample.

2.4.4 IL Radiolysis Principles

The physical processes that dictate the interaction of ionizing radiation with a bulk IL phase are the same as those that occur in water. Incident radiation particles or photons will initially induce ionization and excitation of the anionic and cationic components of the ionic liquid. However the probabilities of this initial interaction leading to the production of primary radiolysis products is very different for an IL than for water. The production of free ions and free radicals depends on the rate of geminate recombination of initially-produced ion pairs within solvent cages formed by the bulk IL phase. The probability of this recombination process depends on the Onsager radius, the distance at which the Coulombic potential equals the thermal energy of the molecules [61],

$$R_s = \frac{e^2}{4\pi\varepsilon_r\varepsilon_o k_b T} \tag{2.3}$$

where R_s is the Onsager radius, e is the electron charge, ε_r is the dielectric permittivity of the medium and ε_o is the dielectric constant of permittivity in a vacuum (unitless), k_b is the Boltzmann constant and T is the temperature (K) (k_bT is the thermal energy). This can be simplified to

$$R_s \propto \frac{e^2}{k_b T \varepsilon_r} \tag{2.4}$$

and the likelihood that an electron will escape is dictated by the dielectric constant [61]. If the kinetic energy is greater than the Coulombic potential, the electron can escape [61]. With a large dielectric constant, the Onsager radius becomes small, and the thermal energy required for an electron to escape decreases. In the case of a small dielectric constant, electron escape is unlikely and recombination predominates.

The probability of the charged species (or radical decay products of electronically excited molecules) escaping geminate recombination to become free ions or free radicals is typically low in ionic liquids because this class of chemicals has relatively low dielectric constants. While the dielectric constants of the phosphonium ionic liquids studied in this work have not been reported, those of other ILs have been measured and reported to be typically < 15 [62]. This is a value which is comparable to the dielectric constants of organic solvents and is much smaller than the dielectric constant of water (80.1 at room temperature [20, 61]). Hence we would expect that the probability of absorbed radiation energy leading to radiolytic decomposition of an IL molecule would be much less than the probability of the same event in water.

2.4.5 Radiolysis of Ionic Liquids

2.4.5.1 *Pulse Radiolysis of Ionic Liquids*

The vast majority of IL radiation studies have utilized pulse radiolysis to examine the fast reactions occurring in the IL on a very short time scale. As discussed previously, ionizing radiation initially ejects an electron from molecules within the medium. These free electrons become thermalized and, in water, become solvated electrons. In comparison to conventional solvents and liquids, ILs respond differently to the electron solvation process; for example, imidazolium ILs contain an ultrafast solvation component that quickly generates the solvated electron, while phosphonium ILs do not and the solvation process is slower [63-65]. The solvation process was correlated to the viscosity of the IL in a series, independent of the anion.

Studies have used electron paramagnetic resonance techniques, time-resolved absorbance pulse radiolysis, and spectroscopic methods to study IL pulse radiolysis. All techniques indicate that ILs possess very different reactivity patterns in comparison to conventional liquid solvents. Furthermore, these studies have illustrated the vast differences between ILs containing different cation and anion species, confirming that generalities of ILs cannot be made. However, studies have given insight to the initial ionization of ILs to aid in the analysis of the resulting chemical reactions.

The consequences of ionizing radiation differ for ILs that have aliphatic cations (such as the phosphonium or ammonium) and those that contain aromatic cations (like the imidazolium). Aromatic cations are efficient electron acceptors, and ionization results in free electron trapping in the anion and cation vacancies [65, 66]. Following this the cations are known to relax from their excited state or undergo dimerization [67]. Aliphatic cations trap electrons electrostatically in their vacancies [65]. As the electron pathway along the alkyl chains and branched structures are blocked, the aliphatic cations (especially those with long alkyl chains) undergo radiolytic decomposition, resulting in the formation of carbon-centered radical cations. As with the cation species, the anions also have an abundance of reaction pathways. Due to the varied nature of the anion structures, ranging from single atoms to branched inorganic chains, predictions of radiolysis pathways are difficult. Often anions will fragment along branching chains from the central anion, only to recombine and form dimer species (though this does not hold true for all anions) [65].

Consistent with the expectation of little radiolytic degradation in ILs, the results of limited studies on the radiation stability of ILs using pulse radiolysis have shown that,

for ionic liquids with cations containing aromatic rings, such as imidazolium and pyridinium, electrons can rapidly be captured by the rings to form neutral radicals [61, 66, 68, 69]. For ILs with alkyl cations, such as tetraalkylammonium salts, electrons can be trapped in metastable F-centers. Both of these processes result in broad absorption bands in the near-IR region. In all cases much smaller primary radiolysis yields (G-values) have been reported for ILs than for water [70]. However, studies on the mechanisms and kinetics of the subsequent reactions of the primary radiolysis products in ILs (such as neutral radicals and those containing metastable F-centers) are limited, presumably due to the fact that each IL provides a unique chemical environment and this discourages such research.

2.4.5.2 *Steady-State Radiation of Ionic Liquids*

There are few studies of the continuous radiolysis of ILs. One of the most notable observations following prolonged irradiation doses was the darkening of the ILs with time [71-73]. This observation, however, is isolated to imidazolium ILs. Studies devoted to the darkening have found that this occurs mostly due to the formation of dimers of imidazolium cations and imadazolium cations containing double bonds [23, 74].

Other studies have shown that long term radiation of ILs can generate many different radiolysis products, where both primary generated species and secondary species formed as a result of the degradation and reactions of primary species [67]. Although a myriad of possible radiolysis products and degradation products exist, input radiation results in only a small amount of degradation of the IL species itself. While the small amounts of radiolysis products present in an IL after irradiation change some of the

physical properties of the IL (viscosity, electrochemical window), many other properties such as the density and refractive indices were unaltered, showing the ILs were largely resistant to radiation [23, 75]. Berthon *et al.* [23] concluded that only a very small amount of degradation products were formed, < 0.5 % mol in fact, following 580 kGy of irradiation.

Few long term gamma radiation studies have been performed on ILs, especially on phosphonium-based ILs. The small body of work has thus far focused on imidazolium and ammonium cation based ILs in particular as most other research has also been performed on these systems. Thus, to our knowledge, this thesis is one of the first studies to provide information on the long term radiation of phosphonium ILs both in contact with a gas phase and a water phase, and aims to fill gaps in the current knowledge.

2.5 REFERENCES

1. E.W. Castner, J.F. Wishart, J. Chem. Phys., 132 (2010) 120901-1 - 120901-9.
2. R.D. Rogers, K.R. Seddon, Science, 302 (2003) 792-793.
3. K.N. Marsh, J.A. Boxall, R. Lichtenthaler, Fluid Phase Equilib., 219 (2004) 93-98.
4. U. Domanska, General Review of Ionic Liquids and Their Properties in Ionic Liquids in Chemical Analysis, M. Koel (Ed.), CRC Press, Boca Raton, Florida (2008) pp. 1-71.
5. P.C. Trulove, R.A. Mantz, Electrochemical Properties of Ionic Liquids in Ionic Liquids in Synthesis, 2nd ed., P. Wasserscheid, T. Welton (Eds.), Wiley-VCH Verlag GmbH & Co. KGaA, Weinhein, Germany (2008) pp. 141-174.
6. B.J. Mincher, G. Modolo, S.P. Mezyk, Solvent Extr. Ion Exch., 27 (2009) 579-606.
7. K. Binnemans, Chem. Rev., 107 (2007) 2592-2614.
8. H. Zhao, S.Q. Xia, P.S. Ma, J. Chem. Technol. Biotechnol., 80 (2005) 1089-1096.
9. A.E. Visser, R.D. Rogers, J. Solid State Chem., 171 (2003) 109-113.
10. A. Heintz, J. Chem. Thermodyn., 37 (2005) 525-535.
11. S.L.I. Toh, J. McFarlane, C. Tsouris, D.W. DePaoli, H. Luo, S. Dai, Solvent Extr. Ion Exch., 24 (2006) 33-56.

12. J. Wishart, Radiation Chemistry of Ionic Liquids:Reactivity of Primary Species in Ionic Liquids as Green Solvents, R.D. Rogers, K.R. Seddon (Eds.), ACS Symposium Series, Oxford University Press, Washington, DC (2003) pp. 381-396.
13. J.F. Wishart, Energy Environ. Sci., 2 (2009) 956-961.
14. N.V. Plechkova, K.R. Seddon, Chem. Soc. Rev., 37 (2008) 123-150.
15. K.J. Fraser, D.R. MacFarlane, Aust. J. Chem., 62 (2009) 309-321.
16. Ionic Liquids in Synthesis, 1st ed., P. Wasserscheid, T. Welton (Eds.), Wiley-VCH Verlag GmbH & Co. KGaA, Weinhein, Germany (2003).
17. P. Bonhote, A.O. Dias, N, Papageorgiou, K. Kalyanasundaram, M. Gratzel, Inorg. Chem., 35 (1996) 1168-1178.
18. R. Hagiwara, Y. Ito, J. Fluorine Chem., 105 (2000) 221-227.
19. A.R. Katritzky, R. Jain, A. Lomaka, R. Petrukhin, M. Karelson, A.E. Visser, R.D. Rogers, J. Chem. Inf. Comput. Sci., 42 (2002) 225-231.
20. CRC Handbook of Chemistry and Physics, 85th Ed., D.R. Lide (Ed.), CRC Press, Boca Raton, FL (2011).
21. K.R. Seddon, A. Stark, M.J. Torres, Pure Appl. Chem., 72 (2000) 2275-2287.
22. J.A. Widegren, A. Laesecke, J.W. Magee, Chem. Commun. (2005) 1610-1612.
23. L. Berthon, S.I. Nikitenko, I. Bisel, C. Berthon, M. Faucon, B. Saucerotte, N. Zorz, P. Moisy, Dalton Trans. (2006) 2526-2534.
24. K.J. Fraser, E.I. Izgorodina, M. Forsyth, J.L. Scott, D.R. MacFarlane, Chem. Commun. (2007) 3817-3819.
25. C.M.S.S. Neves, P.J. Carvalho, M.G. Freire, J.A.P. Coutinho, J. Chem. Thermodyn., 43 (2011) 948-957.
26. C.J. Bradaric, A. Downard, C. Kennedy, A.J. Robertson, Y. Zhou, Green Chem., 5 (2003) 143-152.
27. H.-P. Steinruck, Phys. Chem. Chem. Phys., 14 (2012) 5010-5029.
28. D. Wakeham, P. Niga, C. Ridings, G. Andersson, A. Nelson, G.G. Warr, S. Baldelli, M.W. Rutland, R. Atkin, Phys. Chem. Chem. Phys., 14 (2012) 5106-5114.
29. K.R.J. Lovelock, Phys. Chem. Chem. Phys., 14 (2012) 5071-5089.
30. C.S. Santos, S. Baldelli, Chem. Soc. Rev., 39 (2010) 2136-2145.
31. C.S. Santos, S. Baldelli, J. Phys. Chem. B, 111 (2007) 4715-4723.
32. S.E. Howett, J.M. Joseph, J.J. Noel, J.C. Wren, J. Colloid and Interface Sci., 361 (2011) 338-350.
33. N.V. Sastry, N.M. Vaghela, P.M. Macwan, S.S. Soni, V.K. Aswal, A. Gibaud, J. Colloid Interface Sci., 371 (2012) 52-61.
34. P. Mukherjee, J.A. Crank, P.S. Sharma, A.B. Wijeratne, R. Adhikary, S. Bose, D.W. Armstrong, J.W. Petrich, J. Phys. Chem. B, 112 (2008) 3390-3396.
35. C. Jungnickel, J. Luczak, J. Ranke, J.F. Fernandez, A. Muller, J. Thoming, Colloids Surf., A, 316 (2008) 278-284.
36. F. Gayet, C. Patrascu, J.D. Marty, N. Lauth-de Viguerie, Int. J. Chem. Reactor Eng., 8 (2010) 1-16.
37. H. Gao, J. Li, B. Han, W. Chen, J. Zhang, R. Zhang, D. Yan, Phys. Chem. Chem. Phys., 6 (2004) 2914-2916.

38. J.D. Marty, N. Lauth-de Viguerie, Aggregates in Ionic Liquids and Applications Thereof in Ionic Liquids: Theory, Properties, New Approaches, A. Kokorin (Ed.) [Online] (2011) pp. 409-426, http://www.intechopen.com/books/ionic-liquids-theory-properties-new-approaches.
39. J. Li, J. Zhang, B. Han, L. Peng, G. Yang, Chem. Commun., 48 (2012) 10562-10564.
40. Z. Qiu, J. Texter, Curr. Opin. Colloid Interface Sci., 13 (2008) 252-262.
41. M. Zhao, L. Zheng, Phys. Chem. Chem. Phys., 13 (2011) 1332-1337.
42. R. Vanyúr, L. Biczók, Z. Miskolczy, Colloids Surf., A, 299 (2007) 256-261.
43. J.L. Anderson, V. Pino, E.C. Hagberg, V.V. Sheares, D.W. Armstrong, Chem. Commun. (2003) 2444-2445.
44. R.C. Remsing, Z. Liu, I. Sergeyev, G. Moyna, J. Phys. Chem. B, 112 (2008) 7363-7369.
45. Z. Miskolczy, K. Sebok-Nagy, L. Biczok, S. Gokturk, Chem. Phys. Lett., 400 (2004) 296-300.
46. Y. Zhao, S. Gao, J. Wang, J. Tang, J. Phys. Chem. B, 112 (2008) 2031-2039.
47. N.M. Correa, J.J. Silber, R.E. Riter, N.E. Levinger, Chem. Rev., 112 (2012) 4569-4602.
48. D.P. Acharya, P.G. Hartley, Curr. Opin. Colloid Interface Sci., 17 (2012) 274-280.
49. J.W.T. Spinks, R.J. Woods, An Introduction to Radiation Chemistry, John Wiley & Sons, New York, NY (1990).
50. A.O. Allen, The Radiation Chemistry of Water and Aqueous Solutions, Van Nostrand, New York, NY (1961).
51. I.G. Draganić, Z.D. Draganić, The Radiation Chemistry of Water, Academic Press, New York, NY (1971).
52. Radiation Chemistry: Principles and Applications, Farhataziz, M.A.J. Rodgers (Eds.), VCH Publishers, Weinheim, Germany (1987).
53. J.C. Wren, Steady-State Radiolysis: Effects of Dissolved Additives in Nuclear Energy and the Environment, B. Mincher (Ed.) ACS Symposium Series, Oxford University Press, Washington, DC (2010).
54. J.F. Wishart, A.M. Funston, T. Szreder, A.R. Cook, M. Gohdo, Faraday Discuss., 154 (2012) 353-363.
55. J.F. Wishart, J. Phys. Chem. Lett., 1 (2010) 3225-3231.
56. J.F. Wishart, I.A. Shkrob, The Radiation Chemistry of Ionic Liquids and its Implications for their Use in Nuclear Fuel Processing in Ionic Liquids: From Knowledge to Application, N.V. Plechkova, R.D. Rogers, K.R. Seddon (Eds.), ACS Symposium Series, Oxford University Press, Washington, DC (2009) pp. 119-134.
57. J.M. Joseph, B.S. Choi, P. Yakabuskie, J.C. Wren, Radiat. Phys. Chem., 77 (2008) 1009-1020.
58. Radiation Chemistry: From Basics to Applications in Material and Life Sciences, M. Spotheim-Maurizot, M. Mostafavi, T. Douki, J. Belloni (Eds.) EDP Sciences, France (2008).
59. P.A. Yakabuskie, J.M. Joseph, J.C. Wren, Radiat. Phys. Chem., 79 (2010) 777-785.

60. J.F. Yang, T. Kondoh, K. Kan,Y. Yoshida, Nucl. Instrum. Methods Phys. Res., Sect. A, 629 (2011) 6-10.
61. J.F. Wishart, P. Neta, J. Phys. Chem. B, 107 (2003) 7261-7267.
62. T. Singh, A. Kumar, J. Phys. Chem. B, 112 (2008) 12968-12972.
63. A.M. Funston, T.A. Fadeeva, J.F. Wishart, E.W. Castner, J. Phys. Chem. B, 111 (2007) 4963-4977.
64. N. Ito, S. Arzhantsev, M. Heintz, M. Maroncelli, J. Phys. Chem. B, 108 (2004) 5771-5777.
65. J.F. Wishart, I.A. Shkrob, The Radiation Chemistry of Ionic Liquids and its Implications for their Use in Nuclear Fuel Processing in Ionic Liquids: From Knowledge to Application, N.V. Plechkova, R.D. Rogers, K.R. Seddon (Eds.), ACS Symposium Series, Oxford University Press, Washington, DC, (2009) pp. 119-134.
66. D. Behar, P. Neta, C. Schultheisz, J. of Phys. Chem. A, 106 (2002) 3139-3147.
67. G. Le Rouzo, C. Lamouroux, V. Dauvois, A. Dannoux, S. Legand, D. Durand, P. Moisy, G. Moutiers, Dalton Trans. (2009) 6175-6184.
68. J. Grodkowski, P. Neta, J. Phys. Chem. A, 106 (2002) 5468-547.
69. J. Grodkowski, P. Neta, J.F. Wishart, J. Phys. Chem. A, 107 (2003) 9794-9799.
70. I.A. Shkrob, S.D. Chemerisov, J.F. Wishart, J. Phys. Chem. B, 111 (2007) 11786-11793.
71. L. Yuan, J. Peng, L. Xu, M. Zhai, J. Li, G. Wei, Radiat. Phys. Chem., 78 (2009) 1133-1136.
72. M.Y. Qi, G.Z. Wu, S.M. Chen, Y.D. Liu, Radiat. Res., 167 (2007) 508-514.
73. M.Y. Qi, G.Z. Wu, Q.M. Li, Y.S. Luo, Radiat. Phys. Chem.,77 (2008) 877-883.
74. Z.P. Cui, S.J. Wang, Y.Y. Ao, J. Peng, J.Q. Li, M.L. Zhai, Acta Phys. Chim. Sin., 29 (2013) 619-624.
75. C.J. Rao, K.A. Venkatesan, B.V.R. Tata, K. Nagarajan, T.G. Srinivasan, Radiat. Phys. Chem., 80 (2011) 643-649.

Chapter 3. Experimental Principles and Details

This chapter provides general information regarding the experimental techniques used in this thesis project. Experimental procedures that are common to all experiments are included. As necessary, additional experimental details and information are provided in the appropriate experimental section of later chapters.

3.1 EXPERIMENTAL TECHNIQUES

3.1.1 Gas Chromatography-Mass Spectrometry (GC/MS)

The gas phase that sits above a liquid sample in a test vial is referred to as headspace gas. This gas can contain volatile species that have partitioned from the liquid phase to the gas phase. Gas chromatography-mass spectrometry (GC/MS) was used to study the gas phase headspace above both ionic liquid (IL) and water/IL samples. The technique is particularly useful for determining airborne radiolytic decomposition products. Due to differential partitioning between the mobile (gas) phase and the stationary phase on the walls of the gas chromatograph column, components of a vaporized sample that is introduced into the column are separated, with transport along the column being achieved by the flow of an inert gas phase [1]. A variety of detectors are available for use with the gas chromatograph column, with the mass spectrometer detector being one of the most powerful and useful in compound identification. The mass spectrometer detector allows for precise identification of volatile components existing in the gas phase by providing characteristic mass spectra for the components.

The resulting mass spectra can be displayed to identify species eluting at a specific time as illustrated in Figure 3.1.

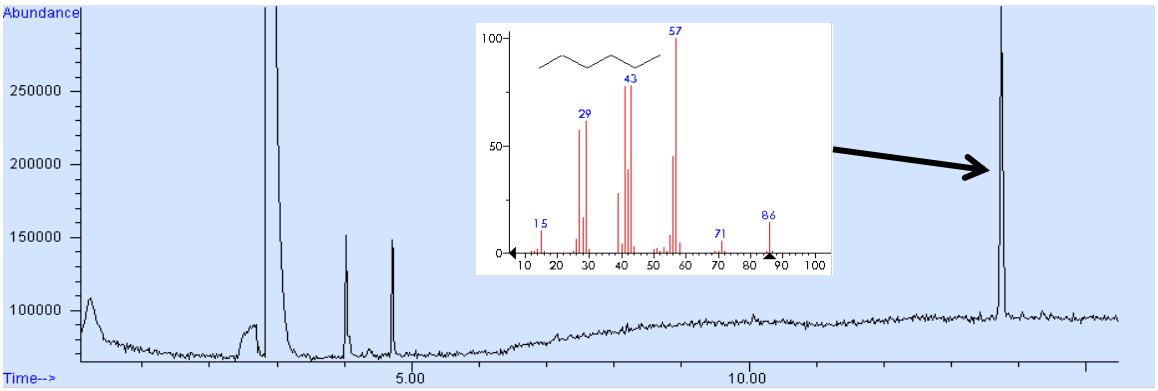

Figure 3.1 Gas chromatogram of the headspace gas from a test with deaerated IL in contact with water and irradiated for 4 hours; inlaid with the mass spectra from the hexane peak

3.1.2 Raman Spectroscopy

Raman spectroscopy is an analytical method that can probe the chemical composition of materials that are capable of Raman scattering [2]. Chemical structures scatter at characteristic frequencies and the spectra resulting from this scattering gives an indication of the bonds and functional groups present in a sample. Raman spectroscopy is a particularly useful tool because spectra can be measured in an aqueous phase without interference since water is not Raman active. Samples require little or no preparation, and can be measured inside a glass vial as well. For these reasons Raman spectroscopy was used to detect species and characterize both the water and the IL phases. However, this technique is only qualitative and cannot give quantitative measures of the species concentrations in either phase.

The Raman spectrometer instrumentation consists of a laser source, a sample illumination and scattered light collection system, and a light detection system. For the analyses performed in this thesis, an attachment to allow the laser to focus perpendicularly to the sample surface was also utilized. When the laser beam strikes a sample, the sample emits photons which are collected by an optical network for detection and analysis.

Raman spectroscopy is possible when the electron cloud surrounding a molecule is polarizable. When an incident photon is able to induce changes in the electronic structure and emission of a scattered photon, the resulting interactions can be classified as Rayleigh scattering, Stokes scattering, or Anti-stokes scattering. The predominant process is elastic, or Rayleigh scattering. Elastic Rayleigh scattering occurs when, following absorption of the incident photon, a molecule is excited to a virtual energy state and then rapidly decays back to the original ground state while emitting a photon with the same energy as the incident photon. Inelastic Raman scattering occurs when the interaction between the incident photon and the molecule results in a change in the vibrational state of the molecule. The scattered photon then has a different energy from the incident photon with the difference corresponding to the energy of the vibration state transition in the molecule. If the scattered photon has less energy than the incident photon (the molecule having been vibrationally excited) the process is termed inelastic Stokes scattering. However, if the scattered photon has more energy than the incident photon the process is termed anti-Stokes scattering. Since both Stokes and anti-Stokes scattering events have a very low probability of occurrence, an intense monochromatic light source (a laser) is necessary to see the scattering clearly. The relative intensities of

Stokes and anti-Stokes scattering are proportional to temperature, which determines the equilibrium populations of the target molecules in particular vibrational states (Boltzmann distributions).

The frequency shift between the incident photon (ν_i) and the scattered photon (ν_f) provide a direct measure of the energy of the vibrational state that has changed. This relationship is given by

$$h\nu_i = h\nu_f \pm \Delta E_{vibration} \quad (3.1)$$

where h is the Plank constant and $\Delta E_{vibration}$ is the energy difference between the initial and final vibrational levels. While Raman scattering can occur for changes in vibrational states of 1 or more quanta, the intensity of the scattering decreases sharply for $\Delta v > \pm 1$. Since most of the molecules of interest in this work are in the ground state ($v = 0$) the Raman spectrum is dominated by a Stokes scattering peak that corresponds to the vibrational energy transition for $v = 0$ to $v = 1$.

3.1.3 Electrochemical Impedance Spectroscopy (EIS)

Differences in the chemical structure and composition of the IL and aqueous phases can be studied using electrochemical impedance spectroscopy (EIS). Changes in chemical structure can induce a change in the conductivity, giving an indication that the composition of a system has changed. Electrochemical impedance spectroscopy was used in this thesis to probe the conductivity of liquid samples to determine if there were any dramatic changes within the water or IL layer as a function of radiation or contact time.

An impedance system can be constructed with any number of 'electrical' elements, including resistors and capacitors, in series or in parallel [3]. A resistor is an element that slows the flow of the current. The magnitude of its resistance is generally proportional to its length and the resistance is inversely proportional to its conductivity and cross-sectional area (with respect to the direction of current flow). Ohm's law links the current that is passing through a resistor, with its resistance (R)

$$I = \frac{\Delta E}{R} \tag{3.2}$$

where I is the current and ΔE is the change in potential across the resistor. A capacitance (C) element can be defined as the derivative of the charge on the element with respect to the applied potential,

$$C = \frac{dQ}{dE} \tag{3.3}$$

where Q is the charge and E is the potential. The derivative of the charge moving through the system with respect to time defines the current, I.

$$I(t) = \frac{dQ(t)}{dt} \tag{3.4}$$

The combination of equations 3.3 and 3.4 provides a relationship between the current and the potential for a capacitor,

$$I(t) = C\frac{dE(t)}{dt} \tag{3.5}$$

In electrochemical impedance spectroscopy, a varying potential is applied to a system using a frequency generator and the resulting frequency dependent current in the system is measured [4, 5]. Normally the potential is varied sinusoidally over several

orders of magnitude of frequencies, ω, which, in our work, was typically 1 Hz to 10^6 Hz. This applied potential generates a sinusoidal current response,

$$I(t) = I_{amp}\sin(\omega t + \theta) \tag{3.6}$$

where I_{amp} is the maximum current amplitude and θ is a phase shift. The impedance (Z) of a system is given by the ratio of the applied potential to the resulting current.

$$Z(\omega t) = \frac{E_{amp}\sin(\omega t)}{I_{amp}\sin(\omega t + \theta)} \tag{3.7}$$

The impedance is purely resistive when the current is in-phase with the applied potential (the phase shift θ = 0). Alternatively, if the phase shift is 90° out of phase the impedance is a purely capacitive response of the system, as shown in Figure 3.2.

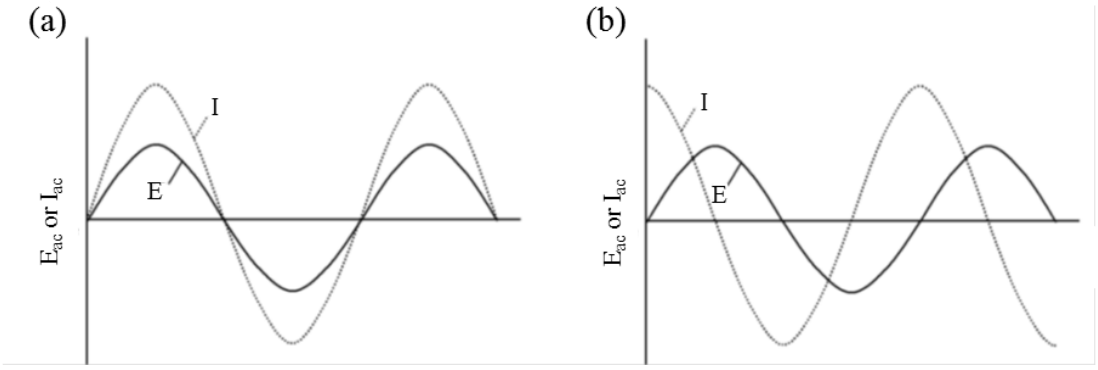

Figure 3.2 The (a) purely resistive and (b) purely capacitive impedance response arising from a given electrochemical impedance experiment [6].

Equation 3.7 can be rewritten to define a complex impedance with real and imaginary components,

$$Z(\omega t) = \frac{E_{amp}\sin(\omega t)}{I_{amp}\sin(\omega t + \theta)} = Z_r(\omega t) + jZ_{im}(\omega t) \tag{3.8}$$

where Z_r and Z_{im} are the real and imaginary components of the impedance, and j is the imaginary unit. The resistance of a system is the real component of the total impedance and the capacitance is contained in the imaginary component, as

$$Z = R - j\frac{1}{\omega C} \tag{3.9}$$

where R is the resistance, ω is the frequency of the applied potential, and C is the capacitance.

Impedance spectra can be presented as either a Nyquist or a Bode plot. A Bode plot consists of two graphs, one with the real part of the impedance (Z_r) as a function of frequency and the second with the phase angle as a function of frequency. For a Nyquist plot the real impedance component is plotted against the imaginary component, and is usually extrapolated to a semicircle (as was done in this work). The Nyquist and Bode plots are used to compare experimental data to modeling results obtained with an equivalent circuit model that consists of resistive and capacitive components. The fit of the modeling results to the measured data is used to extract a value for the resistance of the system and also to identify the number of different resistance and capacitance components required to fit the data. The latter is normally a characteristic of the number of different physical elements in the system (e.g., the number of different phases).

The conductivity of a liquid system (σ) can be determined using the resistance by,

$$\sigma = \frac{1}{R} \cdot \frac{\ell}{A} \tag{3.10}$$

where $\frac{\ell}{A}$ is the cell constant (the ratio of the distance between the two electrodes used to apply the potential (ℓ) to the area of the electrodes (A)). This ratio is normally

experimentally determined using standard solutions of KCl for which the conductivity is known. In this work, the conductivity cell in which the EIS of water/IL systems was measured consisted of a quartz cuvette with two parallel electrodes made of glassy carbon.

3.1.4 Fourier Transform Infrared Spectroscopy (FTIR)

Fourier transform infrared spectroscopy (FTIR) is used for the measurement of the infrared spectra of compounds for the purpose of analysis and structural elucidation as it probes molecular vibrations [7]. The fingerprint region of the spectra (500-1500 cm^{-1}) contains peaks characteristic to specific bonds and within specific compounds, allowing for differentiation between similar structures. Though sensitive to water (the presence of peaks due to water molecule vibrations can occlude other peaks in the spectra), the technique has advantages with respect to Raman spectroscopy because it is easier to use and does not cause fluorescence of a sample. To overcome these disadvantages with Raman spectroscopy, FTIR was used to characterize some of the compounds and particularly the more fluorescent material that was studied.

The FTIR instrument contains four components: a source, a beam splitter, a sample, and a detector. The source light is split by a stationary mirror and moving mirror and is combined again to form an interferogram [8]. Following interaction with the sample, the detector is able to measure the variation in light energy versus time and this is then converted into a readable spectrum by Fourier transformation of the measured light signals.

In order for light energy to be absorbed, a molecular bond must have an electrical dipole moment [8, 9]. This allows the molecule to interact with incoming photons and absorb energy at frequencies associated with transitions between vibrational and rotation states within the molecule; specific infrared absorption bands correspond to specific vibrations in the molecule [7]. The two main types of vibrations in the mid-infrared region (400 cm^{-1}- 4000 cm^{-1})correspond to individual stretching vibrations between chemically bonded atoms and bending vibrations that involve the motion of three chemically bonded atoms (changing the bond angle between the atoms) [7]. The vibrational frequency depends on the bond strength and the masses of the atoms participating in the vibration. Frequencies are thus characteristic of a given chemical group (e.g. O-H stretch), and are further modulated by the chemical environment to give specific values for particular species.

3.1.5 Transmission Electron Spectroscopy (TEM)

The microstructure of samples can be studied using transmission electron microscopy (TEM) [10]. TEM is used in this work for the study of micelles and precipitates present in the aqueous phase of a sample.

A transmission electron microscope operates under the same principles as a light microscope (with light shining through a sample to an eye-piece), but uses electrons rather than visible photons to obtain an image. Thus, samples must be thin enough (20-300 nm) to allow for the efficient transmission of electrons with little loss. The microscope contains a monoenergetic electron source (in our case 100 keV), two condenser lenses for electron beam focus and magnification, and magnetic coils for

electron beam alignment. Samples are prepared on TEM grids and these are mounted on a stage in the focus of the microscope. Once the sample is inserted in the instrument, the instrument is evacuated to permit generation of the electron beam.

Images of the samples studied were obtained using the bright field mode of imaging. In this mode, the flux of incident electrons on a detector (after passing through the sample) dictates the brightness of the image. The size, shape and thickness of areas of the sample are determined by the rate of electron absorption/scattering which creates differential brightness in the image.

The resolution of a TEM is limited by the de Broglie wavelength of the electrons used in the instrument. For our analysis, a 100 keV electron beam is capable of a resolution of 36 pm, a dimension much smaller than the scale of the features that we observed.

3.1.6 Dynamic Light Scattering (DLS)

The formation of colloids and micelles that result from contact of ILs with a water phase is an important aspect of this work and dynamic light scattering (DLS) is useful in the determination of size distributions of colloid scale particles in a solution [11]. With supporting TEM micrographs, the technique gives a microscopic view of colloids and micelles in solution and information on the size distribution profile within a given phase.

Dynamic light scattering data can be collected quickly. The technique requires a very small sample volume, with no sample preparation, and can measure particles with sizes of less than 1 nm with a high molecular weight upper limit (greater than 1000 g/mol). This type of analysis requires that the target particles have a polarizability

that is different from that of the surrounding liquid [12]. A laser is used as an incident light source. After passing through a polarizer (to establish the polarization of the incident light beam), the laser light enters the sample cell and is scattered by material suspended in the cell liquid. The scattered light is collected and detected in an analyzer that measures scattered light intensity as a function of scattering angle, where the location of the detector with respect to the incident laser light defines the scattering angle [13]. By analyzing the intensity fluctuations of scattering light, the diffusion of molecules in the region of study can also be measured using this instrumentation. Brownian motion is related to the size of particles by the Stokes-Einstein equation,

$$D_h = \frac{k_b T}{3\pi\eta D_t} \tag{3.11}$$

where D_h is the hydrodynamic diameter, or particle size, k_b is Boltzmann's constant, T is the temperature, η is the viscosity, and D_t is the diffusion coefficient (as determined from the DLS data) [12, 14]. Software available with the DLS instrumentation can be used to calculate the particle size from the derived diffusion coefficient. The resulting particle size (nominal diameter of the particles (as spherical objects)) can be displayed as a function of intensity, distribution by volume (Figure 3.3), or distribution by number.

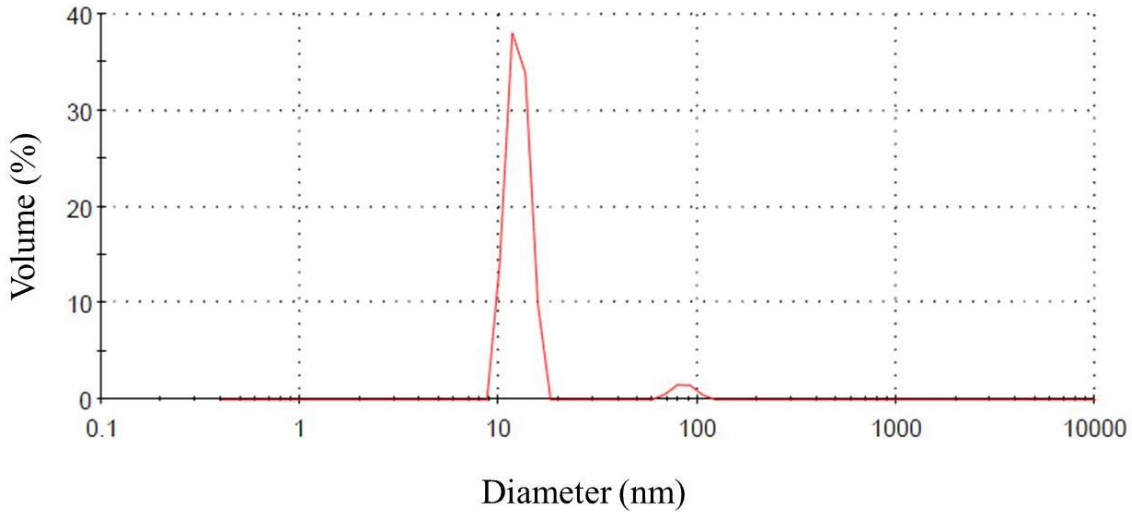

Figure 3.3 A DLS graph illustrating the distribution of particle diameter (nm) versus volume of a water phase sample.

3.1.7 Pulse Radiolysis

Pulse radiolysis is used to apply a short term pulse of ionizing radiation to a system. This pulse initiates fast reactions and is used to study chemical kinetics and primary reaction processes of reactive radicals and ions on a very short time scale (nanoseconds and smaller) [15]. In this work the formation of micelles in ILs in contact with a water phase was studied. This process raises questions about the role of fast reactions occurring in the biphasic system, the role of radiolysis degradation products, and the radiation-induced chemistry that can occur in the water encapsulated within the IL molecule micelles. In order to address these questions, pulse radiolysis and in-situ techniques were used to probe and monitor the biphasic systems.

At Brookhaven National Laboratory, in Upton, NY, the Center for Radiation Chemistry Research facility has the Laser-Electron Accelerator Facility (LEAF). This

facility was designed specifically for pulse radiolysis with a high charge per pulse. Known as one of the fastest facilities globally, the LEAF operates by pulsing a fast laser aimed at an electron gun. Within the electron gun is a light sensitive 6 mm magnesium plug photocathode which emits electrons when UV laser light impinges upon it. The resulting 7 picosecond pulses are sent through a microwave driven accelerator which boosts the energy of the electrons [16]. The electron pulse is collected by a solenoid magnet and directed down a beam line by horizontal and vertical steering dipole magnets. Five integrating current transformers (ICTs) monitor the beam transport to maintain the beam position and profile. The products of the fast electron impact on a target solution are detected using ultraviolet-visible spectroscopy and infrared spectroscopy. Often the species created by electron impact have high molar absorptivity values, and thus fast reactions are easily tracked by monitoring their absorbance decay.

3.1.8 Small Angle Neutron Scattering (SANS)

The small angle neutron scattering (SANS) technique allows for the characterization of structures such as particles in solution, clusters, or precipitates on the nanometer scale [11]. The technique yields information on the number, size and shape of aggregates within the sample, phase transitions, and the location of different molecules or molecular components [11, 17]. In particular, the SANS technique can be a useful tool for studying the micellar structures and inter-micellar interactions in ionic liquid samples. It is a particularly attractive investigative technique because it is noninvasive [17, 18].

Neutron scattering measures the deflection of neutrons in a collimated incident beam by a target. To achieve useful resolution, the technique uses cold (low thermal

temperature = low translational energy or velocity, 'slow') neutrons that have a de Broglie wavelength (λ) that is comparable with the size range of the particles/structures of interest in a given scattering experiment.

In neutron scattering experiments the scattered neutrons are collected and analyzed as a function of the momentum transfer to the neutrons by the scattering events. This can be defined using Bragg wave vectors,

$$q = k_i + k_s \tag{3.12}$$

where q is momentum transfer, k_i is the incident wave vector, and k_s is the scattered wave vector. The primary type of scattering of interest is elastic scattering, where $|k_i| = |k_s| = 2\pi n/\lambda$, where n is the index of refraction. The magnitude of q is then given by

$$q = \frac{4\pi}{\lambda} n \sin\left(\frac{\theta_{sa}}{2}\right) \tag{3.13}$$

where θ_{sa} is the scattering angle. Schematically this type of neutron scattering is illustrated in Figure 3.4 [19].

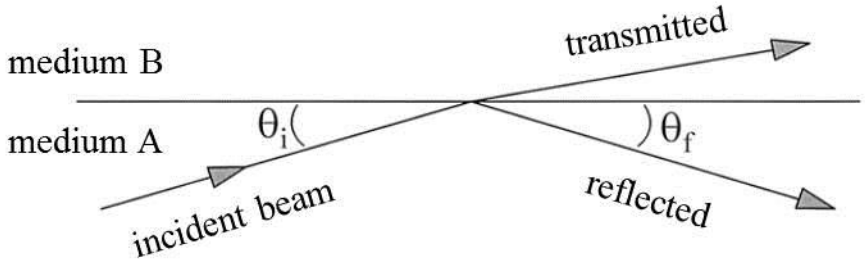

Figure 3.4 The partially transmitted and partially reflected neutron beam resulting from a beam incident on the interface between any two media (A and B).

The refractive index of a medium depends on its scattering length density (SLD). This is a product of the density of atoms per unit volume (ρ) in the medium and their coherent scattering length (*b*), where the coherent scattering length is a property characteristic to the atomic nuclei [19]. It is the distinctive coherent scattering length that makes neutron scattering especially beneficial for the purpose of examining micelles in solution. The scattering of hydrogen varies greatly from the scattering of heavier deuterium, resulting in very different SLD values for these isotopes. Thus, neutron scattering can be especially beneficial for the purpose of studying micelles and their surrounding aqueous solution in contrast matching experiments in which normal water or deuterated water is used.

Small angle neutron scattering instruments use small angles or long wavelengths (and sometimes both) to realize a low value for q. Long neutron flight paths before and after the sample allow for good collimation of the neutrons and precise scattering angle measurements. There are two varieties of SANS instrument neutron selectors to narrow the neutron beam energy distributions. Time-of-flight (TOF) instruments use choppers at the source and a detector to select neutron wavelengths, while utilizing a wide range of the available neutron beam spectral distribution. Alternatively, instruments with broad spectrum neutron sources use velocity detectors to choose a portion of the neutron spectrum.

The SANS analyses described in this work were performed at the National Research Universal (NRU) reactor at Atomic Energy of Canada Limited (AECL), Chalk River Laboratories using the N5 triple axis neutron spectrometer that is operated by the Canadian Neutron Beam Centre (CNBC). The NRU reactor does not have a cold neutron

source and for SANS studies a confocal Soller collimator (CSC) has been designed and implemented. This collimator allows the neutron flux at the sample to increase by a factor of 20, and gives the N5 spectrometer the capability to perform as a SANS instrument.

The NRU instrument is configured according to Figure 3.5 [20]. An extended q range is achieved by using a variety of different neutron wavelengths. Using either a sapphire or beryllium filter before the pyrolytic graphite (PG) monochromator aids in filtering unwanted neutrons. The desired neutron beam is sent through the collimator and the resultant beam converges at a point on the sample. Depending on the experiment, either a pyrolytic graphite filter or a horizontal Soller collimator (HSC) is used to reduce vertical divergence in the beam. The scattered neutrons are filtered through a horizontal Soller collimator before reaching a 32-wire ^{3}He position sensitive neutron detector.

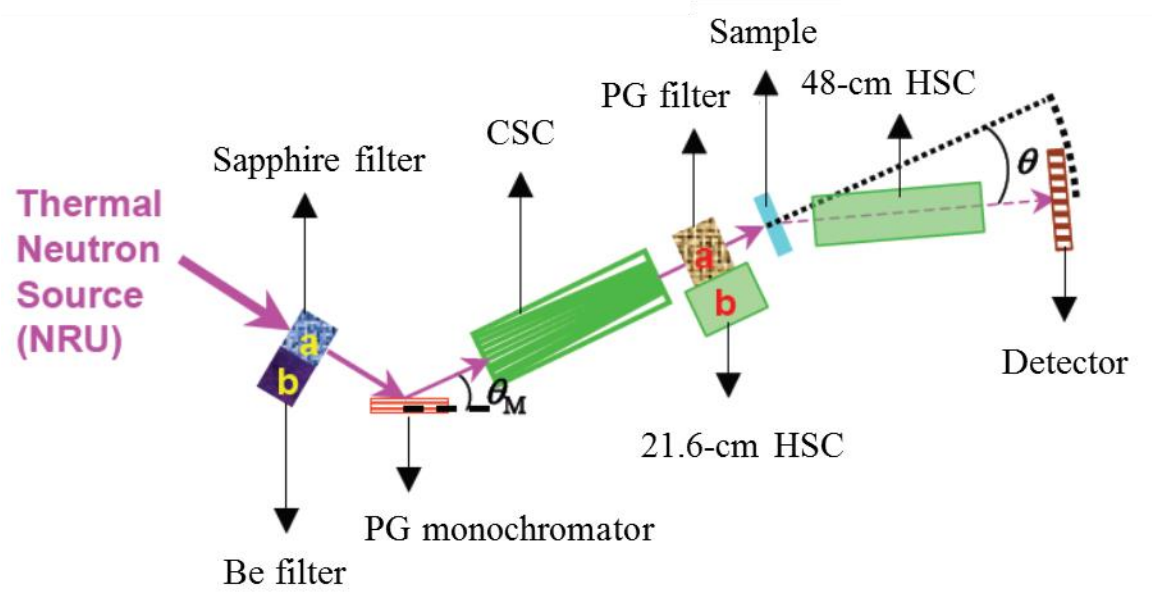

Figure 3.5 A schematic of the adapted N5-SANS instrument [20].

Accumulated neutron scattering intensities are measured and analysis is performed. The raw scattered intensity ($I_{raw}(q)$) is given by

$$I_{raw}q = I_o \Delta\Omega \eta_e T_{sam}(\lambda) V \frac{d\Sigma}{d\Omega}(q) + I_{bgd}(q) \quad (3.14)$$

where I_o is the incident neutron intensity, $\Delta\Omega$ is the sample-to-detector solid angle, η_e is the detector efficiency, $T_{sam}(\lambda)$ is the transmission of a sample, V is the sample scattering volume, and $I_{bgd}(q)$ is the background neutron flux [20]. The term $\frac{d\Sigma}{d\Omega}(q)$ refers to the differential scattering cross section per unit volume. Ultimately, the goal of a SANS experiment is to obtain the $\frac{d\Sigma}{d\Omega}(q)$ of a sample as a function of q. This is related to the size and morphology of the sample. In order to obtain this information, the appropriate data reduction must be performed to yield a SANS curve. This is achieved by normalizing the collected scattered data to the scattered neutron intensity of an empty cell ($I_{emt}(q)$) (the background intensity). This is used to express the reduced intensity [20],

$$I_{red}(q) = \frac{[I_{raw}(q) - I_{bdg}(q)]}{T_{sam}(\lambda)} - \frac{[I_{emp}(q) - I_{bdg}(q)]}{T_{emp}(\lambda)} \quad (3.15)$$

where $I_{emp}(q)$ is the empty cell scattering, and $T_{emp}(\lambda)$ is the transmitted intensity of the empty cell. By putting the reduced intensity ($I_{red}(q)$) on an absolute scale, the reduced intensities merge to result in a single SANS curve from which one can perform data analysis and obtain the system information. A program for data analysis is available at NRU that has been specifically written for this purpose by the research scientists there.

3.2 EXPERIMENTAL PROCEDURES

3.2.1 Sample Preparation

All ionic liquids used in this work were purchased from Sigma-Aldrich and were of the highest purity available (≥ 95%). The purities of the ILs (and the absence of any moisture) were verified using proton nuclear magnetic resonance spectrometry (^{1}H NMR), electrospray ionization-mass spectrometry (ESI-MS) and differential scanning calorimetry (DSC) analysis. The water used in this study was purified by a NANOpure Diamond UV ultrapure water system (Barnstead International) and had a consistent resistivity of 18.2 MΩ·cm. In tests, water/IL samples composed of 2 mL of water and 2 mL of ionic liquid were placed inside 10 mL vials (Agilent Technologies) and sealed with aluminum crimp caps with PTFE/silicone septa. Deaerated samples were prepared by purging the contents of the sealed vials with ultra-high purity argon (Praxair, 99.99% purity) using syringes for 20 minutes prior to irradiation. Aerated samples were prepared by purging the samples with hydrocarbon-free air using the same method.

3.2.2 Sample Irradiation

Irradiation experiments were conducted in a MDS Nordion Gammacell 220 Excel Cobalt-60 irradiator. Test vials containing solutions were placed inside the gamma cell sample chamber and then lowered into the gamma cell irradiation zone, as required. The irradiation zone consisted of 11 tubular pencils containing ^{60}Co arranged in a circle around the sample chamber. The dose rate of the gamma cell during which these experiments were performed varied from ~ 6.4 kGy·h^{-1} to 5.5 kGy·h^{-1} (depending on when experiments were performed, the half-life for decay of ^{60}Co is 5.27 years).

Irradiation was conducted over time periods up to 600 h, during which the samples were periodically removed and tested. Control test vials were also prepared, treated, handled and analyzed in the same manner as test vials, but without any exposure to γ-radiation.

3.2.3 Sample Analysis

Samples were extracted from the test vials at varying times during experiments (generally immediately after completion of an irradiation period). The conductivities of the water and the IL phases were measured using EIS. The EI spectra were obtained using either a BioLogic Science Instruments MCS 200 conductivity instrument, a model 1287 Solatron potentiostat and model 1252 frequency response analyzer, or a model 1260 Solartron frequency response analyzer operated as a stand-alone instrument (depending on instrumentation available). All three sets of equipment yielded equivalent results. Zplot and Zview software packages were used for experiment control and analysis. EIS was performed by varying the frequency range over 1 Hz to 10^6 Hz. The conductivity cell constant was determined prior to each set of analyses using KCl solutions for which the conductivity is known. The cell constant was experimentally determined to vary between 7.5 cm^{-1} and 11.0 cm^{-1} depending on the instrumentation. No error bars are displayed on the graphs showing conductivity measurements because the calculated error is smaller than the graph symbols.

Gas phase analysis was performed by extracting an aliquot of gas from the headspace above the liquids in a test vial using a gas-tight Luer lock syringe (Agilent Technologies). The gas samples were injected into a gas chromatograph with a mass spectrometer detector (GC/MSD, Agilent Technologies 6890 N Network GC System

with 5973 Network Mass Selective Detector). A 60-m long GS-GASPRO column with an internal diameter of 0.36 mm was used with helium as the carrier gas for the sample gas separation. For efficient sample separation, a temperature program was employed. The column temperature started at 35 °C and was held there for 3.50 min. The temperature was then increased linearly at a rate of 25 °C/min to a final temperature of 260 °C and held at this temperature for 3.00 min. The inlet temperature was held constant at 250 °C and the column flow rate was 4.6 mL/min.

The aqueous phase of the samples was analyzed using TEM, Raman spectroscopy, FTIR, and DLS. Due to experimental limitations (viscosity, cloudiness, and density, among others), the IL phase was only analyzed using Raman spectroscopy and FTIR. Raman spectra were obtained using a Renishaw model 2000 Raman spectrometer with a Melles Griot 35 mW HeNe laser at 633 nm. Spectra of both the IL and the water phases were recorded with the laser pointed perpendicular to the side of the sample vial. Infrared spectroscopy was performed on IL samples extracted during the experiments using a Bruker FTIR. Samples were prepared for FTIR analysis by mixing an aliquot of the sample with spectroscopy grade KBr using a mortar and pestle, and then using a press to form pellets. Any solid particles in the aqueous phase were imaged using a Phillips EM 200 transmission electron microscope operating at 100 keV. Sample preparation involved placing aliquots of the aqueous phase on carbon-coated copper grids and allowing them to air dry at room temperature. ImageJ software was used for the determination of the sizes of any particles observed. All DLS and independent particle size measurements were performed using a Malvern Zetasizer Nano-ZS, which has a

detection range of 0.3 nm – 10 µm. Readings of diameter by volume percent were recorded.

3.3 REFERENCES

1. D.A. Skoog, F.J. Holler, S.R. Crouch, Principles of Instrumental Analysis, 6th Ed., Thomson Brooks Cole, Belmont, CA (2007).
2. J.R. Ferraro, K. Nakamoto, Introductory Raman Spectrscopy, Academic Press, San Diego, CA (1994).
3. M.E. Orazem, B. Tribollet, Electrochemical Impedance Spectroscopy, John Wiley & Sons, New York, NY (2008).
4. P. Monk, Fundamentals of Electroanalytical Chemistry, D.J. Ando (Ed.), John Wiley & Sons, Chichester, UK (2001).
5. P.C. Trulove, R.A. Mantz, Electrochemical Properties of Ionic Liquids in Ionic Liquids in Synthesis, P. Wasserscheid, T. Welton (Eds.), Wiley-VCH Verlag GmbH & Co. KGaA, Weinhein, Germany (2008) pp. 141-174.
6. K.J. Daub, A Study of Gamma Radiation Induced Carbon Steel Corrosion, Ph. D. Dissertation, the University of Western Ontario, London, ON, (2013).
7. C. Berthomieu, R. Hienerwadel, Fourier Transform Infrared (FTIR) Spectroscopy, Photosynth. Res., 101 (2009) 157-170.
8. Handbook of Solid State Spectroscopy, D.R. Vij (Ed.), Springer Science + Business Media, LLC, New York, NY (2006).
9. D.L. Pavia, G.M. Lampman, G.S. Kriz, Introduction to Spectroscopy, 3rd Ed., Thomson Learning Inc., Toronto, ON (2001).
10. P.S. Turner, C.E. Nockolds, S. Bulcock, Electron Microscope Techniques for Surface Characterization in Surface Analysis Methods in Materials Science, D.J. O'Connor, B.A. Sexton, R.S.C. Smart (Eds.), Springer-Verlag, Heidelberg, Germany (2003) pp. 99-104.
11. Modern Techniques for Characterizing Magnetic Materials, Y. Zhu (Ed.), Kluwer Academic Publishers, Boston, MA (2005).
12. Dynamic Light Scattering: Applications of Photon Correlation Spectroscopy, R. Pecora (Ed.), Plenum Press, New York, NY (1985).
13. B.J. Berne, R. Pecora, Dynamic Light Scattering with Applications of Chemistry, Biology, and Physics, John Wiley & Sons, New York, NY (1976).
14. R. Pecora, J. Nanopart. Res., 2 (2000) 123-131.
15. J.F. Yang, T. Kondoh, K. Kan, Y. Yoshida, Nucl. Instrum. Methods Phys. Res., Sect. A, 629 (2011) 6-10.
16. J.F. Wishart, A.R. Cook, J.R. Miller, Rev. Sci. Instrum., 75 (2004) 4359-4366.
17. S.H. Chen, Annu. Rev. Phys. Chem., 37 (1986) 351-399.
18. P.S. Goyal, V.K. Aswal, Curr. Sci., 80 (2001) 972-979.
19. Z. Tun, J.J. Noel, D.W. Shoesmith, J. Electrochem. Soc., 146 (1999) 988-994.
20. M.P. Nieh, Z. Yamani, N. Kucerka, J. Katsaras, D. Burgess, H. Breton, Rev. Sci. Instrum., 79 (2008) 095102-1 - 095102-6.

Chapter 4. The Effect of Gamma Irradiation on Gas-Ionic Liquid Interfacial Stability

4.1 INTRODUCTION

Ionic liquids have a variety of properties that make them promising candidates for the purpose of nuclear fuel separations. The radiation stability of several IL classes with various cation and anion combinations have been studied using pulse radiolysis. This work, however, is limited to studies of pure IL systems [1-8]. Mostly confined to ammonium-based ILs (AILs), reports have shown that ILs are relatively radiation resistant, compared to water or organic solvents, because of the smaller probability of 'dry' electrons (produced by radiation impacts) escaping geminate or recombination reactions before they are solvated [5, 9].

This chapter examines the effects of irradiation on gas-IL systems and the implications of having an aerated or deaerated cover gas in contact with an IL. The IL phases were studied using electrochemical and spectroscopic techniques, while the gas phase was studied using chromatography. The study aims to give information on how the radiolytic decomposition of the ILs might be affected by the presence of an interface. A related study of IL radiolytical decomposition when in contact with an aqueous phase is discussed in Chapter 5.

One of the main concerns in this work was the impact of oxygen in the cover gas, a species that could potentially react with ILs or IL fragments. Hence experiments were conducted with aerated and deaerated systems to determine the impact of O_2 in the cover gas. We do not expect a substantial quantity of oxygen to dissolve in the IL phase and

any oxygen reactions with ILs or IL fragments should therefore occur predominantly at the gas-IL interface.

4.2 EXPERIMENTAL

4.2.1 Sample Preparation

The ionic liquids triisobutylmethylphosphonium tosylate (tosylate-IL), trihexyltetradecylphosphonium bis(trifluoromethylsulfonyl)amide (amide-IL), and trihexyltetradecylphosphonium bromide (bromide-IL) were purchased from Sigma-Aldrich, and were of the highest purity available (> 95%). (In our journal article concerning this work the chemical name of the amide-IL (trihexyltetradecylphosphonium bis(trifluoromethylsulfonyl)amide) was referred to as the imide-IL (trihexyltetradecylphosphonium bis(trifluoromethylsulfonyl)imide); since publication date the imide-IL was renamed to the amide-IL. Both notations are acceptable, but for consistency in this thesis we will use the amide-IL notation). Test vials were prepared by placing 2 mL of ionic liquid inside 10 mL test vials (Agilent Technologies). Test vials were purged for 20 minutes prior to irradiation (using syringes) with ultra-high purity argon (Praxair, 99.99% purity) to create a deaerated IL system, or purged with hydrocarbon-free air to create an aerated IL system.

4.2.2 Test Vial Irradiation

Test vials were irradiated in a ^{60}Co gamma cell that, at the time of experiments, provided a uniform absorbed dose rate of 6.4 kGy·h^{-1} (in water) within the vial volume.

Experiments were conducted over an extended period of time during which the vials were periodically inserted into the gamma cell for irradiation for 2 h periods. Experimental constraints did not allow even spacing of the irradiation periods, thus, records were kept for the total duration of the experiment (both the irradiation times and the accumulated irradiation time).

4.2.3 Sample Analysis

4.2.3.1 *Gas Chromatography-Mass Spectrometry (GC/MS)*

During the extended experiments, samples were extracted from the test vials at varying times immediately after completion of an irradiation period. The headspace samples were extracted and injected into the gas sampling port of a gas chromatograph-mass spectrometer (GC/MS), using a gas-tight syringe with a luer lock.

4.2.3.2 *Electrochemical Impedance Spectroscopy (EIS)*

Liquid samples were also extracted using a syringe and analyzed for their conductivity using a BioLogic Science Instruments MCS 200 conductivity instrument, using an electrochemical impedance method over the frequency range of 1 Hz to 200 kHz. The ratio of the gap to the area of the electrodes, or cell constant, was experimentally determined to be 7.5 cm^{-1}. Less than 1% standard deviation was observed from multiple measurements.

4.2.3.3 *Raman Spectrometry*

Raman spectra of the ILs were recorded using a Renishaw model 2000 Raman spectrometer. The laser excitation wavelength was 633 nm; the sample was set up with the laser pointed perpendicular to the sample vial.

4.3 RESULTS

Test vial irradiation was performed for durations up to 86 h. Although studies by other researchers on the γ-radiolysis of ILs containing imidazolium as the cation (but with different anions (PF_6^-, BF_4^-, NTf_2^-)) have shown considerable darkening of the IL with increasing absorbed radiation dose [10-12], we have not observed any darkening in the three ILs studied here, even after prolonged radiation exposures (up to 86 h).

4.3.1 Gas Chromatography Results

The gaseous species in the headspace above the IL phase after irradiation were identified using GC/MS. The major radiolysis products observed from the three different ionic liquids are listed in Table 4.1 along with the chemical structure diagrams of the ILs. The gas phase products observed include: isobutylene (C_4H_8) and toluene ($C_6H_5CH_3$) for the tosylate-IL, ethane (C_2H_6), hexafluoroethane (C_2F_6), fluoroform (CHF_3) and hexane (C_6H_{14}) for the amide-IL, and hexene (C_6H_{12}), and hexane (C_6H_{14}) for the bromide-IL. There were additional minor peaks in the GC/MS spectra that we were not able to identify. Inspection of the products listed above and the related IL structures shows that the products are formed by decomposition of one or both of the anionic and cationic

moieties of the ILs. Similar results were observed by Le Rouzo *et al*. [4] during γ-irradiation of an IL having the same amide anion as we have studied but a different cation. There were no noticeable changes in the gas phase product speciation with increased irradiation time suggesting that the radiolytic decomposition of the ILs reached a steady state quickly with continuous irradiation. Similar decomposition products were detected with both argon and air as cover gases, and none of the identified products contained oxygen. The absence of oxygen addition to the airborne species indicates that reactions at the gas-IL interface contribute very little to the net radiolytic decomposition of ILs.

Table 4.1 The chemical structures of the ionic liquids and their respective radiolytic decomposition products detected in the gas phase.

Ionic Liquid	**tosylate-IL**	**amide-IL**	**bromide-IL**
Chemical Structure	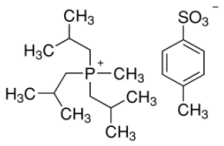	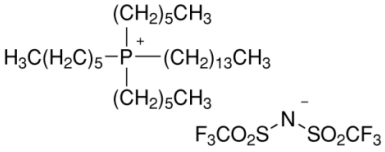	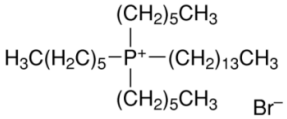
Gaseous Radiolytic Decomposition Products	isobutylene (C_4H_8) toluene ($C_6H_5CH_3$)	ethane (C_2H_6) hexane (C_6H_{14}) hexafluoroethane (C_2F_6) fluoroform (CHF_3)	hexane (C_6H_{14}) hexene (C_6H_{12})

4.3.2 Conductivity Results

The conductivity of the IL phase showed no significant change with irradiation and no dependence on the nature of the cover gas, Figure 4.1. The conductivity of the amide-IL, which was the highest of the three ILs, decreased only slightly during the first

few hours of irradiation before leveling off. These results are consistent with the observation by Berthon *et al*. who also reported minimal change in the conductivity of an IL with increasing irradiation time [3]. For all three ILs tested in this study, the nature of the cover gas had no measurable effect on the conductivity, indicating that very little oxygen reacted with IL components or radiation fragments in the IL phase, since the conductivity can be sensitive to the presence of small quantities of impurities. The absence of oxygen reactions in the IL phase is also consistent with the low quantities of airborne decomposition species observed by the GC/MS analysis.

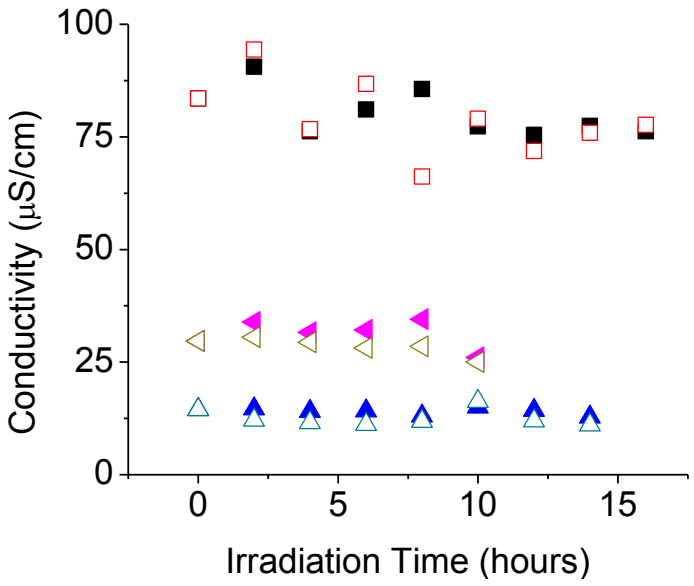

Figure 4.1 Conductivity of ionic liquids in contact with a gas phase as a function of irradiation time:■ □, amide-IL, ▲ △, bromide-IL, and ◀ ◁,tosylate-IL. The solid symbols (■, ▲, ◀) and the open symbols (□, △, ◁) are the data obtained from the ILs in contact with air and Ar, respectively.

4.3.3 Raman Spectroscopy

Raman spectroscopy was performed before and after 8 h of irradiation for the amide and bromide-ILs, Figure 4.2. (Spectra for the tosylate-IL was not collected as ILs must be hydrophobic for our intended industrial application; the tosylate-IL is hydrophilic.) No additional peaks or changes in the relative intensities of the sharp, well-defined peaks were observed after irradiation. Both the Raman spectra and conductivity measurements indicate that the ILs, whether in contact with air or argon are quite radiation resistant.

(a)

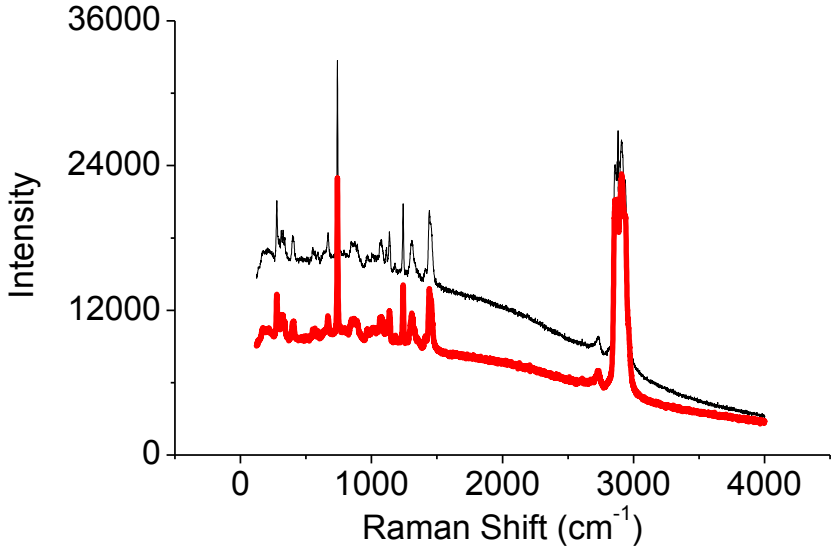

(b)

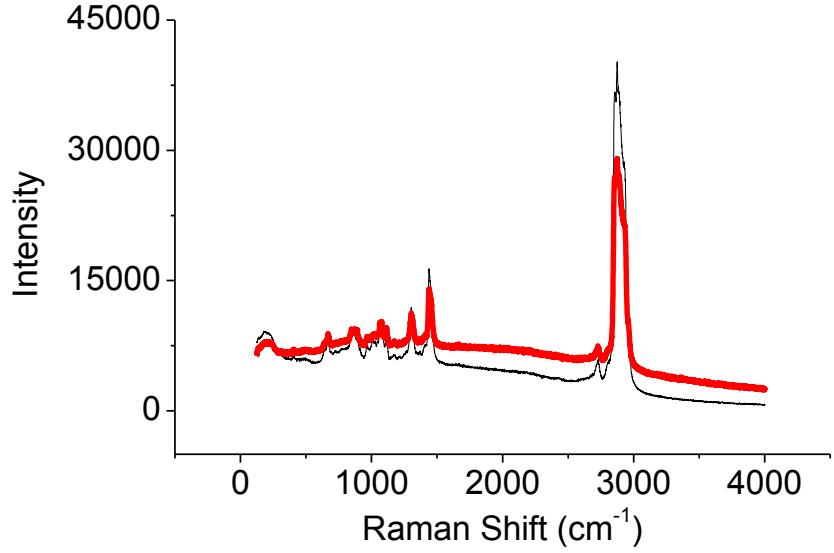

Figure 4.2 Raman spectra of the IL samples in contact with Ar before (thinner lines) and after 8 h irradiation (thicker lines): (a) amide-IL and (b) bromide-IL.

4.4 DISCUSSION

4.4.1 Effect of Radiation on the Gas/IL Biphasic Systems

The effects of γ-irradiation on our gas/IL systems are consistent with our current understanding of the interaction of ionizing radiation with matter, as discussed in section 2.4. In the systems that we studied, the radiation chemistry of the gas phase (due to its low density) was negligible. Changes in the gas phase chemistry would arise as the result of a liquid-to-gas-phase transfer of volatile species [13]. Indeed, the small amounts of gaseous products observed in the headspace in our tests were the volatile organic compounds that would be expected to arise from the radiolytic fragmentation of the ILs (Table 4.1). For example, the hexane observed in the gas phase (vapor pressure at room temperature of 151 mm Hg [14]) is attributed to the separation of a 6-carbon alkyl chain from the amide or bromide IL cation.

The presence of oxygen in the cover gas in contact with an IL had very little impact on the radiolytic gas species observed, the liquid conductivities, or the Raman spectrum of the IL phase. Being a good radical scavenger, oxygen should react readily with any organic radicals created by radiolysis of the ILs to form ketones and aldehydes (that are relatively volatile). As we do not expect a substantial quantity of oxygen to dissolve in the IL phase, any such oxygen reactions with IL decomposition products would occur predominantly at the gas-IL interface. The absence of any oxygenated species in the gas-phase strongly suggests that radiation-induced reactions of organic radicals with O_2 at the gas-IL interface region are negligible.

The Raman spectra also show no evidence of the production of oxygenated species in the IL phase. This result is consistent with little net radiolytic decomposition

of the IL. Although the homogeneous reaction kinetics of solvated electrons and other primary radiolytic products in the IL phase have not been specifically studied, the small yield of solvated electrons and the strong Coulombic field in the IL phase [1] suggests that the net build-up of radiolytic products during long-term radiolysis should be small. As described in section 4.3.2, there was only a small decrease in the conductivity of the amide-IL due to irradiation. Since small amounts of organic compounds dissolved in an IL can have a big impact on the IL conductivity, particularly for a highly viscous IL, this is evidence that the amount of radiolytic decomposition is very small. Hence it is not surprising that we see no evidence of this in the Raman spectra.

4.5 CONCLUSIONS

The effect of radiation on ILs in contact with a gas phase was studied under both aerated and deaerated conditions. Three phosphonium-cation-based ionic liquids, trihexyltetradecylphosphonium bis(trifluoromethylsulfonyl)amide, triisobutylphosphonium tosylate, and trihexyltetradecylphosphonium bromide were studied. All of the ILs exhibited very good radiation resistance to γ-radiation.

Gamma irradiation does not induce substantial chemical decomposition of the IL molecules into smaller fragments. The gaseous species observed in the headspace after irradiation are small volatile organic compounds that are formed in the IL phase via radiolytic decomposition of the ionic liquid molecules. The radiation stability of the ILs in contact with air indicates that interfacial reactions of O_2 with organic radicals that form from radiolysis of the ILs are not important.

4.6 REFERENCES

1. J. Grodkowski, P. Neta, J. Phys. Chem. A, 106 (2002) 5468-5473.
2. D. Allen, G. Baston, A.E. Bradley, T. Gorman, A. Haile, I. Hamblett, J.E. Hatter, M.J.F. Healey, B. Hodgson, R. Lewin, K.V. Lovell, B. Newton, W.R. Pinter, D.W. Rooney, D. Sanders, K.R. Seddon, H.E. Sims, R.C. Thied, Green Chem., 4 (2002) 152-158.
3. L. Berthon, S.I. Nikitenko, I. Bisel, C. Berthon, M. Faucon, B. Saucerotte, N. Zorz, P. Moisy, Dalton Trans., (2006) 2526-2534.
4. G. Le Rouzo, C. Lamouroux, V. Dauvois, A. Dannoux, S. Legand, D. Durand, P. Moisy, G. Moutiers, Dalton Trans., (2009) 6175-6184.
5. J.F. Wishart, P. Neta, J. Phys. Chem. B, 107 (2003) 7261-7267.
6. D. Behar, P. Neta, C. Schultheisz, J. Phys. Chem. A, 106 (2002) 3139-3147.
7. J. Grodkowski, P. Neta, J.F. Wishart, J. Phys. Chem. A, 107 (2003) 9794-9799.
8. I.A. Shkrob, S.D. Chemerisov, J.F. Wishart, J. Phys. Chem. B, 111 (2007) 11786-11793.
9. J. Wishart, Radiation Chemistry of Ionic Liquids: Reactivity of Primary Species in Ionic Liquids as Green Solvent: Progress and Prospects, R.D. Rogers, K.R. Seddon (Eds.), ACS Symposium Series, Oxford University Press, Washington, DC, (2003) pp. 381-396.
10. L. Yuan, J. Peng, L. Xu, M. Zhai, J. Li, G. Wei, Radiat. Phys. Chem., 78 (2009) 1133-1136.
11. M.Y. Qi, G.Z. Wu, S.M. Chen, Y.D. Liu, Radiat. Res., 167 (2007) 508-514.
12. M.Y. Qi, G.Z. Wu, Q.M. Li, Y.S. Luo, Radiat. Phys. Chem., 77 (2008) 877-883.
13. P.A. Yakabuskie, J.M. Joseph, J.C. Wren, Radiat. Phys. Chem., 79 (2010) 777-785.
14. S. Weiguo, A.X. Qin, P.J. McElroy, A.G. Williamson, J. Chem. Thermodyn., 22 (1990) 905-914.

Chapter 5. The Effects of Gamma Radiation on Interfacial Reactions and Transport Processes of Water-Ionic Liquid Systems: Comparison of Bromide and Amide Ionic Liquids

5.1 INTRODUCTION

A separation technology based on the transfer of chemical species through complexation at water/IL interfaces is being developed for nuclear fuel reprocessing and waste stream reduction applications. The separation efficiency of the biphasic system will depend on many parameters including the aqueous oxidation state of the targeted metal ion, interfacial mixing and transport rates, metal-ligand complex formation efficiencies at the water/IL interface, and complex stability in the bulk phases. In the intended application, a water/IL system will be exposed to continuous ionizing radiation that can strongly influence the chemical state of the system and the chemical parameters affecting the separation efficiency of the system. Studies on the effects of radiation on the stability of ILs are rare and have been limited to studies of pure IL phases [1-7]. These studies, mostly confined to ammonium-based ILs (AILs), have shown that ILs are relatively radiation resistant, compared to water or organic solvents, because of the smaller probability of 'dry' electrons, produced by radiation impact on the IL molecules, escaping geminate or recombination reactions before they are solvated [5, 8]. However, how long-term irradiation will affect water/IL biphasic systems and, in particular, the physical and chemical parameters affecting the separation efficiency in these systems have not been studied.

This study investigates the radiation-induced physical and chemical changes in water/IL systems that are exposed to steady-state gamma irradiation. For comparative purposes, two phosphonium-based ILs, which vary considerably in their viscosity, conductivity and miscibility with water, were examined: (a) trihexyltetradecylphosphonium bis(trifluoromethylsulfonyl)amide, and (b) trihexyltetradecylphosphonium bromide. Their chemical structures are shown in Table 5.1. For convenience, these compounds will be referred to further as the amide-IL and the bromide-IL, respectively. Published work on this data refers to the amide-IL as the imide-IL; as noted in chapter 4, these notations are interchangeable. For consistency we will refer to it as the amide-IL.

Table 5.1 The chemical structures of the ionic liquids investigated.

Ionic Liquid	amide-IL	bromide-IL
Chemical Structure	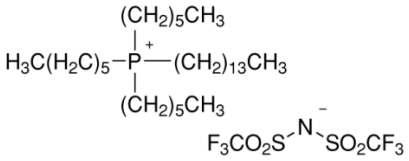	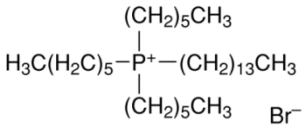

The radiation stability of a water/IL system was not studied for the tosylate-IL (see chapter 4) because this IL is relatively miscible with water; only the relatively immiscible bromide and amide-ILs were studied with water. The bromide and amide-ILs have the same cations, but different anions, and, of the two ILs, the amide-IL has the lower surface tension, lower viscosity, and higher hydrophobicity [9].

5.2 EXPERIMENTAL

5.2.1 Sample Preparation

The two ionic liquids were purchased from Sigma-Aldrich and were of the highest purity available (> 95%). The purity of the ILs and the absence of any moisture in the ILs were verified using proton nuclear magnetic resonance (^{1}H NMR), electrospray ionisation-mass spectrometry (ESI-MS) and differential scanning calorimetry (DSC) analysis. The water used in this study was purified by a NANOpure Diamond UV ultrapure water system (Barnstead International) and had a consistent resistivity of 18.2 MΩ cm. Water/IL samples composed of 2 mL of water and 2 mL of ionic liquid were placed inside 10 mL vials (Agilent Technologies) and sealed with aluminum crimp caps with PTFE/silicone septa. De-aerated samples were prepared by purging the contents of the sealed vials with ultra-high purity argon (Praxair, 99.99% purity), using syringes, for 20 minutes prior to irradiation. Aerated samples were prepared by purging with hydrocarbon-free air in the same manner.

5.2.2 Sample Irradiation

Irradiation was conducted in a ^{60}Co gamma cell (MDS Nordion) that provided a uniform absorbed dose rate of 6.4 kGy·h^{-1} (in water) within the sample volume. The experiments were conducted over a long period of time (up to 600 h), during which the samples were periodically inserted into the gamma cell for irradiation for 2 h periods. These irradiation periods were not evenly spaced, owing to other experimental

constraints. Records were kept of the total duration of the experiment, the irradiation times and the accumulated irradiation time.

5.2.3 Sample Analysis

5.2.3.1 *Gas Chromatography-Mass Spectrometry (GC/MS)*

Samples were extracted from the test vials at varying times during an extended experiment (generally immediately after completion of an irradiation period). For the gas phase analysis, the headspace samples were extracted using a gas-tight syringe with a Luer lock (Agilent Technologies) and injected into the gas sampling port of a gas chromatograph-mass spectrometry detector (Agilent Technologies 6890N Network GC System and 5973 Network Mass Selective Detector).

5.2.3.2 *Electrochemical Impedance Spectroscopy (EIS)*

The conductivities of the IL and water phases were measured using an electrochemical impedance method with a BioLogic Science Instruments MCS 200 conductivity instrument that applies a sinusoidal potential wave and measures the cell impedance as a function of frequency over the range of 1 Hz to 200 kHz. The conductivity cell consisted of a quartz cuvette with two parallel electrodes made of glassy carbon. The cell constant, the ratio of the gap to the area of the electrodes, was experimentally determined to be 7.5 cm^{-1} using standard solutions of KCl (for which the conductivity is known). The standard deviation in the measurements was calculated to be less than 1% from multiple measurements.

5.2.3.3 *Raman Spectroscopy*

Raman scattering measurements were performed using a Renishaw model 2000 Raman spectrometer with a laser excitation wavelength of 633 nm. Spectra of both the IL and water phases were recorded with the laser pointed perpendicular to the side of the sample vial.

5.2.3.4 *Nuclear Magnetic Resonance Spectroscopy (NMR)*

Nuclear magnetic resonance (NMR) spectra were recorded for both original IL and irradiated IL samples in a deuterated acetone solvent using a Varian INOVA 400 MHz spectrometer. All ^{1}H peaks were referenced to a residual acetone peak (acetone d6 = 2.05).

5.2.3.5 *Transmission Electron Microscopy*

Transmission electron microscopy was performed on samples from the aqueous phase of the test vial. Samples were imaged, using a Philips EM 200 transmission electron microscope (TEM) with the electron microscope operating at 100 keV, to investigate whether visible cloudiness was associated with the formation of micelles. TEM samples were prepared by aliquoting small amounts from the aqueous phase onto a carbon-coated copper grid and allowing the grid to air dry at room temperature. Particle diameters for a statistically relevant number of particles (> 100) were estimated using ImageJ software.

5.2.3.6 *Dynamic Light Scattering*

Independent particle-size measurements were performed using light scattering on a Malvern Zetasizer Nano-ZS, which has a detection range of 0.3 nm – 10 μm. Readings of diameter by volume percent were recorded. Similar measures were not performed on the cloudy IL phase because the viscosity and density of the emulsion formed during the tests mad TEM imaging and light-scattering particle size analysis impossible.

5.3 RESULTS

Upon contact with water, the bromide or amide-ILs initially form a distinct phase, a separate layer under the water at the bottom of the sample vial. However, even without irradiation, a third, cloudy layer developed at the water/IL interface. This cloudy layer expanded downwards from the interface as contact time increased and eventually (after > 3 d) converted the entire IL phase into a cloudy phase which we have termed an emulsion (Figure 5.1). Irradiation accelerated the formation of this emulsion; the entire IL phase became cloudy after only 12 h. The shape of the water/IL interface also changed with time (also see Figure 5.1). This reflects changes in the surface tensions at the interface. The development of the emulsion over time was followed by conductivity measurements and Raman spectroscopy.

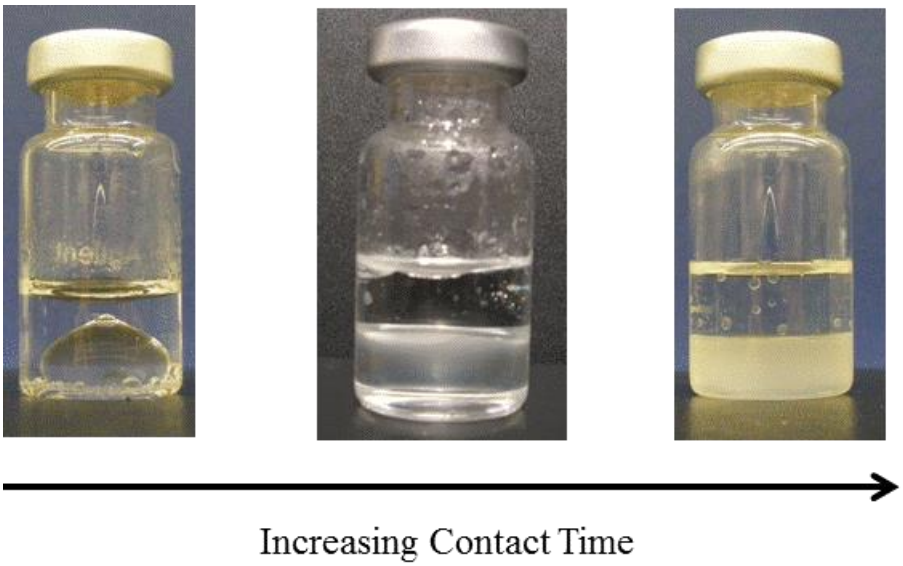

Figure 5.1 Photographs of the water/amide-IL system at increasing contact times showing the development of an emulsion layer. The bottom layer is the IL layer and the top water layer.

5.3.1 Electrochemical Impedance Spectroscopy

The time evolution of the conductivities of both the IL and water phases of the irradiated samples are compared with the conductivities of the un-irradiated samples in Figure 5.2 for the amide-IL and in Figure 5.3 for the bromide-IL. Note that the total irradiation time shown on the upper abscissa scales is non-linear while the total contact time shown on the lower abscissa scales of Figure 5.2 and Figure 5.3 is linear.

(a)

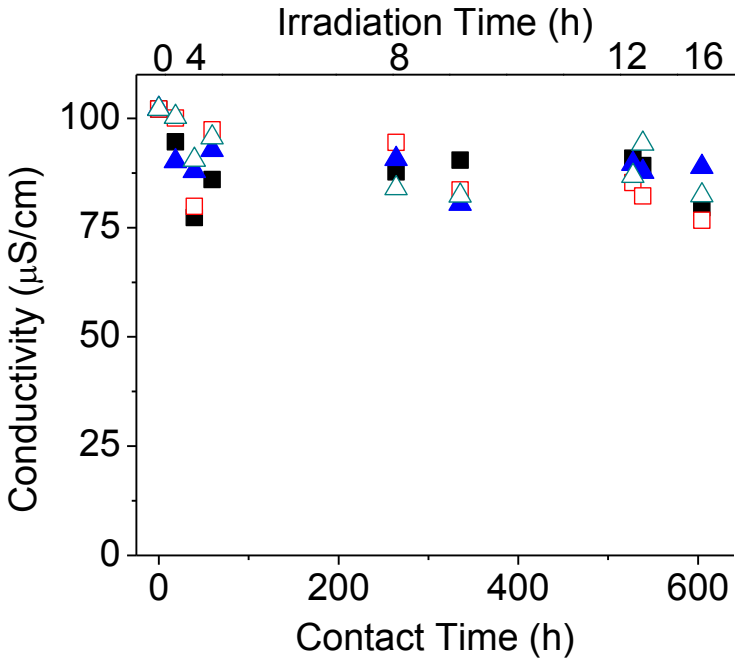

(b)

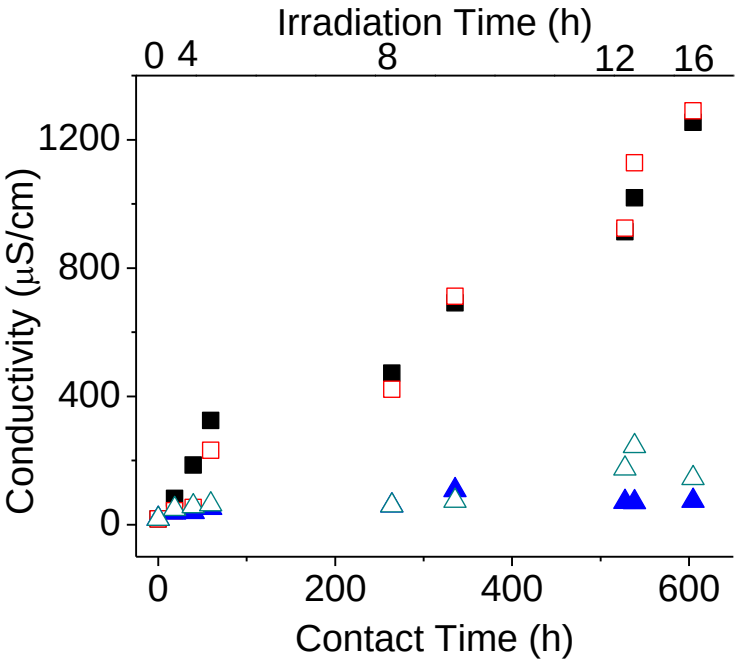

Figure 5.2 Conductivity as a function of total irradiation time (the upper abscissa scale – non-linear) and total contact time (the lower abscissa scale) observed for the water/amide-IL samples: (a) the IL conductivity and (b) the water conductivity. The different symbols represent data obtained under different conditions: ■ aerated and irradiated, □ deaerated and irradiated, ▲ aerated and un-irradiated, and △ deaerated and un-irradiated.

(a)

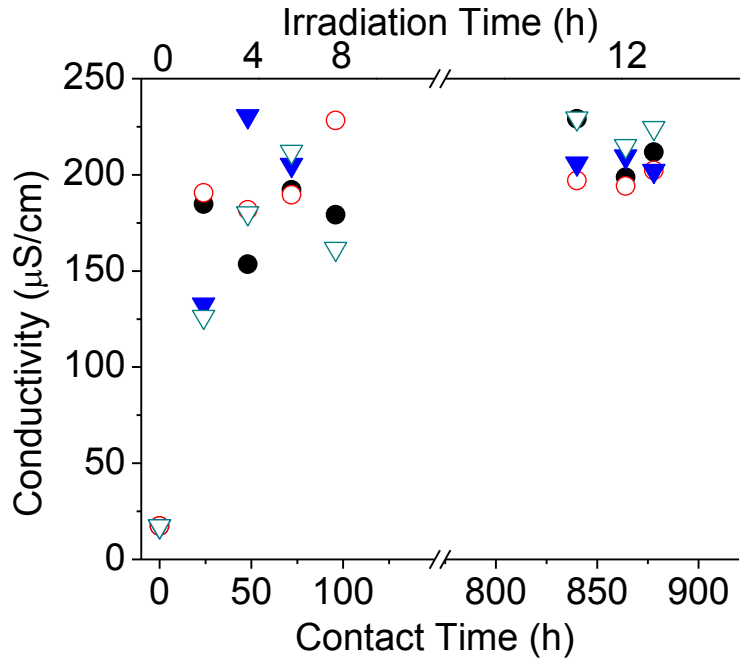

(b)

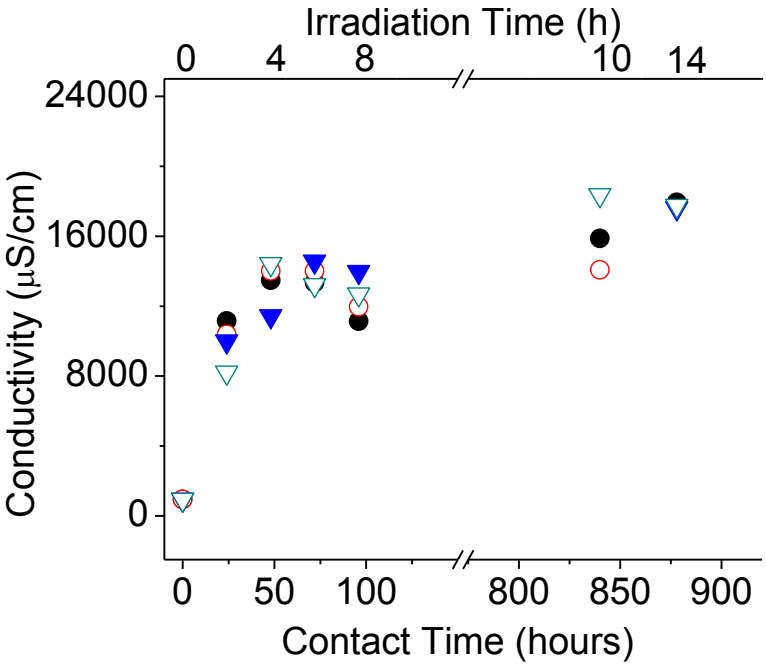

Figure 5.3 Conductivity as a function of total irradiation time (the upper abscissa scale – non-linear) and total contact time (the lower abscissa scale) observed for the water/bromide-IL samples: (a) the IL conductivity and (b) the water conductivity. The different symbols represent data obtained under different conditions: ●aerated and irradiated, ○ deaerated and irradiated, ▼ aerated and un-irradiated, and ▽deaerated and un-irradiated.

The amide-IL layer conductivity was initially high and did not change significantly with increasing contact time with water; if anything, contact with water slightly reduced the IL conductivity (Figure 5.2a). There were no measurable differences between the IL layer conductivities of irradiated and un-irradiated samples. Comparison of Figure 4.1 from Chapter 4 with Figure 5.2a also shows that the conductivity of the IL layer did not depend on whether the IL phase was in contact with a gaseous or aqueous phase during irradiation. For the bromide-IL-water system, the conductivities of both the IL and water layers increased rapidly within the first two hours of contact, but soon reached pseudo-steady state (increasing very slowly thereafter), Figure 5.3. There was no measurable difference in the water or IL conductivities of the irradiated and un-irradiated samples for a given contact time.

For an IL with a relatively higher initial conductivity (the amide-IL), interfacial ion transfer was better followed by monitoring the conductivity of the water layer. The water conductivity is initially very low, and hence, a small change can be more easily observed. Without irradiation, a negligible increase in water conductivity was observed (Figure 5.2b) indicating that the interfacial transfer of the cations and anions of the amide-IL molecules from the IL phase to the water phase is very slow. Gamma-irradiation of water alone did not increase the water conductivity (Figure 5.4). However, γ-irradiation significantly increased the conductivity of the water in contact with the amide-IL, presumably because γ-irradiation accelerates the interfacial transfer of charged species from the IL phase to the water phase in this system. Aeration of the water had no significant impact on the change in conductivity in the water/amide-IL system.

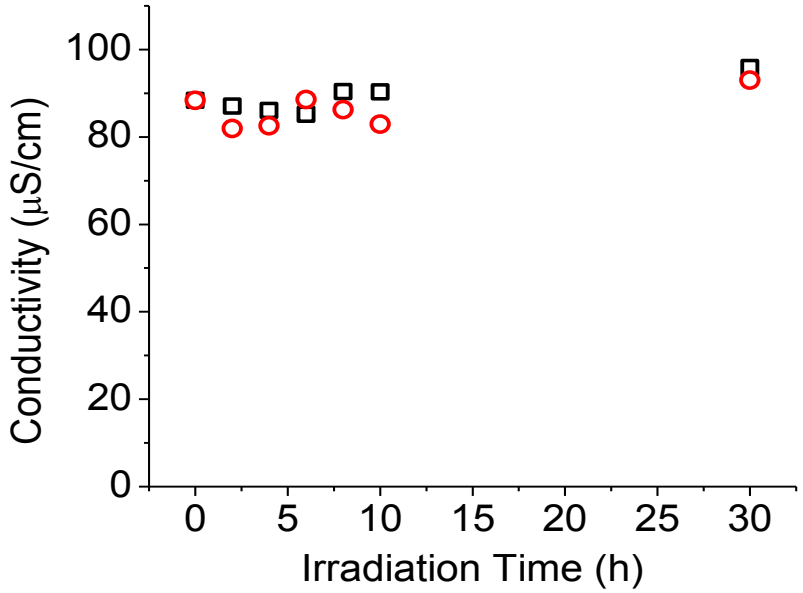

Figure 5.4 Pure water conductivity as a function of irradiation time. The different symbols represent ○ aerated and □ deaerated water.

5.3.2 Raman Spectroscopy

The Raman spectra of the IL and water layers were also taken as a function of time. In Figure 5.5 and Figure 5.6, only the spectra from the un-irradiated and 8-h irradiation cases are shown for ease in comparison of the water/amide-IL and water/bromide-IL systems. The time-dependent behaviour of the spectra for the water/amide-IL system is shown in Figure 5.7, Figure 5.8, and Figure 5.9. For both water/IL systems, γ-irradiation induced few changes in the positions or relative intensities of the sharp, well-defined peaks in the IL phase Raman spectra. One exception was a sharp well-defined peak that was observed at ~ 1700 cm^{-1} in the amide-IL phase spectra taken at longer contact times (> 3 d), see Figure 5.8 and Figure 5.9 (this is discussed further in section 5.4.1). However, γ-irradiation had a significant effect on the intensity

of the broad background band of the IL phase spectra. Irradiation decreased its intensity for the amide-IL, but increased its intensity for the bromide-IL (compare Figure 5.5a and Figure 5.6a). The trends are similar to those observed for the ILs in contact with a gas phase (Figure 4.1), but were much more pronounced when the ILs were in contact with water.

(a)

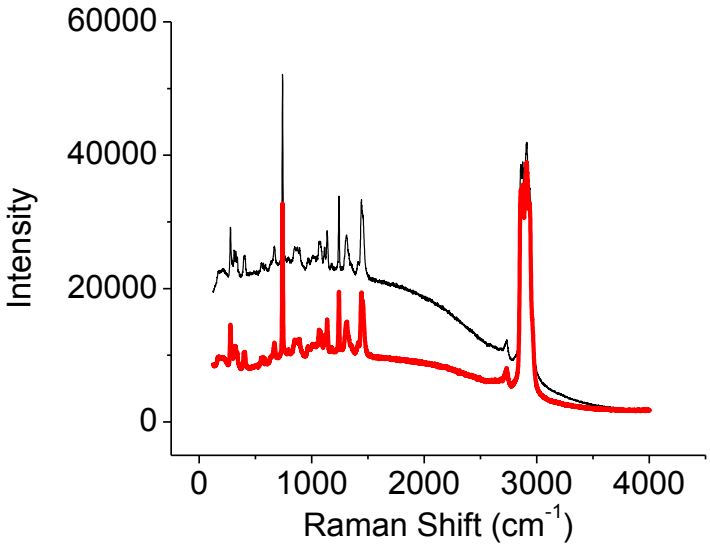

(b)

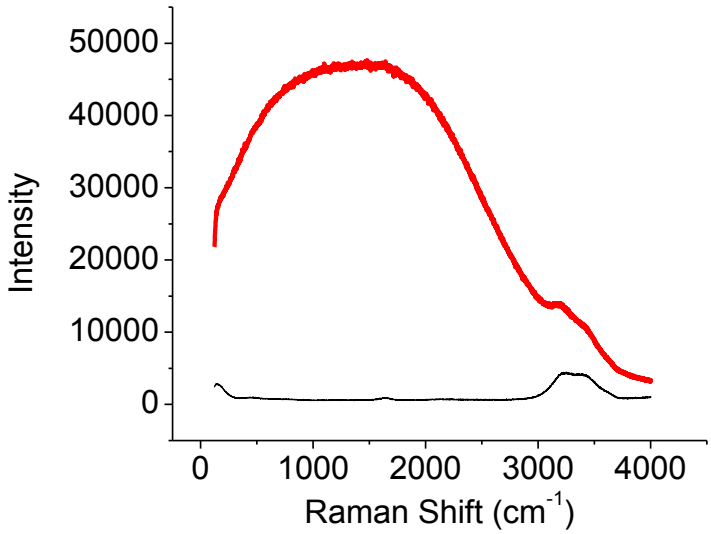

Figure 5.5 Raman spectra of un-irradiated (thinner lines) and 8-h irradiated (thicker lines) water/amide-IL samples: (a) the IL spectra and (b) the water spectra.

(a)

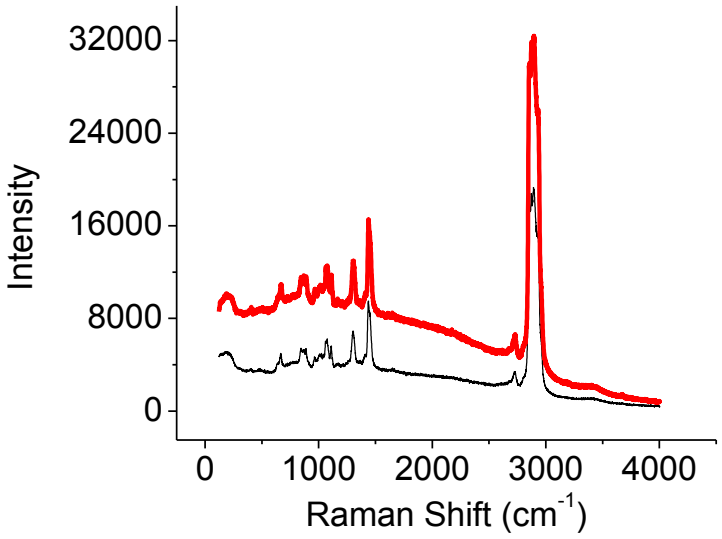

(b)

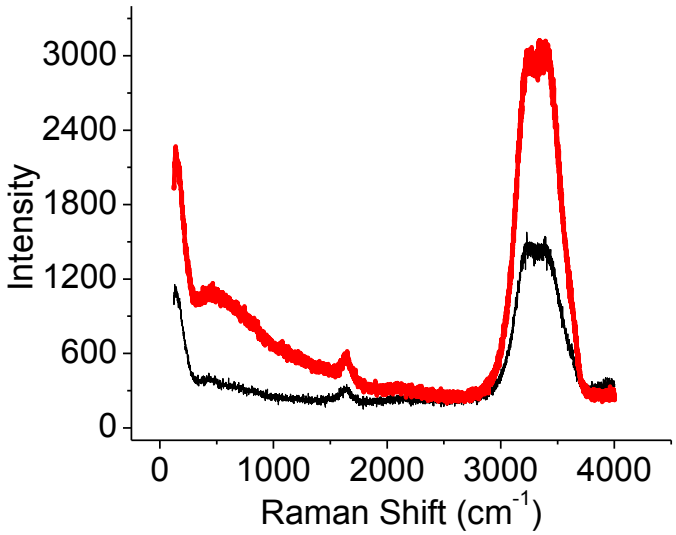

Figure 5.6 Raman spectra of un-irradiated (thinner lines) and 8-h irradiated (thicker lines) water/bromide-IL samples: (a) the IL spectra and (b) the water spectra.

Time dependent changes in the IL-phase Raman spectra due to irradiation were chronologically matched with the changes in the water-phase Raman spectra. For both ILs, the Raman spectra of the respective water layers consisted of similar broad peaks.

However, for the water/amide-IL system, a decrease in the broad band intensity of the IL-phase spectrum accompanied an increase in the broad band intensity of the water-phase spectrum (see Figure 5.5a and Figure 5.5b). On the other hand, for the water/bromide-IL system, the broad band intensities of both the IL and water phase spectra increased (Figure 5.6a and Figure 5.6b). Additionally, in the water/bromide-IL system, only one broad band, centered at ~ 500 cm^{-1}, was observed, Figure 5.6, whereas for the water/amide-IL system two broad peaks, one at ~ 500 cm^{-1} and a second at ~ 2000 cm^{-1}, were observed to coalesce in Figure 5.5.

For the water/amide-IL system, the time-dependent behaviour of the broad band intensity at longer γ-irradiation times was explored in detail. The broad band intensity of the IL-phase spectrum initially decreased, but then increased when the irradiation time was longer than 8 h, Figure 5.7a. The water phase spectrum, however, did not show this behaviour. The broad band intensity continually increased, Figure 5.7b. The time-dependent behaviour of the broad band intensities of both the IL and water spectra at longer times for the water/amide-IL system were similar to those observed for the water/bromide-IL system. One key difference between the two water/IL systems was that the Raman band in the amide-IL case consisted of two bands, which were discernible over long times, Figure 5.7b, while for the bromide-IL case there was only one band, as described above. The simultaneous increases in the band intensities of both the IL and water phases are attributed to increased biphasic mixing, which occurred much faster with irradiation than without. The initial decrease in the broad band intensity of the IL-phase spectrum observed for the water/amide-IL system is attributed to the fact that γ-irradiation was able to promote ion transfer from the IL to water phase (which led to

higher water conductivity), but not able to promote the formation of an emulsion in the IL layer. This leads to effective biphasic mixing in the more viscous and hydrophobic water/IL system, as discussed later in section 5.4.1.

(a)

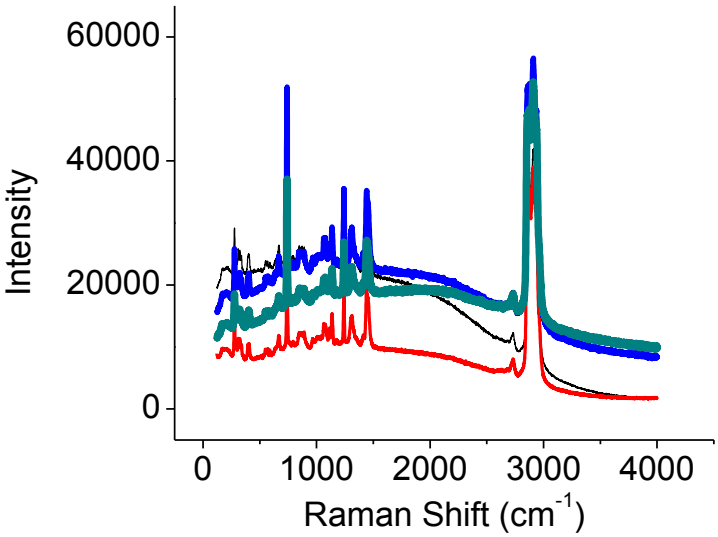

(b)

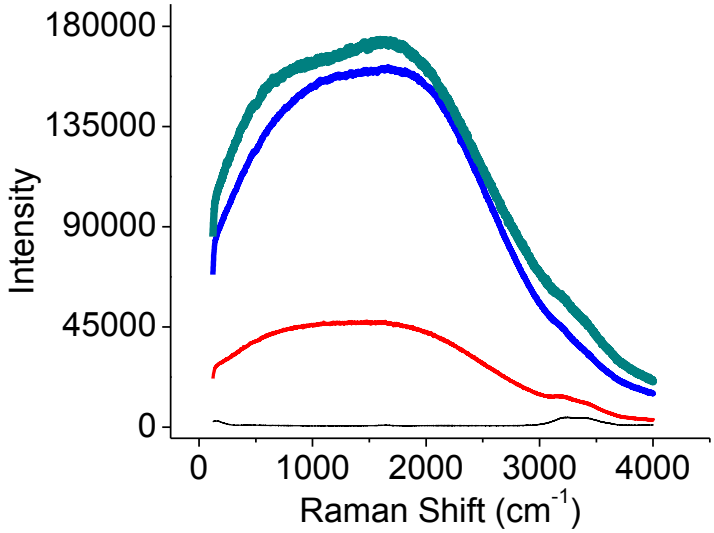

Figure 5.7 Raman spectra of the water/amide-IL samples with no irradiation and taken immediately following irradiation for 6 h (red), 12 h (blue), and 18 h (green) (from the thinnest line to the thickest line): (a) the IL spectra and (b) the water spectra.

The IL and water phase mixing was further explored by allowing un-irradiated and 6-h irradiated water/amide-IL samples to stand for 14 d. After this prolonged time the broad band intensities of both the IL and the aqueous phase spectra increased, as

shown in Figure 5.8 for the un-irradiated and in Figure 5.9 for the 6-h irradiated water/amide-IL samples. Also shown in these figures are the difference spectra that are obtained by subtracting the spectra of samples before contact from spectra taken after 14 d of contact. For a given water/IL system, the broad bands in the difference spectra had the same shape (with minor variations in peak heights), independent of whether the spectrum was obtained from the IL or water phase. However, the broad bands in the difference spectra of the un-irradiated and 6-h irradiated samples were very different, indicating that the origins of the broad bands are different in un-irradiated and irradiated systems.

A well-defined peak at ~ 1700 cm^{-1} in the water spectra of the water/bromide-IL system (Figure 5.5b), also appeared in the IL-phase spectra of the amide-IL (for both un-irradiated and irradiated cases) when the amide-IL had been in contact with water for prolonged times (see Figure 5.8a and Figure 5.9a). This peak is attributed to an adsorbed (or surface) water layer [10, 11], and further suggests that significant phase mixing has occurred.

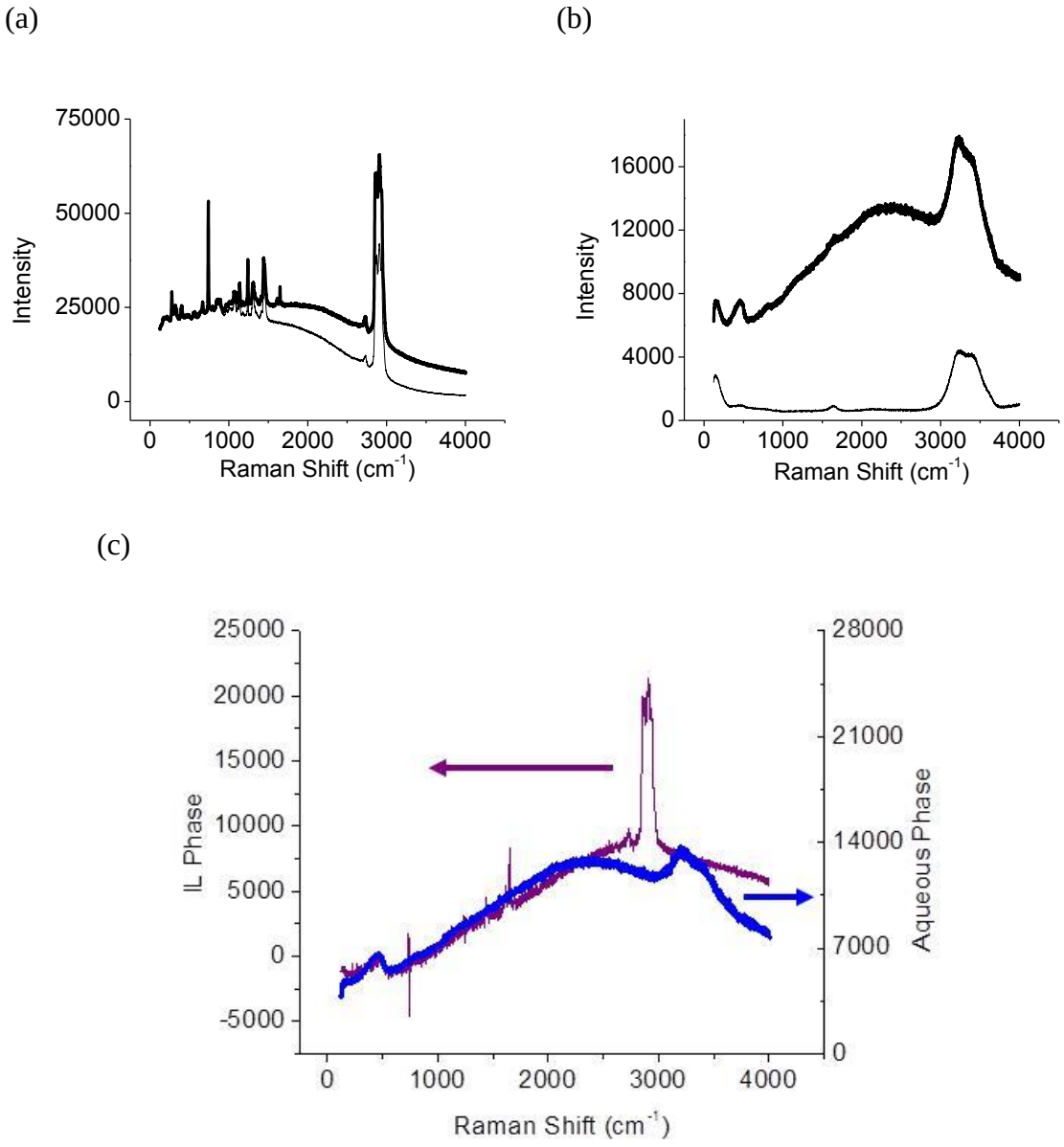

Figure 5.8 Raman spectra of un-irradiated water/amide-IL samples immediately after contact (thinner lines) and after 14-d contact (thicker lines): (a) the IL spectra, (b) the water spectra, and (c) the difference spectra (14-d contact – 0-d contact) of both the IL and aqueous phases.

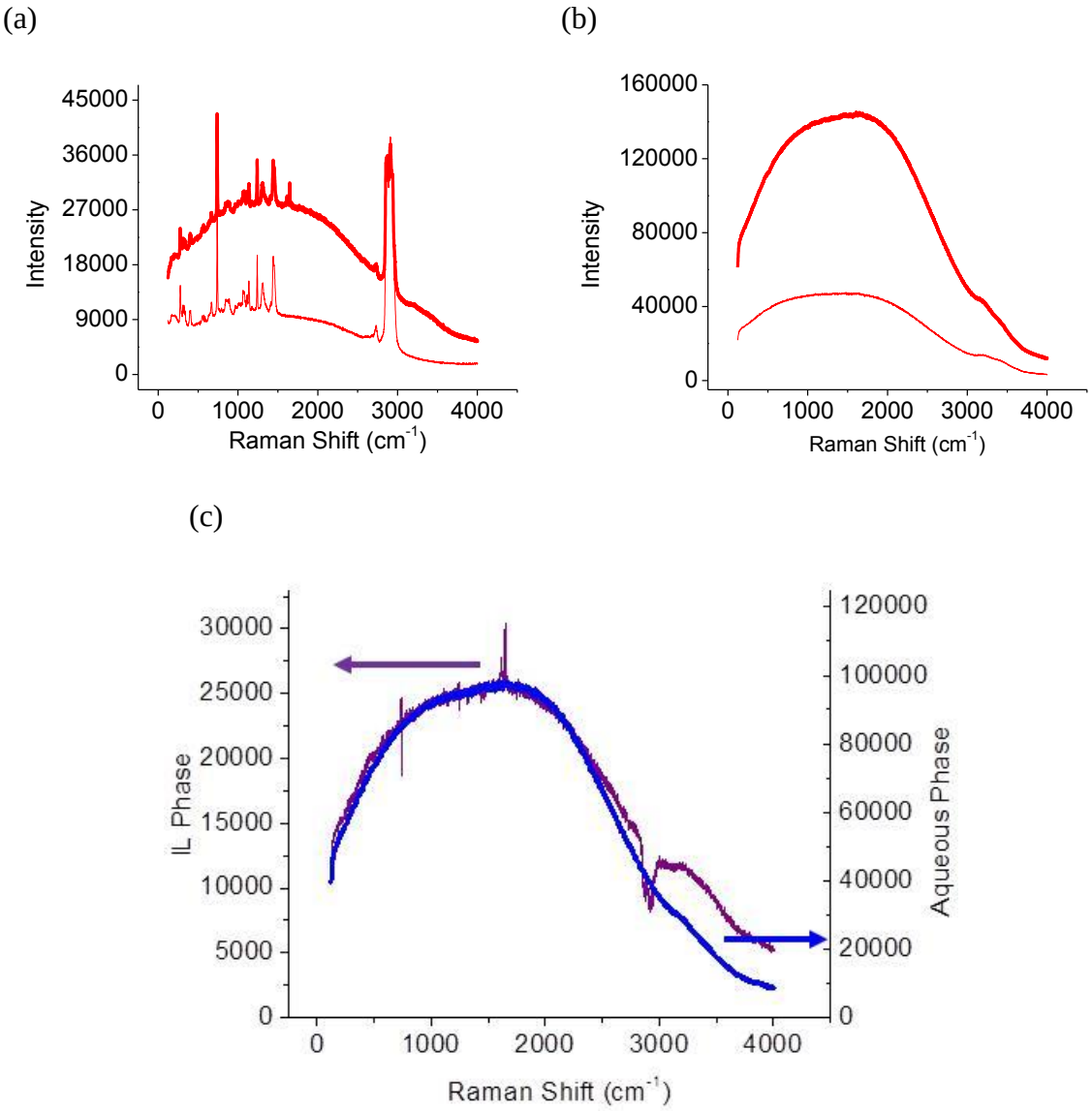

Figure 5.9 Raman spectra of 6-h irradiated water/amide-IL samples immediately after contact (thinner lines) and after 14-d contact (thicker lines): (a) the IL spectra, (b) the water spectra, and (c) the difference spectra (14-d contact – 0-d contact) of both the IL and aqueous phases.

5.3.3 Dynamic Light Scattering

The development of the broad bands in the Raman spectra could be due to the presence of colloidal particles. The presence and sizes of colloidal particles in the aqueous phase of the irradiated and the un-irradiated samples were determined by the

light scattering technique described in section 5.3.3 and the results are listed in Table 5.2. The observed particles in the un-irradiated sample have a bimodal distribution. Approximately half are about 51 nm and half are about 150 nm in size. It is not clear what causes the bi-modal distribution, but the particles may be in various stages of formation or aggregation. The irradiated samples contained particles with relatively uniform size distributions. The average size of the colloid particles was much smaller, 12.5 ± 1.6 nm, for the shorter irradiation case ,and about the same size as the small particles seen in the un-irradiated case, 56 ± 33 nm, for the longer irradiation case. Also the larger particles in the 18 h irradiated case had a very broad distribution in comparison with the other cases.

Table 5.2 The diameter of particles in the aqueous phase and their by % volume of particles for an un-irradiated, and a 6-h and an 18-h irradiated amide-IL samples after being in contact for > 72 h, with the respective standard deviations.

Radiation Time	Diameter, nm (standard deviation)	% Volume
Un-irradiated	150.80 (38.56) 50.90 (8.56)	55.8 44.2
6 h	85.29 (10.86) 12.53 (1.592)	4.0 96.0
18 h	55.95 (33.09)	100.0

5.3.4 Transmission Electron Microscopy

To corroborate the light scattering results, TEM images of particles in water samples were obtained. The TEM images of samples of the aqueous layer that had been in contact with the IL layer for approximately 24 h without γ-irradiation are shown in Figure 5.10. The particles are of varying sizes and mostly spherical in shape. This is

consistent with the particles being micelles [12]. Some particles are oblong and they could be two or more micelles joined together. In Figure 5.10, the pattern observed in the background is due to the water evaporation from the carbon coated grid during sample preparation.

The TEM images were analyzed using ImageJ software to determine the particle size distribution. The sizes determined from the TEM images ranged from 30 nm to 120 nm (Figure 5.11) are in reasonably good agreement with sizes determined from the light scattering particle size analysis.

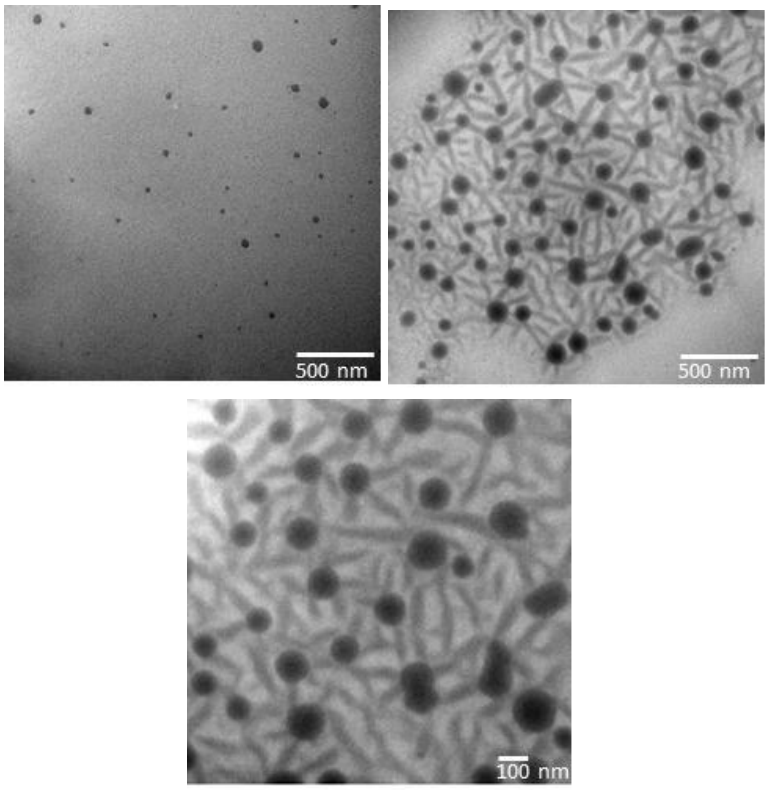

Figure 5.10 TEM images of the particles in the aqueous phase following 24 h of contact with the IL phase.

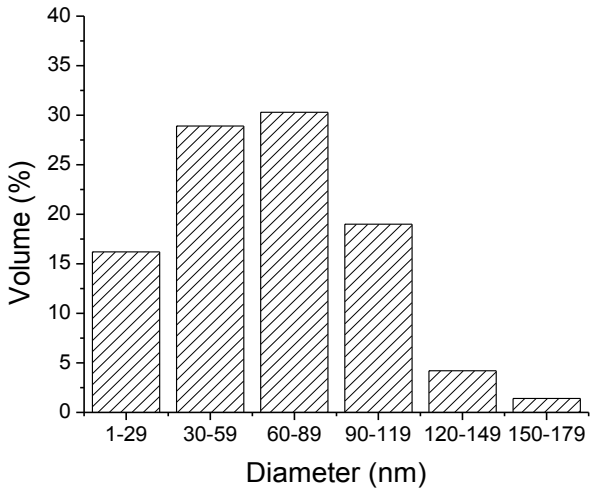

Figure 5.11 The diameter of the colloidal particles collected from the aqueous phase by % volume.

5.4 DISCUSSION

5.4.1 Effect of Radiation on Water/IL Systems

When not in contact with an IL, water, whether aerated or deaerated, does not exhibit increased conductivity due to irradiation, even for prolonged irradiation times (Figure 5.5). Accordingly, any changes in the conductivity of water in contact with the IL are the result of transfer of species from the IL phase to the water. Transfer of the bromide ion (from the bromide-IL) to the aqueous phase is expected to occur relatively easily owing to the hydrophilic nature of the bromide anion. Since HBr is a much stronger acid than water, the exchange OH^- and Br^- between the IL and aqueous phases would shift the acid base equilibrium in the water to a more acidic pH. Consequently, the anion exchange would also increase the total concentration of ions in the water phase and thereby increase its conductivity, as we have observed in Figure 5.3b. The simultaneous

increase in the bromide-IL phase conductivity is attributed to the fact that the IL phase gains water molecules, as we will discuss in section 5.4.1. These water molecules reduce the surface energy and the viscosity of the IL phase. The conductivities of both the aqueous and IL phases reach near steady state levels within 2 d, when the partitioning of the anions reaches phase equilibrium. Our conductivity measurements show that γ-irradiation has a negligible effect on the interfacial charge transfer in the water/bromide-IL system. This is likely because of the efficiency of the anion interfacial transfer that occurs in the absence of radiation.

For the water/bromide-IL system, the Raman spectra of both the bromide-IL and water phases show a broad background band, centered at ~500 cm^{-1}, that increased with time, Figure 5.5. This observation is attributed to an increase in the light scattering probability by colloidal particles or micelles. The increases in the background band intensities in the spectra were observed both with and without γ-irradiation. Since the increase was present without γ-irradiation, any additional increase due to irradiation was difficult to observe for this system, just as changes in conductivity due to irradiation of this system were also difficult to observe.

For the water/amide-IL system, in the absence of irradiation, the transfer and exchange of anionic species between the amide-IL and water phases is slower because the amide-IL does not have an equivalent small mobile ion and, hence, the aqueous conductivity rises more slowly than in the water/bromide-IL system, Figure 5.2b. The smaller change in conductivity for the water/amide-IL system in the absence of radiation makes it easier to observe any conductivity changes caused by γ-irradiation of this system, Figure 5.2b. Note that the water conductivity of the water/amide-IL system, even

after 16 h irradiation, was still an order of magnitude lower than the conductivity of the water observed in the water/bromide-IL system, with or without irradiation.

For both the bromide and amide ILs, prolonged contact with water eventually converted the IL phase into a cloudy emulsion. Gamma-irradiation significantly accelerated the formation of this emulsion and this effect was particularly pronounced in the water/amide-IL systems. Emulsion formation in both the presence and the absence of radiation is indicative that mixing occurs readily between the two phases. To verify the movement of water into the IL phase, ^{1}H NMR spectroscopy was performed once the emulsion layer formed. After a prolonged contact period, the upper water layer was decanted from a test vial and a small sample of the emulsified IL phase was dissolved in deuterated acetone. The ^{1}H NMR spectrum contained signals consistent with the phosphonium ionic liquid as well as an unambiguous water peak at 2.86 ppm (the NMR spectra not shown). No other NMR peaks were observed and their absence is consistent with the presence of very low concentrations of the radiolytic decomposition products of the IL.

5.4.2 Radiation-Induced Micelle Formation

The light scattering analysis and TEM images show the presence of spherical particles. We characterize these particles as micelles. The formation of micelles, reverse micelles, and microemulsions have previously been observed for a variety of ionic liquids dissolved in water [13-16]. In ILs with long-tail hydrocarbon groups in their cation or anion moiety, the long alkyl chains can also give rise to the surfactant activity [13]. In this study, both the bromide and amide ILs have the same cation which includes long

alkyl groups. The formation of micelles explains the emulsification of the IL layer starting at the water/IL interface and expanding downwards for our water/IL systems (as shown in Figure 5.1). Jungnickel *et al.* [17] have shown that ILs dissolved in water can form micelles when the IL concentration reaches the critical micelle concentration (CMC). They also demonstrate that the CMC is a function of the type and concentration of impurities in the IL as well as the alkyl chain length in the IL moiety [16]. The amide and bromide-ILs examined in this study are highly hydrophobic and immiscible (particularly the amide-IL), and their CMCs are expected to be smaller than those reported for less miscible ILs [38-40]. We have not established the CMC values for the ILs studied here as the primary focus of this study was the radiation stability of the systems. Nevertheless, it is clear that there will be an IL concentration gradient at the water/IL interface and the IL concentration somewhere along this gradient is sufficiently high to promote micelle formation at or near the interface under our conditions.

As mentioned above, ion transfer between the amide-IL and water phases is expected to be slow. While the anion in the amide-IL monomer is more easily transferable to the water phase than the cation, and an exchange of amide-IL anions and water anions (i.e., OH^-) occurs to some extent, the interfacial ion transfer will be somewhat limited by even slower cation exchange. The result of this slow migration will be the creation of both concentration and charge gradients in the interfacial region that persist for some time. This results in a concentration gradient of IL monomers through the water/IL interfacial region, with the anions in the water phase pulling cations away from the interfacial region and into the water phase. The concentration of the IL monomers in the water phase will increase with time and eventually reach the CMC near

the interface, and micelles can begin to form. The hydrocarbon radiolytic decomposition products of the ILs may provide loci for the formation of the micelles, lowering the local effective CMC and accelerating micelle formation.

While we have only directly detected micelles within the aqueous phase using TEM, we would expect both micelles and reverse micelles to form at, or near the interface between aqueous and IL phases. Regular micelles will form with the long alkyl chains of the IL cations (hydrophobic non-polar hydrocarbon tails) oriented towards the centre of the micelles IL anions or aqueous anions will surround the micelles and be loosely paired with the positively charged center of the cations (the hydrophilic polar heads of the IL), as depicted in Figure 5.12a. Reverse micelles with the hydrophobic tails oriented outwards and the polar heads oriented towards the center will also form at the interface, Figure 5.12b. These can carry water (at the centre of the reverse micelles) into the IL phase.

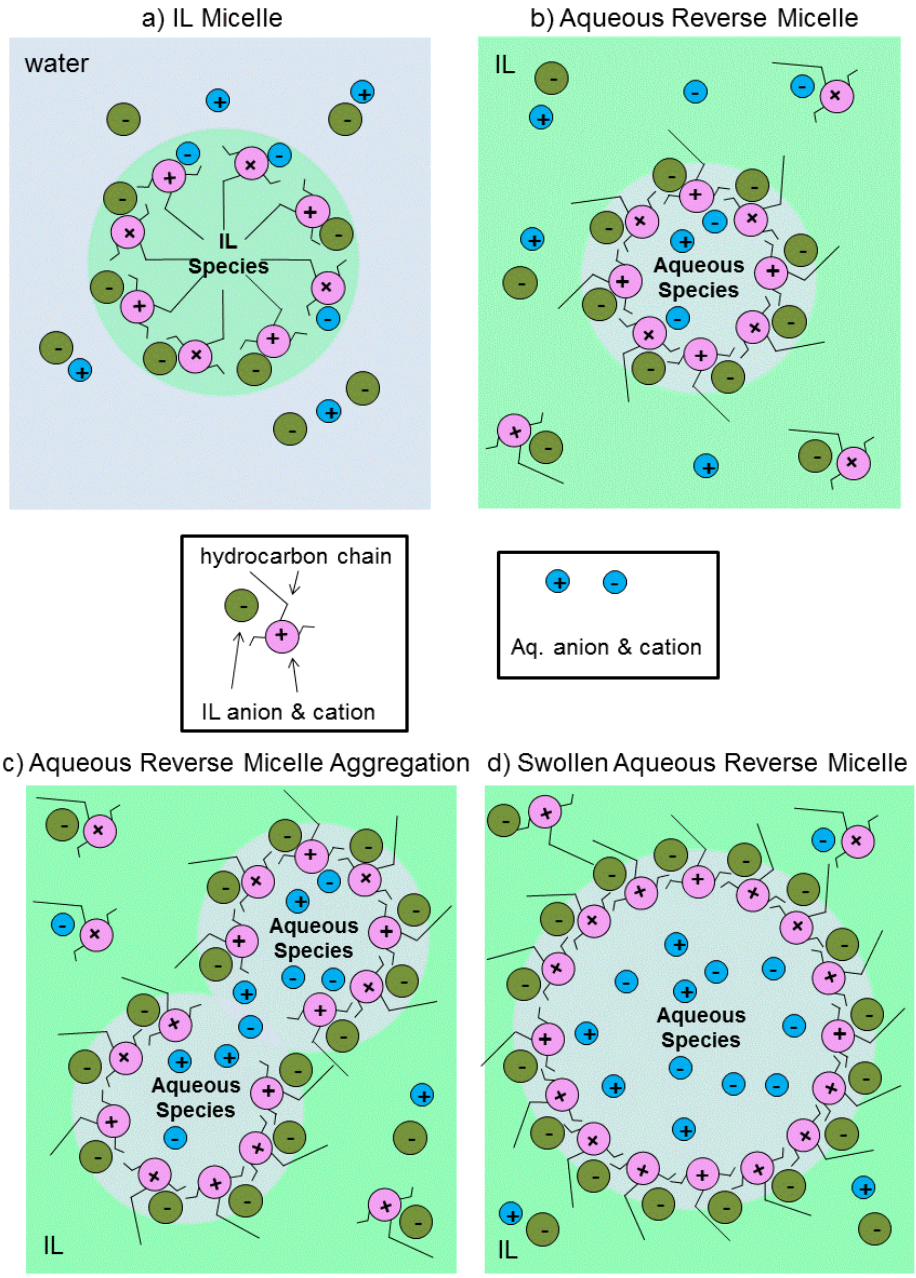

Figure 5.12 Schematic diagrams of the proposed structures of: a) IL micelle, b) aqueous reverse micelle, c) aggregation of aqueous reverse micelles, and d) the resulting swollen aqueous reverse micelles following aggregation.

To explain the accelerating effect of radiation on the emulsification process and the changes in the conductivity and Raman broad band intensities, a mechanism is

proposed that involves formation of micelles at the water/IL interface and their migration into the bulk phases. In this mechanism, the formation of micelles and reverse micelles at the water/IL interface induces mixing of the two phases. As the mixing increases the micelles formed at the interface migrate into the bulk aqueous or IL phases where they can aggregate and swell. Those micelles migrating to the aqueous phase are observed as predominantly single spheres (TEM images in Figure 5.10) with the anionic and cationic headgroups forming the outer micelle structure and the alkyl chain tails oriented inwards. However, even under conditions where the micelle concentration is small (short contact times with no γ-irradiation), some agglomeration of the micelles is observed, as seen in the lower right quadrant of Figure 5.10. Reverse micelles will migrate into the hydrophobic IL phase where they are favoured to aggregate at a faster rate to become swollen micelles and aggregates, as depicted in Figure 5.12.

Migration of reverse micelles from the interfacial region into the IL phase carries water molecules into the IL phase. Eventually, as the density of the reverse micelles increases, swollen reverse micelles in the IL phase lose their individual identity and a uniform emulsion is formed, as depicted in Figure 5.13. This is the emulsion layer, separate from both the aqueous phase and the clear IL phase seen in Figure 5.1. We suspect that this emulsion layer is protected by layers of micelles at the aqueous-emulsion and IL-emulsion interfaces. Under our conditions, the emulsion is seen as a cloudy layer that grows into the IL phase while the water phase remains clear. Miskolczy *et al.* [18] observed in their study of micelle formation in the aqueous phase of imidazolium ILs that the turbidity of the aqueous phase increased with an increase in the micelle concentration. In our study, the increase in turbidity is much more pronounced in the IL phase.

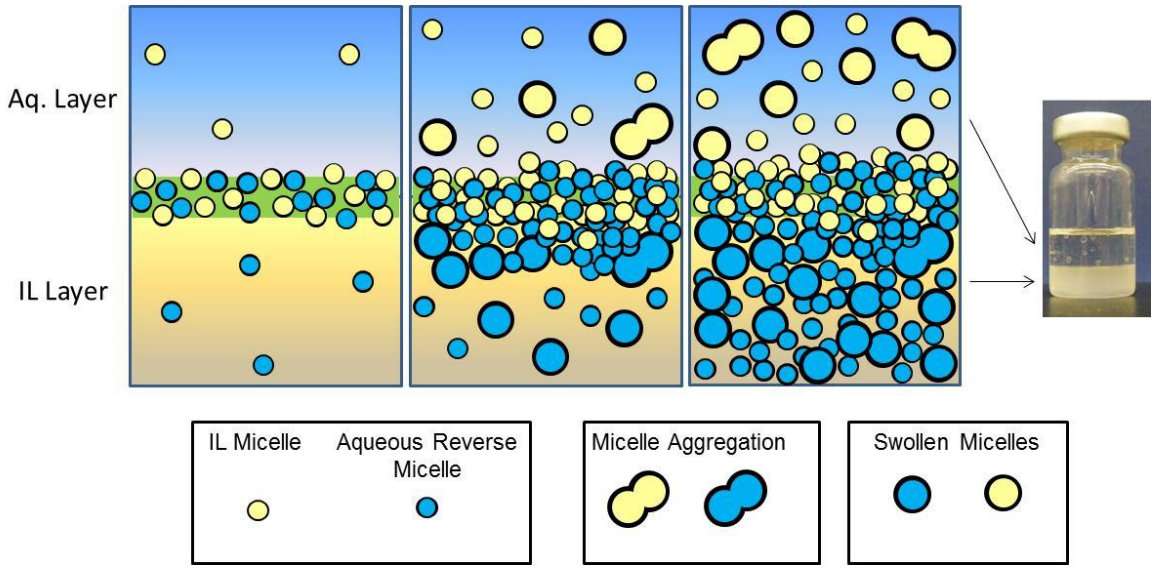

Figure 5.13 Schematic of the proposed development of an emulsion layer.

The proposed mechanism for micelle formation is consistent with the observed changes in the broad band intensities in the IL and water phase Raman spectra as a function of contact time, as well as the effect of γ-irradiation on the evolution of the spectra. In the absence of irradiation, the intensity of the broad band centered at ~ 2000 cm^{-1} increased with time in both the IL and water phase Raman spectra for the water/amide-IL system, Figure 5.8. This broad band also increased with contact time as shown in the Raman spectra of the 6-h irradiated samples, Figure 5.9. However, with irradiation, there was an additional broad band centered at 500 cm^{-1} that developed with contact time. This band was also present, but at a much lower intensity, in both the water and IL phase Raman spectra of the un-irradiated samples (Figure 5.8), and also in the water spectrum of the irradiated bromide IL-water sample (Figure 5.6b). We attribute the broad band centered at ~ 2000 cm^{-1} to scattering associated with the amide anions in the IL micelles and we attribute the band centered at ~ 500 cm^{-1} to scattering from the IL

cations of the micelles (since the amide and bromide-ILs share the same cation). The single atom bromide ion cannot be detected in Raman spectra. For the amide-IL, γ-irradiation initially decreases the intensities of the broad bands in the Raman spectrum of the IL phase while increasing the intensities of those in the Raman spectra of the water phase, Figure 5.5. This behaviour is attributed to IL transfer from the IL phase to the water phase, increasing both the IL anion and cation concentrations in the aqueous phase. After long irradiation periods (> 10 h) the broad band intensities increase in both phases, Figure 5.7. We attribute this behaviour to an increase in IL monomer concentration at or near the IL-water interface and the formation of micelles that can then disperse into both the water and IL phases.

In general, γ-irradiation increases the transfer rates of IL ions to the water phase and accelerates micelle and reverse micelle formation. The exact mechanism by which γ-radiolysis of the IL-water system affects the interfacial charge transfer process is not yet clear. However, it is known that steady-state γ-radiolysis of water can significantly alter the electrochemical potential of water alone [19]. Similarly, IL radiolysis can alter the electrochemical potential of the IL phase (although to a much smaller extent). These changes could result in an increase in the potential gradient at the water/IL interface, which could drive an increase in the charge transfer rate across the interface. This is not a novel proposal. An increase in the corrosion potential on carbon steel has previously been attributed to an increase in potential gradient at the water-metal interface under γ-irradiation [19].

An increase in the interfacial ion transfer rate from γ-radiolysis would accelerate micelle formation, as the CMC would be reached faster. In addition, impurities are

known to affect the surface energy of the water-micelle interface and impurities could, in turn, significantly affect the CMC [17]. Radiolysis of the IL produces IL fragments in the IL phase. Due to their immiscibility with water, these small organic radiolysis products become "trapped" at the interface. Although the total numbers of these organic molecules may be quite low, they could accumulate at the interface and affect interfacial properties that control the rates of micelle formation.

5.5 CONCLUSIONS

Two phosphonium-cation-based ionic liquids, trihexyltetradecylphosphonium bis(trifluoromethylsulfonyl)amide, and trihexyltetradecylphosphonium bromide were studied. The ILs are relatively radiation resistant, and γ-irradiation does not induce substantial chemical decomposition of the IL molecules into smaller fragments (as previously discussed in Chapter 4).

In immiscible water/IL systems, biphasic mixing occurs during extended periods of contact between the two fluids, even in the absence of radiation. We suggest that this mixing occurs as a result of transfer of IL ions into the water phase. As the concentration of these ions reaches the critical micelle concentration micelles and reverse micelles form at or near the interface. Migration of these micelles into both phases induces a mixing of the two phases and the interfacial region expands, further accelerating the formation of micelles and reverse micelles. In the IL phase reverse micelles absorb aqueous species to swell and aggregate. The eventual result is formation of a distinct emulsion layer that exists as a separate phase from both the aqueous or IL phase.

The presence of γ-irradiation accelerates the formation of the emulsion phase. This was attributed to the formation of small organic molecules by radiolytic decomposition of the IL and the action of these molecules as loci for micelle formation at the interface.

Easy and rapid formation of an emulsion in an IL-water system could have both good and bad implications. For applications where the capture of ions from the aqueous phases by the IL is desired, a uniform emulsion would increase the contact area between the IL molecules and water bearing target impurities.

5.6 REFERENCES

1. J. Grodkowski, P. Neta, J. Phys. Chem. A, 106 (2002) 5468-5473.
2. D. Allen, G. Baston, A.E. Bradley, T. Gorman, A. Haile, I. Hamblett, J.E. Hatter, M.J.F. Healey, B. Hodgson, R. Lewin, K.V. Lovell, B. Newton, W.R. Pitner, D.W. Rooney, D. Sanders, K.R. Seddon, H.E. Sims, R.C. Thied, Green Chem., 4 (2002) 152-158.
3. L. Berthon, S.I. Nikitenko, I. Bisel, C. Berthon, M. Faucon, B. Saucerotte, N. Zorz, P. Moisy, Dalton Trans. (2006) 2526-2534.
4. G. Le Rouzo, C. Lamouroux, V. Dauvois, A. Dannoux, S. Legand, D. Durand, P. Moisy, G. Moutiers, Dalton Trans. (2009) 6175-6184.
5. J.F. Wishart, P. Neta, J. Phys. Chem. B, 107 (2003) 7261-7267.
6. D. Behar, P. Neta, C. Schultheisz, J. Phys. Chem. A, 106 (2002) 3139-3147.
7. J. Grodkowski, P. Neta, J.F. Wishart, J. Phys. Chem. A, 107 (2003) 9794-9799.
8. J. Wishart, Radiation Chemistry of Ionic Liquids: Reactivity of Primary Species in Ionic Liquids as Green Solvents: Progress and Prospects, R.D. Rogers, K.R. Seddon (Eds.), ACS Symposium Series, Oxford University Press, Washington, DC, (2003) pp. 381-396.
9. S.L.I. Toh, J. McFarlane, C. Tsouris, D.W. DePaoli, H. Luo, S. Dai, Solvent Extr. Ion Exch., 24 (2006) 33-56.
10. G.E. Walrafen, L.A. Blatz, J. Chem. Phys., 59 (1973) 2646-2650.
11. D.M. Carey, G.M. Korenowski, J. Chem. Phys., 108 (1998) 2669-2675.
12. Y. Moroi, Micelles: Theoretical and Applied Aspects, Plenum Press, New York, NY (1992).
13. Z. Qiu, J. Texter, Curr. Opin. Colloid Interface Sci., 13 (2008) 252-262.
14. M. Zhao, L. Zheng, Phys. Chem. Chem. Phys., 13 (2011) 1332-1337.
15. R. Vanyúr, L. Biczók, Z. Miskolczy, Colloids Surf., A, 299 (2007) 256-261.

16. J.L. Anderson, V. Pino, E.C. Hagberg, V.V. Sheares, D.W. Armstrong, Chem. Commun. (2003) 2444-2445.
17. C. Jungnickel, J. Luczak, J. Ranke, J.F. Fernandez, A. Muller, J. Thoming, Colloids Surf., A, 316 (2008) 278-284.
18. Z. Miskolczy, K. Sebok-Nagy, L. Biczok, S. Gokturk, Chem. Phys. Lett., 400 (2004) 296-300.
19. K. Daub, X. Zhang, J.J. Noël, J.C. Wren, Electrochim. Acta, 55 (2010) 2767-2776.

Chapter 6. The Effects of Gamma-Radiation on Interfacial Reactions and Transport Processes of Water/Ionic Liquid Systems: Comparison of Amide and Dicyanamide Ionic Liquids

6.1 INTRODUCTION

In Chapters 4 and 5, phosphonium ionic liquids were prepared and the effects of gamma radiation on the gas/IL and water/IL samples were investigated. More specifically, Chapter 5 investigated the effects of radiation on two phosphonium ILs containing the same cation but differing anions. In this chapter, the effect of radiation on trihexyltetradecylphosphonium bis(trifluoromethylsulfonyl)amide and trihexyltetradecylphosphonium dicyanamide will be investigated and compared. Being that both ILs contain the same trihexyltetradecylphosphonium cation and amide-containing anion structures, the ILs possess very similar physical and chemical properties. By comparing the two ILs under identical conditions, information on the consequences of radiation induced interfacial processes can be examined and further understood. The structures of the ILs and their respective physical and chemical properties are shown in Table 6.1.

Table 6.1 The chemical structures of the ionic liquids investigated, as well as their chemical and physical properties (chemical and physical properties measured at 25 °C).

Ionic Liquid	Amide-IL	Dicyanamide-IL
Structure	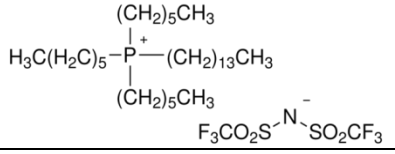	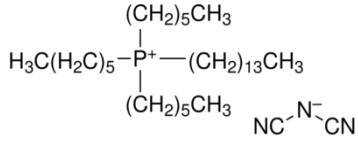
Density (g/mL) [1]	1.08	0.92
Viscosity (cP) [2]	292.5	280.4
Miscible with Water [2]	No	No
Theoretical Glass Transition Temperature (°C) [1]	-91	-78
Gaseous Products Detected After Radiation Exposure	ethane (C_2H_6) hexane (C_6H_{14}) hexafluoroethane (C_2F_6) fluoroform (CHF_3)	dichloromethane (CH_2Cl_2)

6.2 EXPERIMENTAL

6.2.1 Sample Preparation

The ionic liquids trihexyltetradecylphosphonium bis(trifluoromethylsulfonyl)amide and trihexyltetradecylphosphonium dicyanamide were purchased from Sigma-Aldrich (purity ≥ 95%), which will hereafter be referred to as the amide-IL and the dicyanamide-IL. The structures of the amide-IL and the dicyanamide-IL can be found in Table 6.1. Purified water from a NANOpure Diamond UV ultrapure water system with a resistivity of 18.2 MΩ·cm was used in the tests. Test vials were prepared by placing 2 mL of water and 2 mL of an ionic liquid inside a 10 mL Pyrex vial and sealing the vial with an aluminum crimp cap containing a PTFE/silicone septum. Sealed vials were de-aerated by purging with ultra-high purity argon using syringes. The purging was done immediately before irradiating the vials.

6.2.2 Sample Irradiation

Sample vials were irradiated in a ^{60}Co gamma cell at a dose rate of 5.5 $kGy \cdot h^{-1}$. Irradiated sample vials were removed from the gamma cell after exposure times ranging from 1 h to 168 h and analyzed immediately. Control samples were also prepared, treated and analyzed in the same way, except that they were held without exposure to gamma-radiation. To ensure that observed differences between irradiated and non-irradiated control samples were the consequences of irradiation, we attempted to minimize the period during which the IL and water were in contact with each other outside of the radiation field. For irradiated samples, this contact time was ~25 min pre-irradiation and ~5 min post-irradiation, which in total was much less than the typical irradiation time.

6.2.3 Sample Analysis

6.2.3.1 *Gas Chromatography-Mass Spectrometry*

Immediately after irradiation, gas phase analysis was performed by extracting an aliquot of gas from the headspace above the liquids in the test vial using a gas-tight Luer lock syringe. These gas samples were injected into a gas chromatograph with a -mass spectrometer detector using helium as the carrier gas.

6.2.3.2 *Electrochemical Impedance Spectroscopy*

A frequency response analyzer (Solartron, model 1260), operated as a stand-alone instrument, was used to make conductivity measurements on the liquid components of

the samples. ZPlot® software (Scribner Associates) was used for experimental control. The conductivities of the water and IL phases of our samples was determined from electrochemical impedance spectroscopy (EIS) measurements, performed over a frequency range of 1 Hz to 1 MHz in a specialized conductivity cell. The conductivity cell constant was determined prior to each set of experiments using KCl solutions and was experimentally determined to be 10.6 cm^{-1} at the time of experiments with the amide-IL, and 11.0 cm^{-1} at the time of experiments with the dicyanamide-IL.

6.2.3.2.1 *Electrochemical Impedance Spectroscopy: Fitting with a Contaminant*

Due to time constraints and availability of lab equipment the amide-IL and dicyanamide-IL experiments were performed at different periods of time. Between the dicyanamide-IL and the amide-IL experiments (a period of a few weeks) the electrochemical cell was borrowed and returned with a contaminant adhered to the inside of the cell. Despite repeated attempts and efforts to remove the contaminant, cleaning efforts were not successful. Thus, the EI spectra of the amide-IL samples had to be carefully analyzed due to the presence of a contaminant in the conductivity cell which unevenly coated the glassy carbon electrodes. Fortunately, dicyanamide-IL samples were run completely before lending the conductivity cell. These spectra were fit easily by determining the intercept of the Nyquist plot along the real (Z') axis.

Repeated experiments and fitting was performed to ensure measurements were of the resistivity (inverse conductivity) of the IL or water phase within the cell, and not the contaminant. This was confirmed by fitting amide-IL measurements and comparing the

results to previous amide-IL measurements for which the conductivity was already known (from Chapter 4 and 5).

For the case of the amide-IL phase, the resulting Nyquist plot in Figure 6.1b shows one large semi-circle with a second, smaller semi-circle developing out of the first. The Bode plots, Figure 6.1a, show very close overlap, with the phase angle Bode plot showing almost complete overlap, and only minimal differences in the impedance modulus as the spectra shift to a lower frequency.

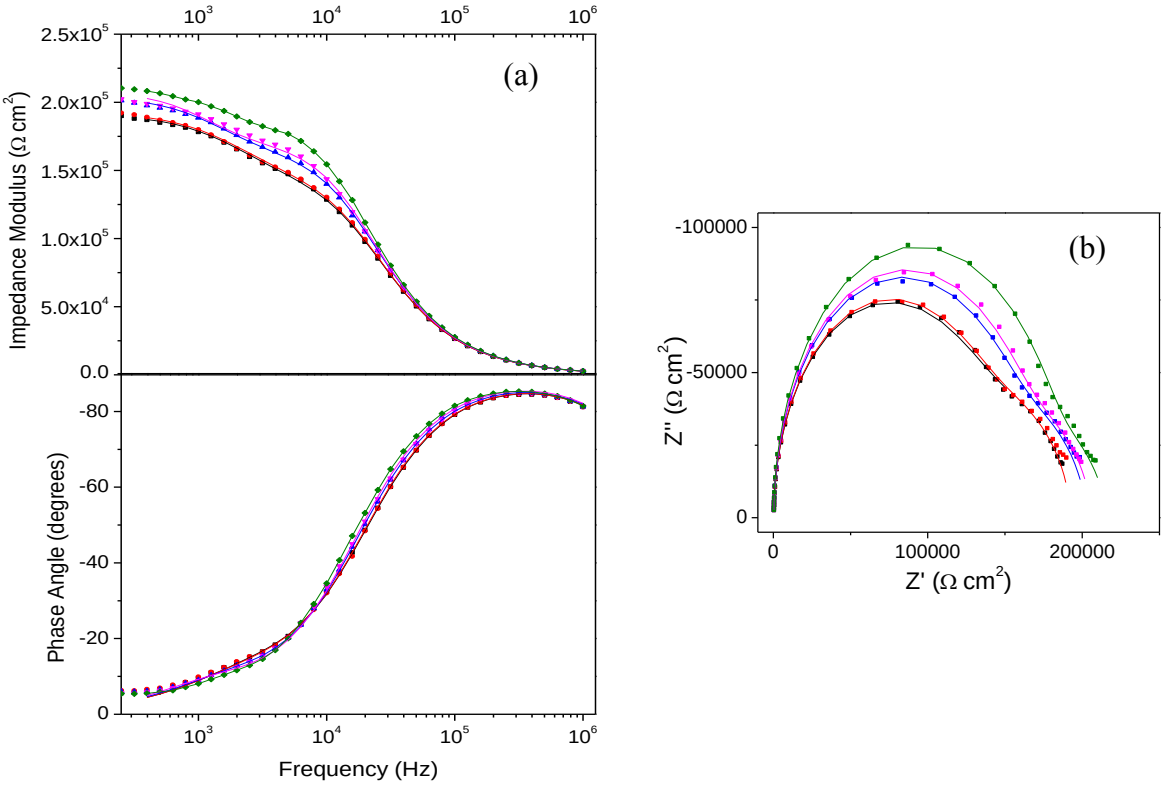

Figure 6.1 The electrochemical impedance spectra for the IL phase of the amide-IL sample. The (a) Bode plots and (b) Nyquist plot shows the signals at ■ 0 h irradiation, ■ 24 h irradiation, ■ 72 h irradiation, ■ 120 h irradiation, and ■ 168 h irradiation.

The resulting equivalent circuit, Figure 6.2 was composed of a resistor (R1) and constant phase element (CPE1) representing the wiring to the electrochemical cell and the impurity coating glassy carbon electrodes on one side of the electrochemical cell. In parallel, a second resistor (R3) denotes the resistance of the IL sample in the cell. Following this, again in parallel, is a final resistor (R2) and constant phase element (CPE2) representing the impurity coated on the glassy carbon electrodes as the signal exits the cell. Using this model, all parameters within the selected data resulted in an error of < 5%.

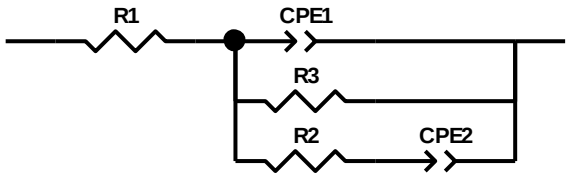

Figure 6.2 The equivalent circuit modeling the amide-IL plots in contact with the water phase.

As the conductivity increased dramatically, the Bode and Nyquist plots (Figure 6.3) of the water phase from the water/amide-IL samples also illustrated many differences. When the frequency shifted to a lower value, the impedance modulus in Figure 6.3a showed much more variation between samples of different irradiation times. With increased irradiation time, the impedance modulus shifted to lower values, resulting in a lower resistivity and higher conductivity. The phase angle Bode plot (lower half of Figure 6.3a) showed the development of a second peak, which only continued to grow

larger with increased irradiation time, and illustrated a shift to a higher frequency as experiments progressed. This is consistent with the transfer of ions from the IL phase to the water phase, producing the second peak and reducing the resistivity of the water layer. Dramatic changes are illustrated in the Nyquist plot (Figure 6.3b), with the size of the semi-circles diminishing greatly. At values of high resistivity, the contaminant is not visible on the Nyquist plot. However, with the increased ion transfer to the water layer, the contaminant signal becomes very apparent as the resistivity shifts to a lower value.

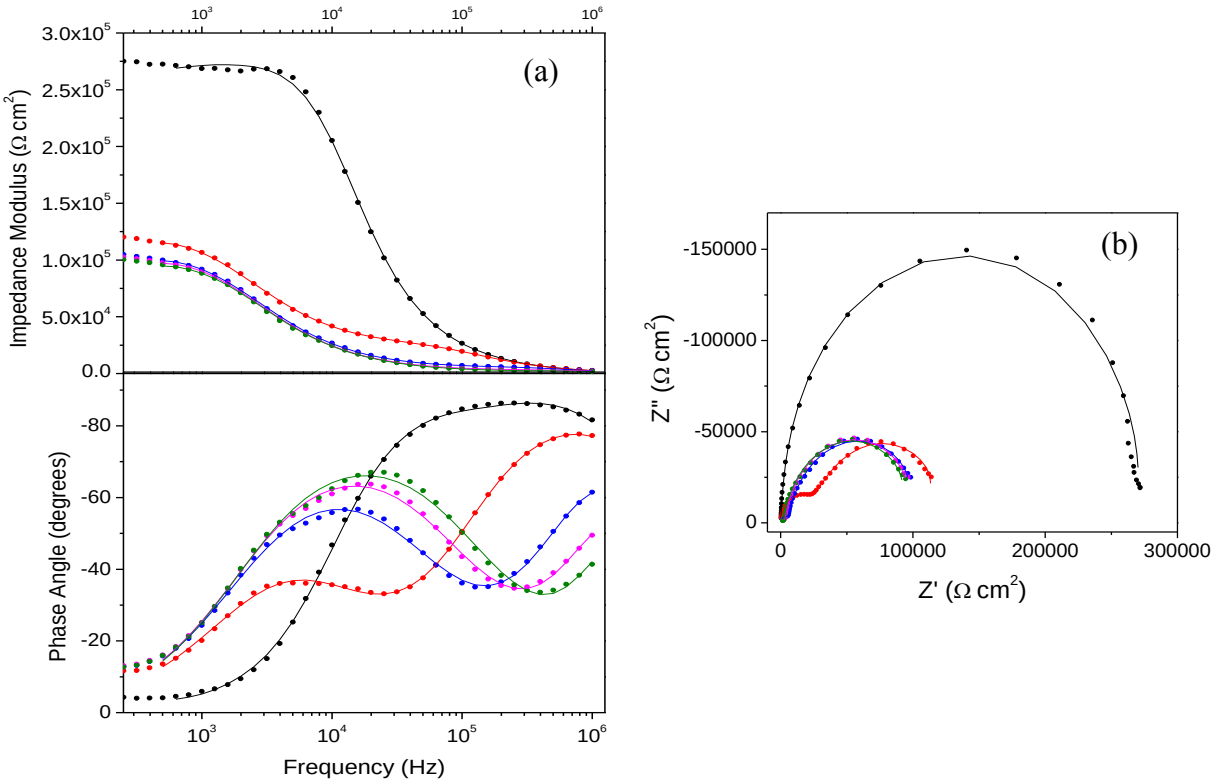

Figure 6.3 The electrochemical impedance spectra for the water phase of the amide-IL sample. The (a) Bode plots and (b) Nyquist plot shows the signals at ● 0 h irradiation, ● 24 h irradiation, ● 72 h irradiation, ● 120 h irradiation, and ● 168 h irradiation.

The equivalent circuit to represent the data was composed of a variety of resistors and constant phase elements in parallel (Figure 6.4). The wiring and other resistance from the instrumentation is represented by a resistor (R1). A second resistor (R2) and a constant phase element (CPE1) represent the contaminant coating the glassy carbon electrodes. The resistivity of the water layer is obtained from the third resistor in series (R3), which is in series with a second constant phase element (CPE2). The resistance from the contaminant is represented by a fourth, and final resistor (R4) and the final constant phase element (CPE3). The resistance of the water layer was known from previous experiments performed using the uncontaminated cell and the resulting Nyquist plot. Therefore R3 was assigned based on the equivalent circuit fit and prior experimental knowledge. When modeled in this manner, the error within the selected data was < 5%.

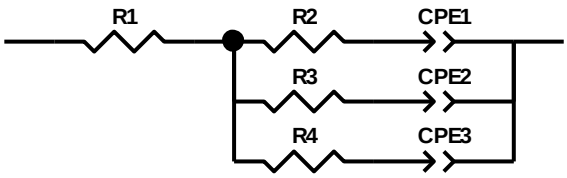

Figure 6.4 The equivalent circuit modeling the water phase plots in the biphasic water/amide-IL system.

6.2.3.3 *Fourier Transform Infrared Spectroscopy*

Infrared spectroscopy was performed on IL samples extracted during the experiments using a Fourier transform infrared spectrometer. Samples were prepared for

FTIR analysis by mixing liquid aliquots or solid precipitate with spectroscopy grade KBr and using a press to form pellets.

6.2.3.4 *Transmission Electron Microscopy*

Transmission electron microscopy was used to further investigate the identity of the water phase. Samples from the aqueous phase were collected and imaged using a transmission electron microscope operating at 100 keV. Sample preparation involved placing aliquots of the aqueous phase on carbon-coated copper grids and allowing them to air dry at room temperature.

6.3 RESULTS

6.3.1 Ionic Liquids in Contact with Argon Gas

6.3.1.1 *Gas Chromatography-Mass Spectrometry*

Gaseous species in the headspace of test vials containing only an ionic liquid sample, after irradiation, were identified using the GC/MSD and are listed in Table 6.1. Previous experiments have indicated that similar radiolytic decomposition products are produced, regardless of whether the gaseous environment is aerated or deaerated (as discussed in Chapter 4) [3]. The absence of oxygenated organic gaseous species indicates that reactions at the gas/IL interface contribute little to the radiolytic degradation. For this reason, only deaerated samples were investigated. In the case of the amide-IL, the gas phase products identified include ethane (C_2H_6), hexafluoroethane

(C_2F_6), fluoroform (CHF_3), and hexane (C_6H_{14}). The presence of these species can be attributed to radiolytic decomposition of the IL, and their volatility accounts for their transfer into the gas phase. Only one gaseous organic species, dichloromethane (CH_2Cl_2), was identified in the gas phase in contact with the dicyanamide-IL. Dichloromethane was a surprising find since the dicyanamide-IL does not contain chlorine atoms and therefore cannot yield dichloromethane as a radiolysis product. The dichloromethane is likely residual from the synthesis of the dicyanamide-IL; in the synthetic process the dicyanamide-IL is washed with dichloromethane on a column [4, 5]. The volatility of this organic solvent allows it to transfer easily into the gas phase above the IL.

6.3.1.2 *Electrochemical Impedance Spectroscopy*

Changes in the IL phase during irradiation were monitored using electrochemical impedance spectroscopy (EIS) measurements to determine the conductivity, Figure 6.5. Of the two ILs studied, the amide-IL had the lower conductivity. In contrast, the dicyanamide-IL had a higher conductivity, ~150 $\mu S \cdot cm^{-1}$, a value that is consistent with the findings of Vaughan et al. [1]. Although there was some scatter in the conductivity values for both ILs, neither showed a significant change in conductivity with irradiation time. This finding is in accordance with other studies of ILs irradiated and in contact with a gas phase [6, 7].

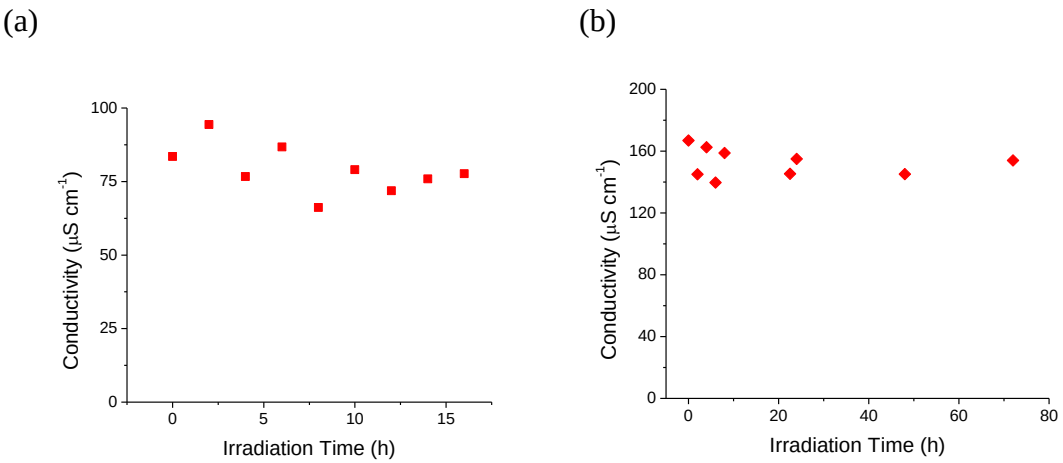

Figure 6.5 Conductivity as a function of irradiation time for (a) amide-IL and (b) dicyanamide-IL samples.

6.3.2 Ionic Liquids in Contact with Water

The stability of both ILs in contact with an aqueous phase was studied. Of the two ILs, the dicyanamide-IL is the more conductive and slightly less viscous [8, 9]. When the samples were prepared, the dicyanamide-IL floated atop the water layer due to its density being less than that of water. In contrast, the amide-IL is denser than water and forms a layer below the water layer.

6.3.2.1 *Trihexyltetradecylphosphonium Bis(trifluoromethylsulfonyl)amide*

6.3.2.1.1 *Electrochemical Impedance Spectroscopy*

In the water/amide-IL system, the conductivity of the IL phase showed little change from its initial value (Figure 6.6a), as we previously observed in Chapter 5. This is illustrated in the electrochemical impedance spectra of the amide-IL, which changed significantly with increased irradiation or contact time (Figure 6.1).

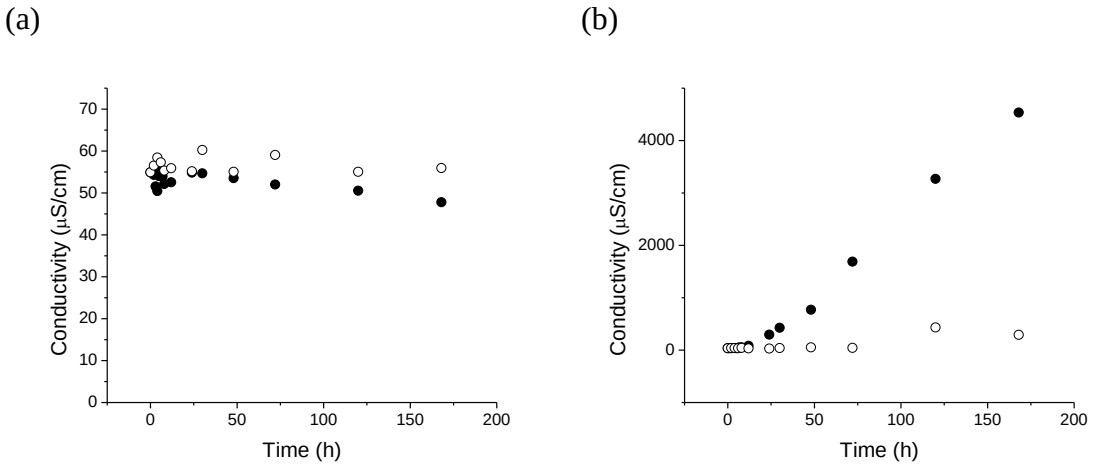

Figure 6.6 Conductivity as a function of contact time for the water/amide-IL system: (a) IL layer and (b) water layer. Symbols differentiate data from ● irradiated and ○ non-irradiated samples.

Again consistent with previous observations in Chapter 5, the conductivity of the water phase increased with time and exposure to radiation, Figure 6.6. There is a suggestion of an incubation period for the amide-IL before the water conductivity begins to rise sharply with irradiation. As discussed in section 6.2.3.2.1 the EI spectra were carefully analyzed taking into account contaminant issues.

At longer irradiation and contact times cloudy regions, indicative of emulsification, began to develop in the IL layer near the water interface (growth of such an emulsion has been observed previously [3] and was discussed in depth in Chapter 5). This cloudy region expanded downwards from the water/amide-IL interface over time. The emulsion was observed in both the presence and absence of irradiation, but irradiation accelerated the development of the emulsion. As a result of the development of this emulsion at the water/amide-IL interface, the shape of the interface changed and

became less distinct. Because the emulsion layer in the amide-IL has been studied and discussed in Chapter 5, it will not be discussed in great detail here.

6.3.2.2 *Trihexyltetradecylphosphonium dicyanamide*

6.3.2.2.1 *Electrochemical Impedance Spectroscopy*

In the biphasic dicyanamide-IL and water sample, contact with water induced the same conductivity changes in both irradiated and non-irradiated systems, as seen in Figure 6.7a. The initial conductivity of ~150 $\mu S \cdot cm^{-1}$ increased sharply with increasing time of exposure to water before leveling off at 300 – 350 $\mu S \cdot cm^{-1}$. The steady state was established after ~25 hours of contact. This behavior is similar to that observed in the bromide-IL sample, discussed in Chapter 5, but dramatically different from the trend observed in the amide-IL system.

Contrasting the IL phase, irradiation had a clear impact on the conductivity of the aqueous phase, Figure 6.7b. The water layer conductivity was initially very low (~10 $\mu S \cdot cm^{-1}$) and, in the absence of irradiation, increased slowly and continuously over the entire duration of our tests. However, in the presence of radiation, the conductivity of the water layer increased dramatically at an approximately linear rate, rising to ~900 $\mu S \cdot cm^{-1}$ after 100 h of radiation exposure. As discussed earlier, we know that this increase in conductivity cannot be attributed to the irradiation of water alone [3]. Rather, the increase is most certainly a consequence of the transfer of ions from the IL phase to the aqueous phase.

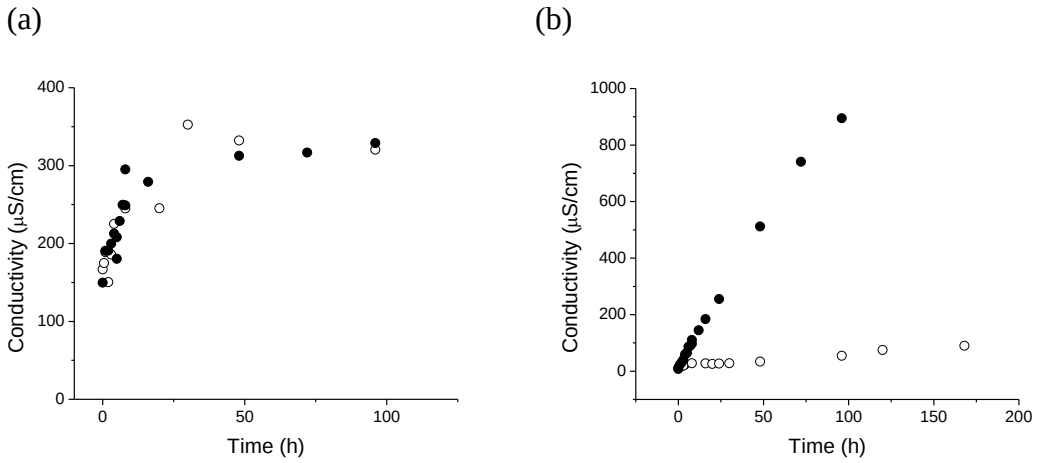

Figure 6.7 Conductivity as a function of contact time for the water/dicyanamide-IL samples: (a) IL layer and (b) aqueous layer. Symbols differentiate data from ● irradiated and ○ non-irradiated samples.

6.3.2.2.2 Fourier Transform Infrared Spectroscopy

After more than 8 h of irradiation, a white precipitate could be seen accumulating in the water/dicyanamide-IL sample. The precipitate settled quickly at the bottom of the vial in the aqueous layer (Figure 6.8), while neither the water nor IL layers appeared cloudy.

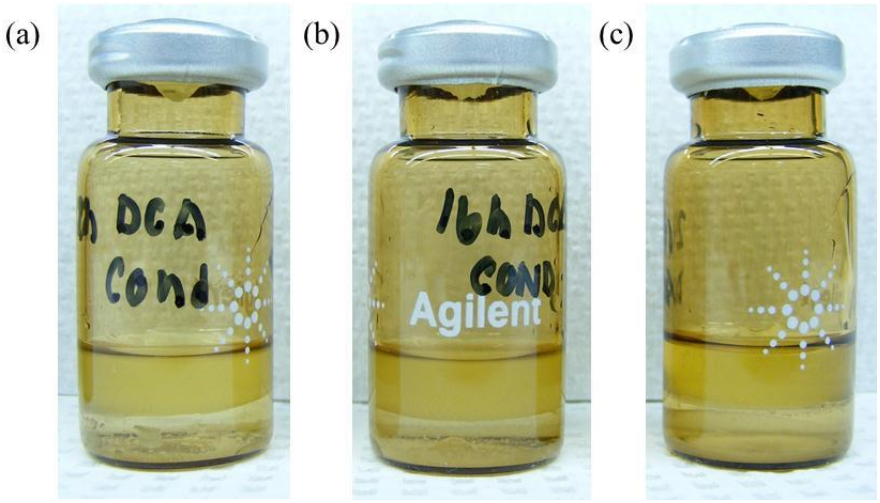

Figure 6.8 Photographs of vials containing water/dicyanamide-IL after irradiation for (a) 12 h, (b) 16 h, and (c) 24 h. The upper layer in the vial is the IL phase and the lower layer is the water phase. A white precipitate can be observed at the bottom of each vial. The initially colourless glass of the vials has been darkened by radiation exposure.

To characterize the white precipitate, aliquots containing the precipitate were collected from the water phase and placed on glass slides. The water was allowed to evaporate from the slides and the white precipitate was gently scraped from the slides. Next the FTIR spectrum of the dried precipitate was collected. The FTIR spectrum of the precipitate and that of the pure dicyanamide-IL have a strong overlap in the main peaks of the dicyanamide-IL (Figure 6.9), with only slight variations in the CN stretching vibrations at 2100-2220 cm^{-1}. However, the precipitate also has additional sharp peaks in the region 1000-1800 cm^{-1} and a broad band centered on ~3300 cm^{-1}. The FTIR peaks indicate that the dicyanamide anion is a main component of the precipitate, while the broad band peaks is consistent with the incorporation of OH or water into the precipitate [10, 11].

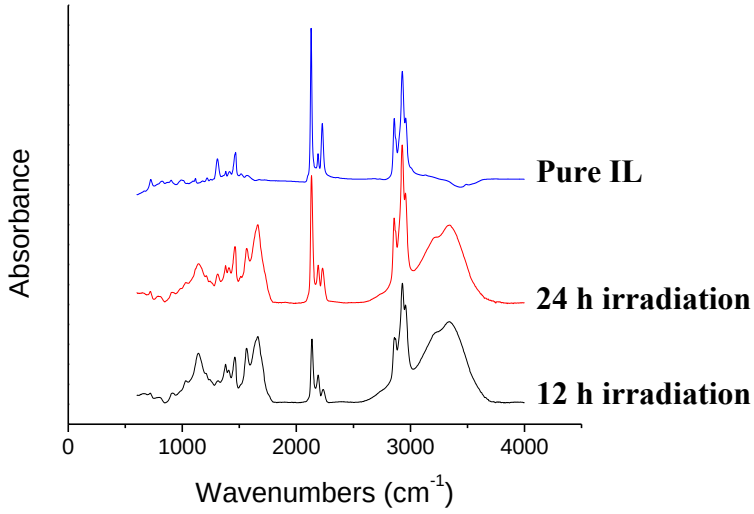

Figure 6.9 FTIR spectra of pure dicyanamide IL and of the precipitates formed after irradiation of a water/dicyanamide IL sample for 12 h and for 24 h.

Particles suspended in the aqueous phase were captured on a TEM grid and TEM images were obtained (Figure 6.10). The TEM images showed a fine particulate, with particles in the nanometer size range (hence their suspension in the aqueous phase). Using ImageJ software, the particle size distribution was examined in further detail, Figure 6.11 . The particulate size distribution ranged from 10 nm to over 120 nm, with some larger agglomerated precipitate species, independent of radiation time. The vast majority of particles hovered around the 20 – 30 nm size diameter size distribution.

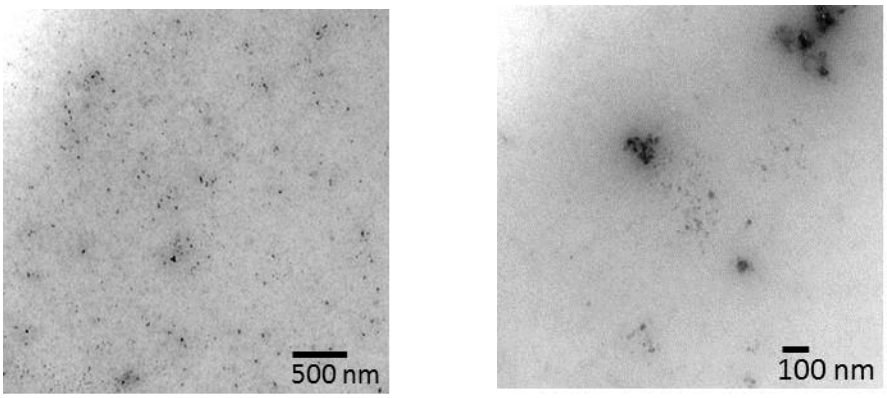

Figure 6.10 TEM images of particulates in the aqueous phase of the water/dicyanamide-IL system following 16 h of irradiation.

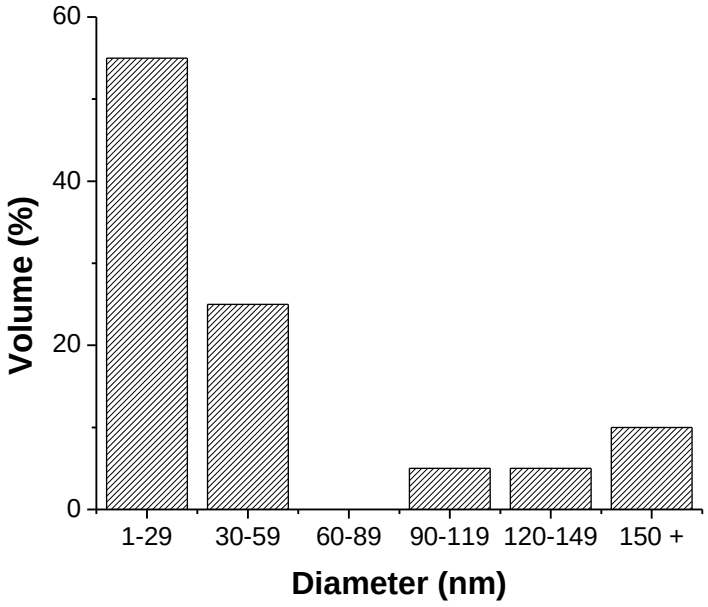

Figure 6.11 The diameter of the particles by % volume collected from the aqueous phase and studied using TEM

6.4 RESULTS

6.4.1 Effects of Radiation on Gas/IL Systems

The conductivity measurements show no or very little change in the conductivities of the ILs with irradiation. This is consistent with the headspace gas analysis, which detected few volatile radiolysis products. The net radiolytic degradation of the ILs was expected to be very small due to their low dielectric constant [12]. The probability of an excited or charged species formed by absorption of ionizing radiation and then escaping recombination in a liquid is proportional to the dielectric constant of the medium [3, 13]. As discussed in Chapter 2, the dielectric constants of ILs are comparable to those of organic solvents, and favor recombination, as opposed to charged species separation and the consequently observed radiolytic degradation.

6.4.2 Effects of Radiation on Water/IL Systems

The conductivity of the amide-IL was minimally impacted by water/IL contact, and maintained a constant conductivity, with only a slightly negative trend, when exposed to water; instead the interaction involved micelle formation and emulsification, as previously described in detail [9]. The conductivity of the dicyanamide-IL, however, did increase over time as a consequence of being in contact with the aqueous phase. This observation is consistent with the analysis of the precipitate isolated from the aqueous phase in contact with the dicyanamide-IL, which found that the precipitate contained the dicyanamide anion. If dicyanamide anions are transferred from the IL phase to the aqueous phase, then anions from the water must likewise transfer to the IL phase in order to avoid excessive electrical charge differences between the two phases. The water can provide only hydroxide anions. The entry of OH^- ions into the IL would be expected to increase the IL layer conductivity, both because the decrease in IL purity would decrease the IL viscosity (thereby increasing ionic mobility) and because OH^- ion is more mobile than the IL ions.

Micelle formation that occurs in the amide-IL (discussed in chapter 5) and the dicyanamide-IL phases (discussed later in 6.4.3) can contribute to the conductivity observations. The conductivity of the IL is envisioned to occur by electron hopping [14, 15]. Micelles do not migrate at substantial rates, and this slow movement will hinder electron hopping between charged species. In the amide-IL, micelle formation occurs relatively quickly. The fast formation of micelles in the sample can account for the fact that no large increase is observed in the conductivity when the water and IL phase come into contact (promoting ion transfer). This micelle formation can also account for the

small negative trend in conductivity. In the dicyanamide-IL micelle formation is also seen to hinder the electron hopping mechanism that occurs. Micelles in the dicyanamide-IL formed at a slower rate than in the amide-IL. At increased irradiation and contact times it can be seen that the conductivity of the IL phase reached a steady-state, Figure 6.7. The later formation of micelles results in the delayed steady-state conductivity, as they subsequently hinder the electron hopping mechanism.

In both the amide and dicyanamide water/IL systems, the water phase conductivity increased linearly with irradiation time. The magnitude of change in the water conductivity was similar for both ILs and the time dependence was similar. Though the amide-IL tests were run for longer irradiation periods than the dicyanamide-IL tests (more than 150 h), the increase in the water conductivity continued at a rate that was approximately constant with time.

In the water/amide-IL system there may be signs of an induction period of several hours duration before the aqueous phase conductivity began to rise. While there is insufficient information to comment further on the observation of an induction period, this may be due to the larger size of the amide-IL anion, and increased hydrophobicity. The general increase in conductivity of the water layer is not surprising, since we have previously shown that radiation facilitates inter-phase mixing in water/IL systems [9]. Pure water is a rather poor conductor, and so the addition of ions from the IL phase should increase its conductivity.

From the amide-IL results, and due to the similarities between the two ILs, it was initially expected that micelles would also be observed on the TEM grid prepared from the aqueous layer in the dicyanamide-IL system. However, in the dicyanamide-IL

system, no visible emulsion layer formed in either the IL or water phases, even after long periods of irradiated or non-irradiated contact. TEM images of the aqueous phase did not show evidence of any micelles, but rather detected the nanometer-scale precipitate dispersed throughout the water phase. Precipitate formation has not been observed in our previous IL studies. The FTIR results show that the same precipitate is formed regardless of irradiation time. Comparing the FTIR spectra of the precipitate to that of the pure IL (Figure 6.9) one can see that there are few significant differences between the pure IL and the precipitate product. Although we have not been able to conclusively identify this precipitate, it is likely that it is either a salt compound used in the synthesis of the dicyanamide-IL, or a phosphonium dicyanamide salt formed during our experiments.

6.4.3 Radiation-Induced Nanoemulsion

Precipitate formation only occurs in those samples with 8 h or more of irradiation, indicating that the formation requires energy to drive the process. It was also interesting to observe that the precipitate formed had a uniform size distribution, with particles ranging from 10 nm to over 120 nm, and the highest volume % of particles between 20−30 nm. A bimodal distribution was observed, with the smaller precipitate species likely formed in the micelles as the sizes correspond to the size of micelle species observed in chapter 5. The larger sized species are agglomerations of the primary produced species. The distribution observed indicated that the precipitate may form via micelle formation in the aqueous phase, as it is known that the formation of nanoparticles within micelles allow for control in the size and shape of resulting precipitate and particulate [16].

Micelles, reverse micelles, and emulsion systems have been observed in a variety of IL systems, including our own [3, 17-20]. However, a new type of emulsion system, the water-in-oil nanoemulsion, has been described for the first time only recently [21-23]. Although microemulsions and conventional emulsion systems have many similarities, nanoemulsions differ in that they are visually transparent and are not thermodynamically stable [24]. The input of energy into a biphasic system containing two immiscible liquids (and often a surfactant) can result in the formation of a nanoemulsion system [21, 24]. Micelles and reverse micelles formed in the nanoemulsion have the same identity as that of a regular emulsion system, with the radius of the micelles formed approximately 100 nm or less (though this definition is not yet widely adopted, with some nanoemulsion systems having radii of $\geq$ 250 nm) [24, 25]. The instability of these systems in the absence of energy causes them to breakdown if given sufficient time. One of the main applications for the nanoemulsion systems is for the production of nanoparticles as the size and composition of the micelles are controlled in the system and the micelles can act as nanoreactors [21].

Although we have no visual proof, a nanoemulsion system is likely present in our biphasic water/dicyanamide-IL system. In the presence of radiation, the biphasic system receives an intensive amount of energy. As radiation produces degradation products and promotes the transfer of ions across the interface and the formation of micelles, a nanoemulsion can form. The formation only occurs beyond 8 h of irradiation time due to the large amount of energy required for formation. As the dicyanamide-IL contains the same cation as the amide-IL, giving surfactant activity, it is envisioned that the formation of micelles and reverse micelles occurs in the same manner at the interface as described

in Chapter 5 (Figure 5.12), before dispersing into their respective phases. In the aqueous phase the IL droplets or pools that are encapsulated within the micelles act as nanoreactors, promoting the formation of nanoparticles and precipitate within the small confined volume. Precipitate formation is therefore uniform because of the regulated size of the reverse micelles present in the nanoemulsion. Due to the thermodynamic instability of the nanoemulsion system, in the absence of radiation the biphasic system breaks down to the initial two phases (IL and water). However, the precipitate formed within the micelles remains, settling in the aqueous phase. Confirmation of the nanoemulsion would require an energy intensive environment with in situ analytical techniques, which were not available at the time of experiments.

The implications of this behavior for applications in separations processes in which ILs are used to extract metal ions are not entirely clear at this stage. Certainly precipitate formation would complicate the process by adding a third phase to the mixture, necessitating that filtration or settling steps be added to the separations process. It also results in the consumption of the IL, an expensive component of the process that would need to be recycled. The formation of micelles and emulsion layers has beneficial aspects – the interfacial contact area of water and IL would be greatly increased, facilitating much more rapid phase separation of the metal ions - but also detrimental ones – the emulsion may be difficult and time-consuming to coalesce, impeding the removal of metal ions and recycling of the IL in the separations process.

6.5 CONCLUSIONS

Although a variety of previous papers have discussed and compared the physical properties of ionic liquids under various conditions, this is the first work to compare the effects of long term irradiation on trihexyltetradecylphosphonium bis(trifluoromethylsulfonyl)amide and trihexyltetradecylphosphonium dicyanamide ILs in biphasic (gas/IL and water/IL) systems.

The ILs studied were both relatively radiation resistant; however, γ-radiation influences the rate of formation of micelles and the formation of a white precipitate (in the case of the dicyanamide-IL). Even in the absence of radiation, the transfer of IL ions into the aqueous phase occurs, in spite of the immiscibility of the two phases, though irradiation greatly accelerates and enhances this transfer. The consequences of this ion transfer differ between the dicyanamide and the amide-ILs. In the latter case, the ion transfer acts to increase the IL ion concentration in the water layer until the critical micelle concentration is achieved an emulsion layer is formed. The emulsion formation in the amide-IL is stable, and forms in the presence and absence of radiation. However, in the water/dicyanamide-IL, it is suggested that nanoemulsion formation causes the production of a fine precipitate within the micelles formed. The nanoemulsion formed in the dicyanamide-IL biphasic system is not thermodynamically stable, and forms only with the input of high amounts of energy into the system. Upon removal from the gamma cell chamber, the system breaks down and leaves a fine precipitate in the aqueous layer. Currently, however, this precipitate has not been fully characterized, though it does appear to incorporate the dicyanamide anion of the IL.

In summary, we can conclude that irradiation impacts both the dicyanamide-IL and the amide-IL when they are in contact with an aqueous phase. The implications of emulsion layer and precipitate formation for applications of these ILs in separations and extractions are currently unresolved. It is, however, very probable that the formation of the type of precipitate observed here would not be desirable in a separations process.

6.6 REFRENCES

1. J.W. Vaughan, D. Dreisinger, J. Haggins, ECS Trans., 2 (2006) 381-392.
2. Cytec Inc. Cyphos® Phosphonium Salt Information Sheets [available online].
3. S.E. Howett, J.M. Joseph, J.J Noël, J.C. Wren, J. Colloid Interface Sci., 361 (2011) 338-350.
4. J.C.F. Diogo, F.J.P. Caetano, J.M.N.A. Fareleira, W.A. Wakeham, C.A.M. Afonso, C.S. Marques, J. Chem. Eng. Data, 57 (2012) 1015-1025.
5. D.R. MacFarlane, S.A. Forsyth, J. Holding, G.B. Deason, Green Chem., 4 (2002) 444-448.
6. L. Berthon, S.I. Nikitenko, I. Bisel, C. Berthon, M. Faucon, B. Saucerotte, N. Zorz, P. Moisy, Dalton Trans., (2006) 2526-2534.
7. G. Le Rouzo, C. Lamouroux, V. Dauvois, A. Dannoux, S. Legand, D. Durand, P. Moisy, G. Moutiers, Dalton Trans., (2009) 6175-6184.
8. K.J. Fraser, E.I. Izgorodina, M. Forsyth, J.L. Scott, D.R. MacFarlane, Chem. Commun. (2007) 3817-3819.
9. C.M.S.S. Neves, P.J. Carvalho, M.G. Freire, J.A.P. Coutinho, J. Chem. Thermodyn., 43 (2011) 948-957.
10. A. Safavi, N. Maleki, F. Farjami, Colloids Surf. A, 355 (2010) 61-66.
11. A.C. MacMillan, T.M. McIntire, J.A. Freites, D.J. Tobias, J. Phys. Chem. B, 116 (2012) 11255-11265.
12. J.F. Wishart, I.A. Shkrob, The Radiation Chemistry of Ionic Liquids and its Implications for their Use in Nuclear Fuel Processing in Ionic Liquids: From Knowledge to Application, N.V. Plechkova, R.D. Rogers, K.R. Seddon (Eds.), ACS Symposium Series, Oxford University Press, Washington, DC, (2009) pp. 119-134.
13. J.F. Wishart, P. Neta, J. Phys. Chem. B, 107 (2003) 7261-7267.
14. W. Wang, R. Balasubramanian, R.W. Murray, J. Phys. Chem. C, 112 (2008) 18207-18216.
15. A. Skrzypczak, P. Neta, J. Phys. Chem. A, 107 (2003) 7800-7803.
16. C.T. Seip, C.J. O'Connor, Nanostruct. Mater., 12 (1999) 183-186.
17. Z. Qiu, J. Texter, Curr. Opin. Colloid Interface Sci., 13 (2008) 252-2622.
18. M. Zhao, L. Zheng, Phys. Chem. Chem. Phys., 13 (2011) 1332-1337.

19. J.L Anderson, V. Pino, E.C. Hagberg, V.V. Sheares, D.W. Armstrong, Chem. Commun. (2003) 2444-2445.
20. R. Vanyúr, L. Biczók, Z. Miskolczy, Colloids Surf. A, 299 (2007) 256-261.
21. C. Solans, P. Izquierdo, J. Nolla, N. Azemar, M.J. Garcia-Celma, Current Opin. Colloid Interface Sci., 10 (2005) 102-110.
22. N. Usón, M.J. Garcia, C. Solans, Colloids Surf. A, 250 (2004) 415-421.
23. K. Landfester, M. Willert, M. Antonietti, Macromolecules, 33 (2000) 2370-2376.
24. D.J. McClements, Soft Matter, 8 (2012) 1719-1729.
21. J. Li, J. Zhang, B. Han, L. Peng, G. Yang, Chem. Commun., 48 (2012) 10562-105644.

Chapter 7. Investigating Short Term Energy Transfer and Radiation Absorption in Water/Ionic Liquid Systems

7.1 INTRODUCTION

The most important and interesting phenomena observed during the course of the studies on the effect of radiation on the water/ionic liquid (IL) systems was not irradiation-induced chemical decomposition of the IL molecules, but rather the micelle formation and phase mixing between the two immiscible liquids that was accelerated by irradiation. The presence of reverse micelles and an emulsion in an IL phase in contact with water provides an interesting chemical system that can be used to study the effects of a very small liquid volume and the water/IL interface on the reaction kinetics of solvated (IL-solvated or hydrated) electrons. Studies of the production and decay kinetics of an IL-solvated or hydrated electron require that the system to be probed and monitored on short time scales using fast pulse radiolysis and in-situ techniques.

This chapter describes an initial study on the short-term radiolysis chemistry in water/IL systems. This work was conducted in collaboration with Dr. James Wishart at the Laser-Electron Accelerator Facility (LEAF) at Brookhaven National Laboratory (Upton, New York). LEAF employs pulse radiolysis techniques to study chemical reactions and other phenomena by subjecting samples to short pulses of high-energy electrons and following the reactions using various detection methods, including time-resolved spectroscopy. The LEAF facility is equipped with instrumentation that exists in only a handful of global facilities.

7.2 TECHNICAL BACKGROUND

7.2.1 Hydrated and IL-Solvated Electrons

The radiolytic formation of hydrated electrons in water was described in detail in Chapter 2. This section focuses on the formation of solvated electrons in an IL solvent. Each radiation particle (or for γ-radiation, the primary electron produced from the Compton interaction of matter with a γ-photon) undergoes many collisions when it passes through matter. In an IL, inelastic collisions result in either the ionization or excitation of the IL molecule:

$$IL \xrightarrow{\text{fast e (or } \gamma\text{−ray)}} IL^{*} \text{ or } (IL^{\bullet+} + e^{-}_{hot}) \qquad (7.1)$$

where IL* is an excited IL component (either cation or anion) [1, 2]. The electron ejected from ionization by a primary electron has a sufficient kinetic energy to ionize other IL components (and hence is termed a hot electron). Due to its excess energy, the hot electron can ionize or excite another neighbouring solvent molecule and generate another electron with less kinetic energy. The energy of this electron is not high enough to ionize or excite another molecule (and is often referred to as a sub-excitation electron), but has sufficient energy to escape the Coulombic influence of the counter IL cation (and thereby avoid geminate recombination). The secondary electron collisions lead to the formation of a spur (a local cluster of 2-3 ion and electron pairs or excited species) near each primary electron collision site. The electrons ejected from the molecules are sometimes referred to as free electrons, as opposed to bound electrons. However, such electrons are not completely free of the influence of the counter cation, $IL^{\bullet+}$.

The electrons formed in a spur with sufficient kinetic energy move away from the counter IL cations and the spur expands. As the spur expands, the electrons dissipate their excess kinetic energy through collisions with solvent molecules in less energetic processes, such as vibrational and rotational excitation, or translational energy transfer (heating). Eventually, after numerous elastic and inelastic collisions, the hot electron thermalizes. The time and number of collisions required for thermalization is expected to be shorter in an IL than in water because the opportunities for intra- and intermolecular energy transfer are greater with bulky IL molecules that have high densities of vibrational and rotational energy states. How fast the electrons can escape geminate recombination with the counter IL cations before the electrons are thermalized determines the chemical consequence of the ionization.

The ionization of a solvent molecule creates an excess electron locally and solvent molecules possessing dipole moments reorganize themselves around the electron with positive charge centres oriented inwards to form a solvated electron (e^-_{solv}). The dipole relaxation (or solvation) time in water is very fast; it occurs in less than 10^{-12} s for electrons (and less than 10^{-11} s for other ions) [3-5]. In ethanol, the solvation of an excess electron takes 6.9 ps [6]. The dipole relaxation time is much slower in an IL due to quasi-ordering (repeating units) of the cation and anion moieties of the IL. For example, it has been reported that the solvation of an electron in *N*,*N*-Diethyl-*n*-methyl-*n*-(2-methoxy)ammonium bis(trifluoromethanesulfonyl)imide occurs in 26 ps [7]. The rate of solvation of an electron in an IL is also found to correlate to with the IL viscosity and a solvation time (for a molecular ion) as slow as on the order of nanosecond has been reported [8, 9].

While being thermalized and solvated, free electrons will continue to be subject to geminate recombination with a counter solvent cation. The probability of surviving geminate recombination depends on the dielectric constant of the solvent medium and can be related to the Onsager radius as discussed in chapter 2 [1, 10].

The shorter thermalization time, longer solvation time, and lower dielectric constant of an IL, compared to water, all predict a lower radiolytic yield of solvated electrons in an IL compared to water. This is what is observed. The radiolytic yields (or G-values) for solvated electrons are about 0.07–0.08 μmol $\cdot J^{-1}$ (in the nanosecond time region) for ILs [1, 11, 12]. The G-value for hydrated electrons in water is much larger, 0.27 μmol$\cdot$ J^{-1} (in the nanosecond time region) [13].

In water, the hydrated electron is believed to be confined in a roughly spherical cavity, with a radius of 0.22 to 0.24 nm, and to occupy an *s*-type ground electronic state, Figure 7.1. Its spectrum is characterized by a broad electronic absorption near 1.7 eV (~ 700 nm). This band can be thought of as arising from a transition from the *s* state to an excited *p* state [14]. The characteristic absorption spectrum of the hydrated electron in water is shown in Figure 7.2 [1, 15-18]. It has a peak maximum at 715 nm. Its high extinction coefficient, $\varepsilon_{715nm} = 1.9 \times 10^4\ dm^3$ at room temperature, allows for direct in-situ measurement of hydrated electrons using absorption spectroscopy.

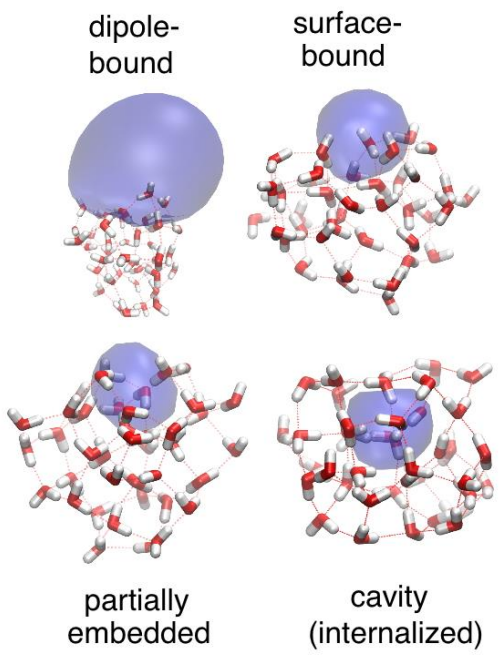

Figure 7.1 Hydrated electrons in water clusters. Images are taken from [19].

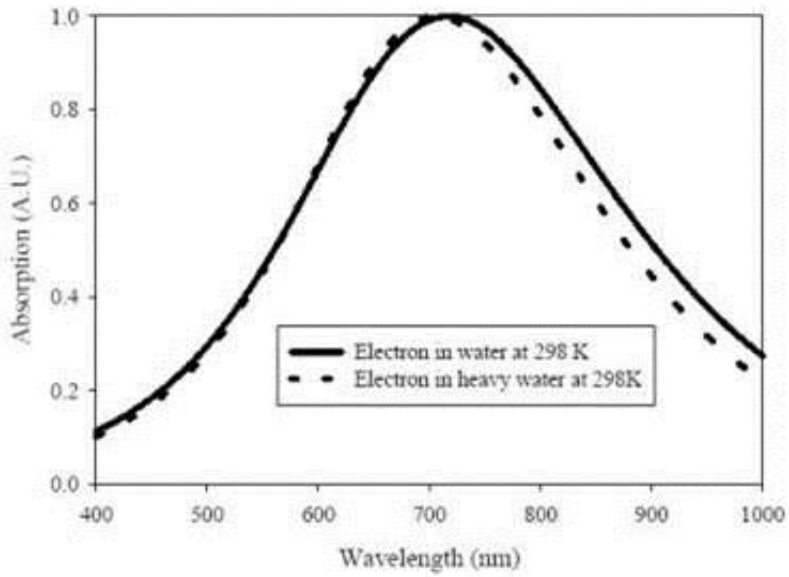

Figure 7.2 The characteristic absorption spectrum of the hydrated electron in normal water and heavy water [18].

Solvated electrons in ILs (referred to here as IL-solvated electrons) are less studied, but are often described as an electron trapped in a solvent matrix, much like an F-centre in ionic crystals [10]. It has been reported that the solvated electrons in ILs have absorption in the near infrared region (~ 900 to 1400 nm) with, similar to hydrated electrons, a broad spectral band and a decay characteristic to their high reactivity [1, 2]. For example, the absorption spectrum of the solvated electron in methyltributylammonium bis(trifluoromethylsulfonyl)imide shows a very broad absorption band peaking at 1410 nm with $\varepsilon_{1410\,nm} = 2.2 \times 10^4$ L•mol^{-1}•cm^{-1} (Figure 7.3).

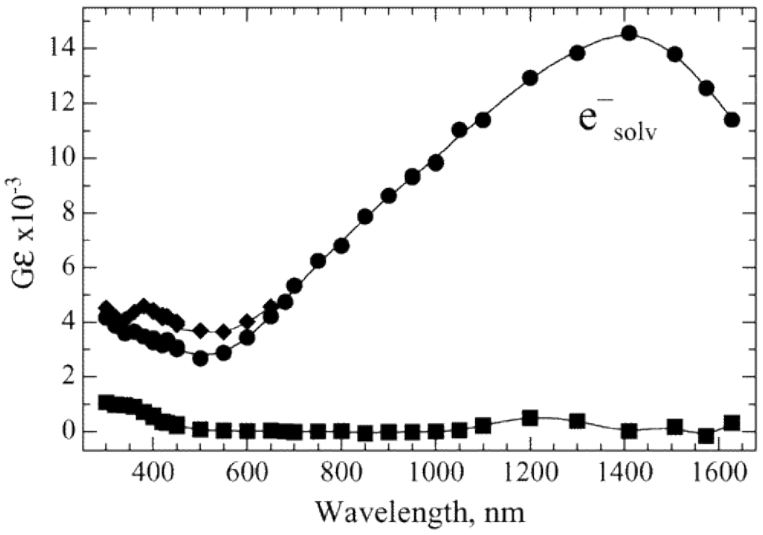

Figure 7.3 The absorption spectrum of a solvated electron observed after pulse radiolysis of methyltributylammonium bis(trifluoromethylsulfonyl)imide; (♦) species with a 50 ns lifetime, (●) species with a 300 ns lifetime, and (■) residual absorbance at 1 μs [1].

The decay rate of IL-solvated electrons varies depending on the type of IL [1]. In methyltributylammonium bis(trifluoromethylsulfonyl)imide the decay time was found to be 3.3×10^6 s^{-1} (giving a lifetime of 300 ns) [1]. No decay constant has been reported for

the phosphonium ILs studied here. The lifetime of a hydrated electron in pure water at neutral pH is known to be on the order of 1 μs [20]. In pure water the main decay path for a hydrated electron is the reaction with H_3O^+. The lifetime of hydrated or IL-solvated electrons will be shortened in the presence of solutes or surfaces (or interfaces) that can react easily with them. Measurements of changes in the decay kinetics of solvated electrons have been successfully employed to obtain second-order rate constants for hydrated or solvated electron reactions with various solutes [21].

7.2.2 Project Objective and Methodology

The studies described in earlier chapters have shown that, even in the absence of radiation, micelles and reverse micelles develop at the interface between a highly viscous IL and water. Slow exchange of ions between the two phases and the surfactant activity of the long alkyl chains on the phosphonium cation facilitate the micelle and reverse micelle formation. The formation of micelles further promotes interfacial mixing and an emulsion layer develops from near the water/IL interface and slowly expands further into the IL phase, see Figure 7.4.

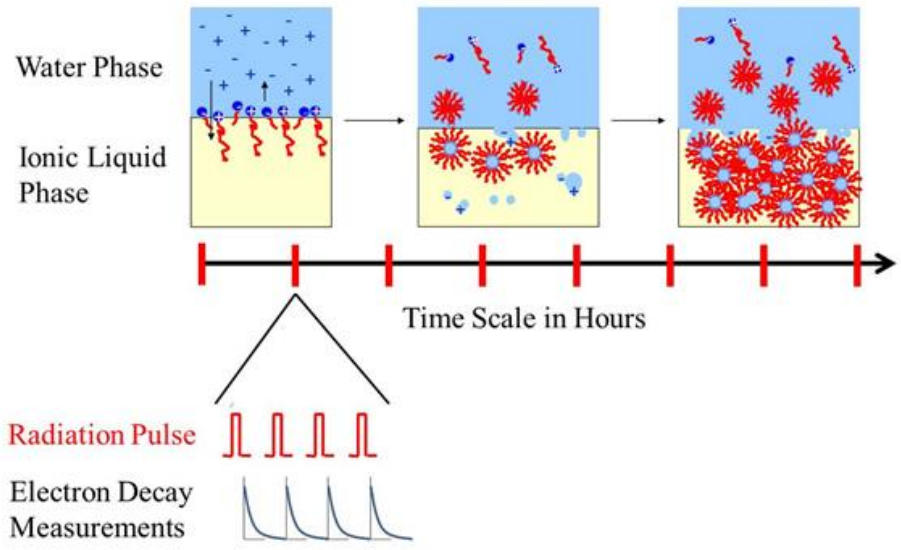

Figure 7.4 Schematic of the time evolution of an water/IL system. Vertical red lines along the time scale are times for application of the pulse radiolysis.

The presence of reverse micelles and an emulsion in a water/IL system provides an interesting opportunity to study the effect of very small solvent volumes and high surface areas on the dynamic behaviour of solvated electrons. The production and decay of solvated electrons formed by pulse radiolysis at set time intervals can be followed over the time period of the emulsification of the water/IL system, by applying radiation pulses at intervals as illustrated in Figure 7.4. At each interval the sample was pulsed repeatedly to collect the spectra in the ultraviolet-visible and infrared region For these experiments, radiation is delivered to the system in very short pulses (of length 150 ps). The decay of solvated electrons that are produced by these pulses are then followed using the light absorption technique.

In this initial study the water/amide-IL and water/dicyanamide-IL systems whose biphasic mixing behaviours were observed to be different were investigated. Although

the pure imidazolium dicyanamide-IL has been previously studied by other groups, the phosphonium-based ILs have not been studied [22, 23].

7.3 EXPERIMENTAL

The polarity of the two ILs used in these tests (amide-IL and dicyanamide-IL) was measured using Reichardt's betaine-30 dye (betaine-30, Sigma Aldrich), which is visually dark blue at neutral and basic pH values (≥ 7) and exhibits a green hue at acidic pH values. Neutral and basic pH values are desired in these experiments to minimize solvated electron quenching by acidic species. Initial dye tests indicated that the amide-IL received from Sigma Aldrich was too acidic and required further purification, while the dicyanamide-IL did not require such treatment (Figure 7.5). To purify the amide-IL, 150 μL aliquots of 200 mM NaOH (Sigma Aldrich) were added to the amide-IL to counter the acidic impurities. After mixing for 30 min, water (purified to a consistent resistivity of 18.2 MΩ·cm (Milli-Q Plus PF)) was added to the mixture to extract the basic NaOH aqueous phase using centrifugation, and the amide-IL was recovered from the centrifuge. This rinsing was carried out a total of three times. Any excess water remaining in the IL after the final separation was removed using a rotary evaporator followed by drying in an oven at 50 ºC. A Karl Fischer titration of the IL after drying confirmed that the water content in the amide-IL was < 2000 ppm. The dicyanamide-IL sample did not need to be purified and a Karl Fischer titration of this IL indicated that its water content was less than < 2000 ppm.

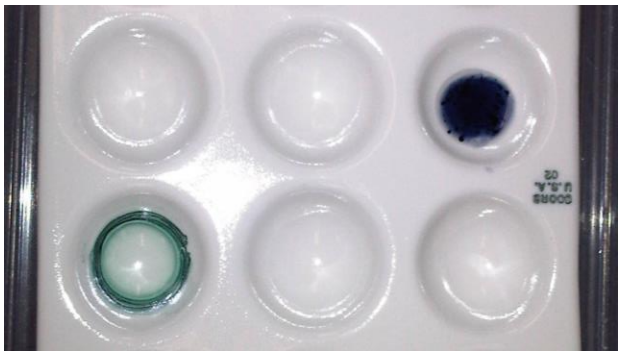

Figure 7.5 The betaine-30 dye test of the amide-IL (lower left corner) exhibiting a green hue that indicates the presence of acidic impurities and the test of the dicyanamide-IL (upper right corner) exhibiting a blue hue that indicates the presence of basic impurities.

Prior to each experiment, aliquots of water and IL were bubbled with argon for 20 min to remove any dissolved oxygen (which could react with the solvated electron). The two phases were then added to a 1-cm path length cuvette to form the water/IL system. The test cuvette was topped with a septum cap.

Experiments were performed at the Brookhaven National Laboratory Laser-Electron Accelerator Facility. Using an RF photocathode, the electron accelerator was able to produce electron pulses of 150 picosecond width. The radiolytic dose deposited in the test sample was between 20-30 gray per pulse. To minimize the impact of radiated heating of the samples, the temperature of the targets was maintained at a constant 21 ºC. A pulsed xenon arc lamp provided incident light for solvated electron absorption analysis. Band-pass filters were used to select the appropriate wavelengths for analysis. Either FND-100Q silicon (≤ 1050 nm) or GAP-500 InGaAs (≥ 900 nm) photodiodes collected transient absorption signals which were digitized using a Tektronix TDS-680B oscilloscope [1]. Data from the oscilloscope was collected and processed using custom routines written in LabVIEW (National Instruments). The data was analyzed with Igor

Pro software (WaveMetrics, Inc., Lake Oswego, OR) using customized programs developed at LEAF.

7.4 RESULTS AND DISCUSSION

7.4.1 Trihexyltetradecylphosphonium Dicyanamide

7.4.1.1 *Transient Absorption Spectra*

The dicyanamide-IL test samples were prepared in cuvettes as pure IL or water/IL systems. The absorption spectra of the pure dicyanamide-IL showed very low absorbance in range of 500 – 1700 nm and no distinct absorption bands could be identified. However, the absorption spectra of the water/dicyanamide-IL system, after contact for 2 days, exhibited several broad bands, Figure 7.6. The absorption appears to include a broad band with its maximum at ~900 nm, a second broad band at ~1400 nm (best seen in the 16 ns spectrum) and possibly another band at ~650 nm. Initially, the band at 900 nm dominates the spectrum, but at later times the bands at 1400 nm and 650 nm become more important and the absorption intensity of the broad band at 900 nm is virtually absent after 16 ns. These results suggest that at least three different transient species are produced in the water/dicyanamide-IL systems by pulse radiolysis.

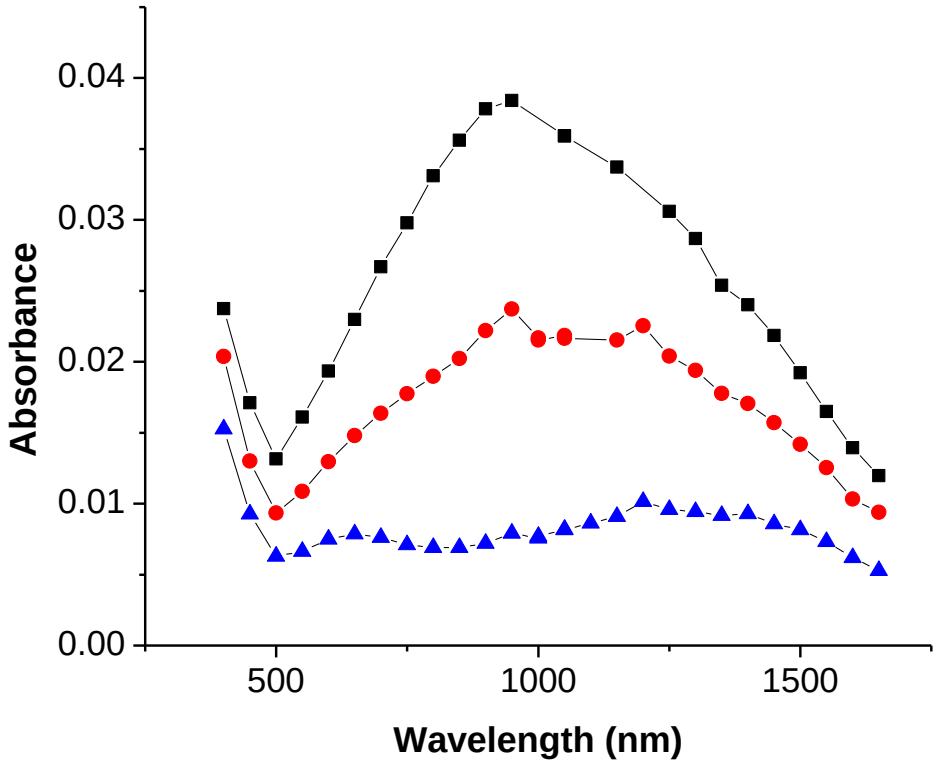

Figure 7.6 The transient absorption spectra of a dicyanamide-IL/water system after 2 d of contact time; spectra obtained ■ 4 ns, ● 16 ns, and ▲ 50 ns after pulse application.

7.4.1.2 *Decay Profiles*

To determine what these transient species might be, the decay kinetics of the transient species were followed by monitoring the absorbances at wavelengths near the band maxima, 650nm, 900 nm and 1400 nm. Due to significant overlaps between the absorption bands of the transient species the decay profiles at band maxima showed complex behaviour. All of the decay profiles required two first-order decay constants for a good fit with the data over the time period of 0 - 1 μs:

$$I_t = I_{z,1} \cdot e^{-k_1 t} + I_{z,2} \cdot e^{-k_2 t} \qquad (7.2)$$

where I_z and I_t represent absorption intensities at time zero and t, respectively, and k_1 and k_2 represent the first-order decay rate constants for the species 1 and 2 responsible for the absorbance.

7.4.1.3 *Decay Behaviour of the Absorbance at 900 nm*

The decay profiles of the absorbance at 900 nm obtained for pure dicyanamide-IL and water/dicyanamide-IL systems are compared over a short time period (50 ns following a radiation pulse) in Figure 7.7 and at longer times in Figure 7.8. The decay profiles obtained at 650 nm are also shown in Figure 7.7 and are discussed in section 7.4.1.4. Also shown in Figure 7.8 are the fits to the absorbance profiles using equation 7.2. The decay constants determined from these fits are listed in Table 7.1.

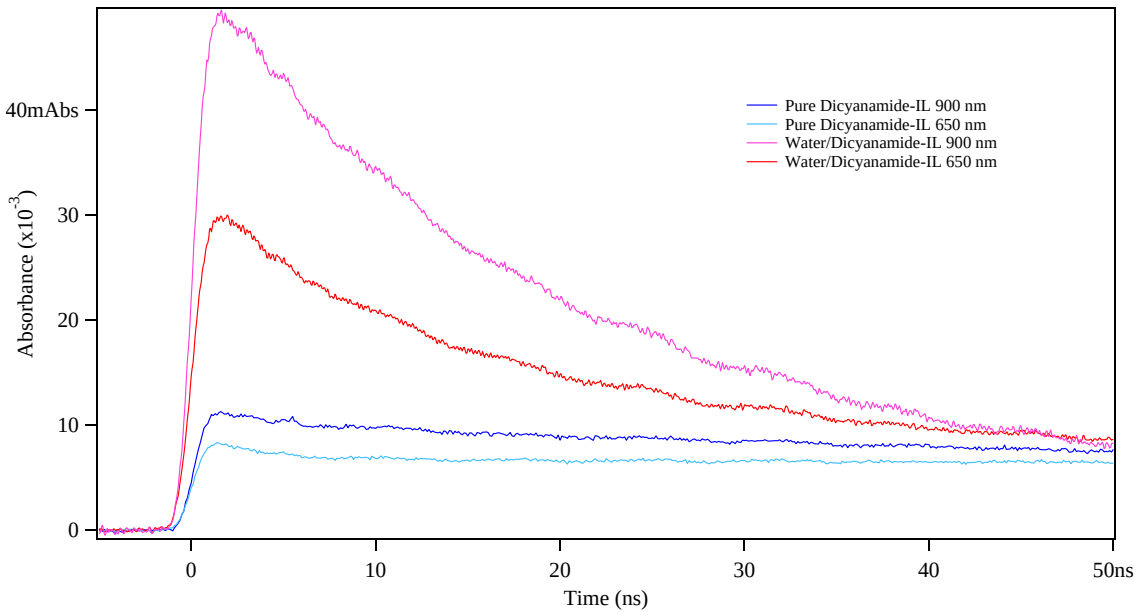

Figure 7.7 The decay curves for the pure dicyanamide-IL at 650 nm (light blue) and 900 nm (dark blue), and for water/dicyanamide-IL at 650 nm (red) and 900 nm (fuchsia).

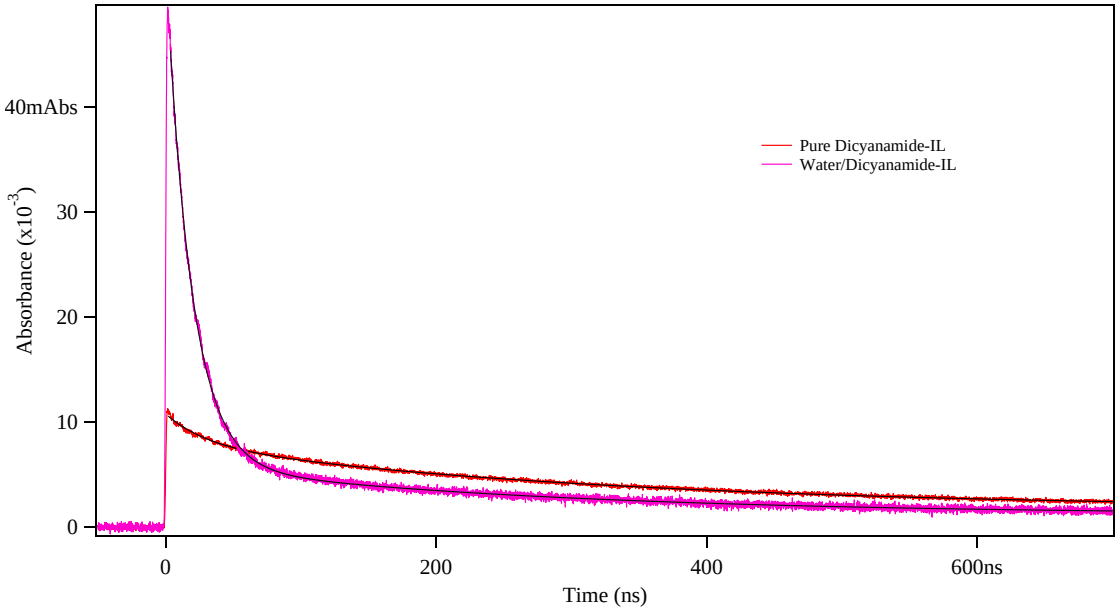

Figure 7.8 The decay profiles of the absorbance at 900 nm obtained for pure dicyanamide-IL (red) and the water/dicyanamide-IL system (fuchsia). The black lines (superimposed on most of the curves) are the fits of the absorption equation 7.2.

Table 7.1 Decay constants determined from fits to the absorbance profiles using equation 7.2.

Samples	**pure dicyanamide-IL**		**water/dicyanamide-IL**	
	k_1 (s^{-1})	k_2 (s^{-1})	k_1 (s^{-1})	k_2 (s^{-1})
1400 nm **1350 nm** **1300 nm**			4.5×10^7 4.2×10^7 4.6×10^7	8.7×10^6 7.9×10^6 8.4×10^6
900 nm	3.4×10^7	3.0×10^6	5.2×10^7	3.5×10^6

Figure 7.7 shows that the absorption intensity at 900 nm at short times is much greater in the water/dicyanamide-IL system than in pure dicyanamide-IL. This indicates

that the radiolytic yield of the transient species responsible for the absorption at 900 nm is significantly higher in the IL/water system than in pure IL.

The need to use two decay constants to fit the experimental data indicates that there are two different species responsible for the absorbance at 900 nm. The faster decay process (associated with decay constant k_1) has rates of 3×10^7 s^{-1} and 5×10^7 s^{-1} for the pure dicyanamide-IL and water/dicyanamide-IL, respectively. The decay rate is slightly higher in the water/dicyanamide-IL system than in pure dicyanamide-IL and both rate constants are faster than those expected for chemical-reactions of hydrated or IL-solvated electrons. These rate constants are on the order magnitude of radiative decay rates of allowed electronic transitions [1]. Hence, the fast decay component of the absorption band with its maximum at 900 nm is assigned to an electronically excited IL species, IL*, formed by pulse radiolysis.

The 2^{nd} decay constants obtained from the absorbance profile at 900 nm are an order of magnitude smaller and the same (within experimental uncertainty) in the pure dicyanamide-IL and in the water/dicyanamide-IL, (3.0×10^6 s^{-1} and 3.5×10^6 s^{-1} respectively). These values are on the same order of magnitude as the decay rates of IL-solvated electrons that have been reported for other pure ILs [1]. Because we see the same decay in both the IL and the water/IL samples, we attribute the slower decaying absorbance at 900 nm to the presence of electrons solvated in dicyanamide-IL. As discussed in section 7.4.1.5, the broad absorption band centred at 1400 nm that becomes more visible at longer times (Figure 7.6) is also attributed to the dicyanamide-IL-solvated electron. While the absorption band centred at 1400 nm significantly overlaps with the band centred at 900 nm, at longer times this overlap is much reduced by the fast decay of

the electronically excited IL species. At these longer times the decay constant of the IL-solvated electron is better obtained from the absorbance profile at 1400 nm.

7.4.1.4 *Decay Behaviour of the Absorbance at 650 nm*

The short-term (< 50 ns) decay profiles of the absorbance at 650 nm obtained for the pure dicyanamide-IL and dicyanamide-IL/water systems are shown in Figure 7.7. For both systems, the decay profiles show that, although the absorption intensity at 650 nm is significantly lower than that at 900 nm, the decay rate at 650 nm is similar to that obtained at 900 nm. This is consistent with the transient absorption spectrum being dominated by the strong broad band with its maximum at 900 nm (Figure 7.6). The short-term decay profile at 650 nm is mostly due to the decay of the electronically excited IL species that is responsible for the band with its maximum at 900 nm.

At longer times after the radiation pulse (> 100 ns) the absorbance at 650 nm shows a very different decay profile, Figure 7.9. The absorbance decay rate at 650 nm decreases and then it increases again at longer times (50 – 200 ns). This decay profile indicates the presence of an additional transient species that contributes to the absorbance at 650 nm. The decay rate of this transient species was obtained from the absorption decay over the range 0.3 – 1.0 μs. The decay rate constant of this transient species was determined to be 2.5×10^6 s^{-1} in the water/dicyanamide-IL and 1.3×10^6 s^{-1} in the pure dicyanamide-IL. The broad absorption band centred at 650 nm and the values of the decay constants for this band suggest that the transient species responsible for the absorption could be a hydrated electron. Existence of a hydrated electron in pure dicyanamide-IL, given our efforts to remove water from the test material, is difficult to

explain. However, the absorbance in pure dicyanamide-IL is very small and we may be just seeing the behaviour of the tail of the absorption by a species that absorbs at wavelengths below 500 nm (Figure 7.6). We have not studied this absorption or identified the responsible species.

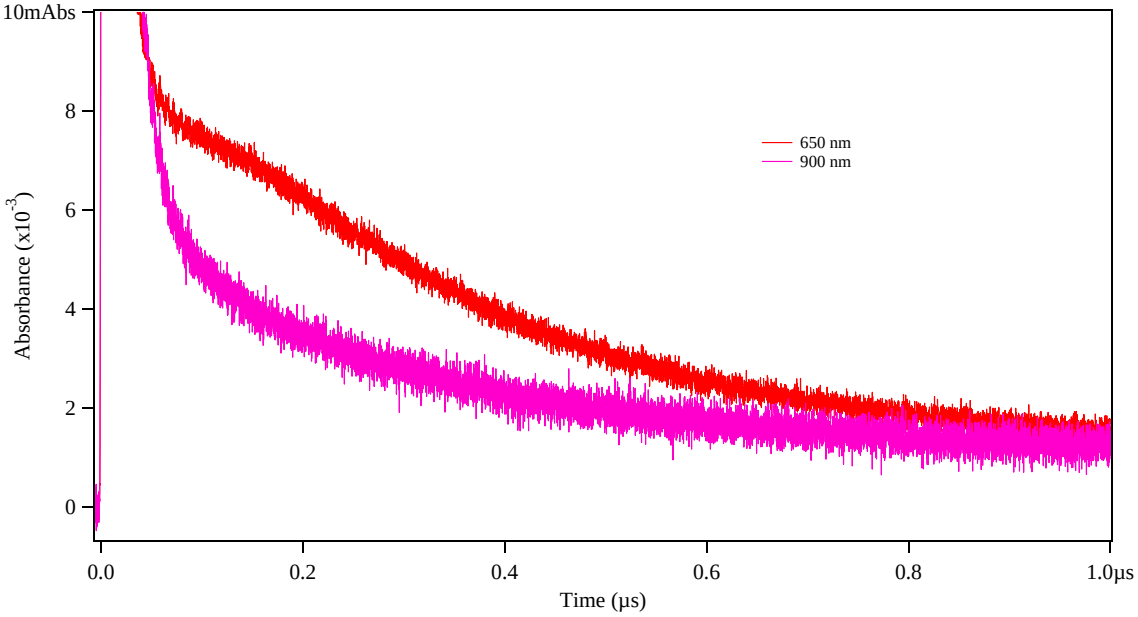

Figure 7.9 The decay curves for the water/dicyanamide-IL system at 650 nm (red) and 900 nm (fuchsia).

7.4.1.5 *Absorbance Decay Profiles at 1300 - 1400 nm*

Decay profiles at wavelengths around 1400 nm were also obtained for the the water/dicyanamide-IL system (Figure 7.10). Due to limited access time to the LEAF facility, the decay profiles for pure dicyanamide-IL at these wavelengths were not obtained. As for the absorbance at 900 nm, the decay at 1400 nm required two decay constants for a good fit (also shown in Figure 7.10). The two decay constants obtained from this fit are listed in Table 7.1.

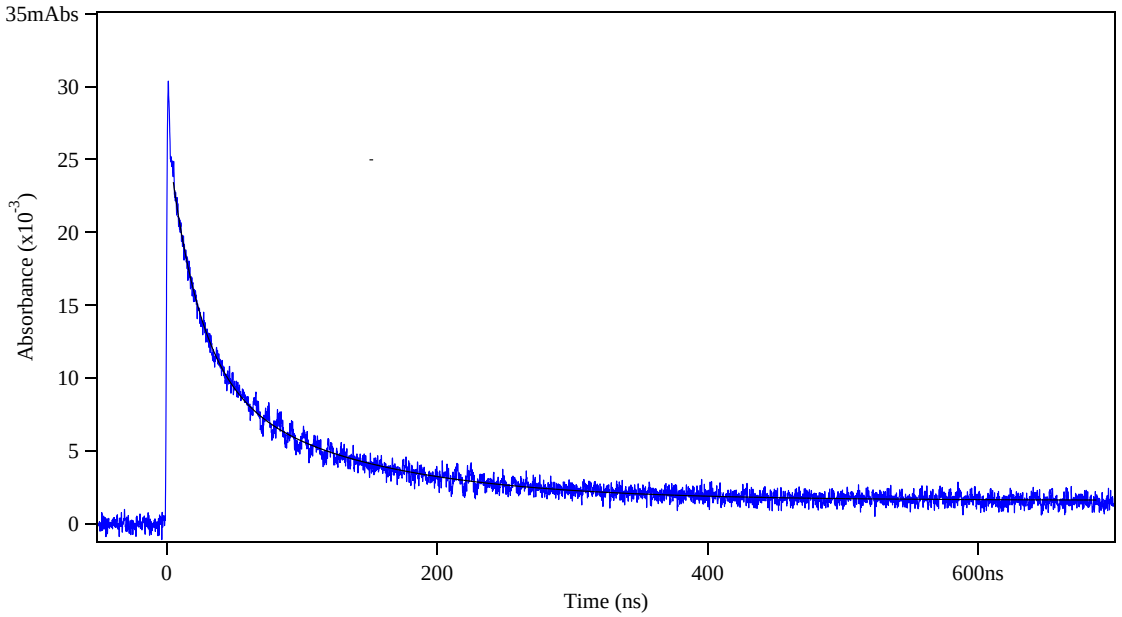

Figure 7.10 The decay profile of the absorbance at 1400 nm for the water/dicyanamide-IL system. The black line superimposed on the data is the fitted line.

The 1st decay constant obtained from the absorbance profile at 1400 nm is similar in value to the 1st decay constant obtained at 900 nm. As described above, the electronically excited IL species are likely responsible for the strong absorption band with its maximum at 900 nm and the tail of this band at 1400 nm can explain the similarity in the short-term decay constants. However, a broad absorption band centred at 1400 nm is clearly visible at longer times when most of the electronically excited IL species has decayed away (Figure 7.6). Measurements at 1300 nm and 1350 nm all produced the same decay constants as those obtained at 1400 nm showing that overlap from a band at 900 nm is no longer important at the longer times.

The 2nd decay constants obtained from the absorbance at wavelengths in the range of 1300 nm - 1400 nm are $(8.4 \pm 0.4) \times 10^6$ s^{-1} (Table 7.1). These values are on the same order of magnitude as the decay rates of IL-solvated electrons that have been reported for pure ILs [1]. We believe the IL-solvated electron is responsible for the broad absorption band with its maximum at 1400 nm (Figure 7.6) and that this 2nd decay constant is due to the decay of the IL-solvated electron in water/dicyanamide-IL.

The decay rate of the IL-solvated electron obtained from the absorbance profile at 1400 nm is about twice as large as the 2nd decay constant derived from absorption at 900 nm which we also attributed to the decay of the IL-solvated electron. However, we believe that the absorbance decay at 900 nm, even at long times, is compromised by a contribution from faster electronic decay processes. The 2nd decay constant derived from the absorbance at 1400 nm, at which other IL-solvated electrons are known to have maxima, more accurately reflects the decay rate constant for the IL-solvated electron. This decay constant is determined to be $(8.4 \pm 0.4) \times 10^6$ s^{-1} in the water/dicyanamide system. To date, the decay profiles at wavelengths longer than 900 nm have been studied only for water/dicyanamide-IL and the effect of the dispersed water phase on the lifetime of the IL-solvated electron could not be determined. However, the similarity of the 2nd decay constants obtained at 900 nm and 1400 nm suggests that the effect of water micelles on the decay of the IL-solvated electron is small.

7.4.1.6 *Summary on the Transient Species Observed in the Dicyanamide-IL*

It has been reported that solvated electrons in some other ILs have broad absorption spectra that peak typically around 1000 nm, but with some variation

depending on the different ILs [1, 2]. We have also observed a broad absorption band centred around 900 nm for the dicyanamide-IL. However, analysis of the time dependent behaviour of this absorbance is best fit with two decay constants and this indicates that two different transient species are responsible for the absorbance at this wavelength. The 1^{st} decay rate constant for the absorbance at 900 nm is high, $3\text{-}5 \times 10^{7}$ s^{-1}. Thus, this decay rate is attributed to the radiative decay of an electronically excited IL species. The initial absorbance at 900 nm is significantly higher in the water/dicyanamide-IL system than in pure dicyanamide-IL, indicating that the radiolytic yield of the electronically excited IL species during the 150 ps radiolysis is increased when the IL is dispersed in a water phase (in micelle forms).

Our results indicate that the dicyanamide-IL solvated electron has a broad absorption band with its maximum at 1400 nm and that this band contributes to absorption at 900 nm. The 2^{nd} decay constant observed for the absorbance at 900 nm is attributed to the decay of the dicyanamide-IL solvated electrons. Due to the strong absorption at 1400 nm by the electronically excited IL species the short-term absorbance profile at this wavelength is still influenced by the decay of IL*. However, the 2^{nd} decay constant at 1400 nm is 8.7×10^{6} s^{-1} (lifetime of 120 ns) and it is attributed to the decay of the IL-solvated electron. Due to a lack of data on the decay profiles at 1400 nm in the pure dicyanamide-IL, the effect of the presence of the dispersed water phase (in micelle forms) on the production and decay of the IL-solvated electron is yet to be determined.

7.4.2 Trihexyltetradecylphosphonium Bis(trifluoromethylsulfonyl)amide

Transient spectra were also collected for amide-IL and water/amide-IL systems (Figure 7.11). The spectra of a water/amide-IL system exhibited two bands, a narrower band centred at ~ 450 nm and a broader band in the wavelength range of 500 – 900 nm. Due to limited facility access time, we were not able to obtain the spectra at longer wavelengths. The spectra of the amide-IL systems show no absorption band with a maximum at 900 nm like that seen in dicyanamide-IL systems. This result further supports our proposal that the 900 nm band observed in the dicyanamide-IL is due to an electronically excited species of that IL, since each IL molecule will produce a unique set of electronically excited species upon radiolysis.

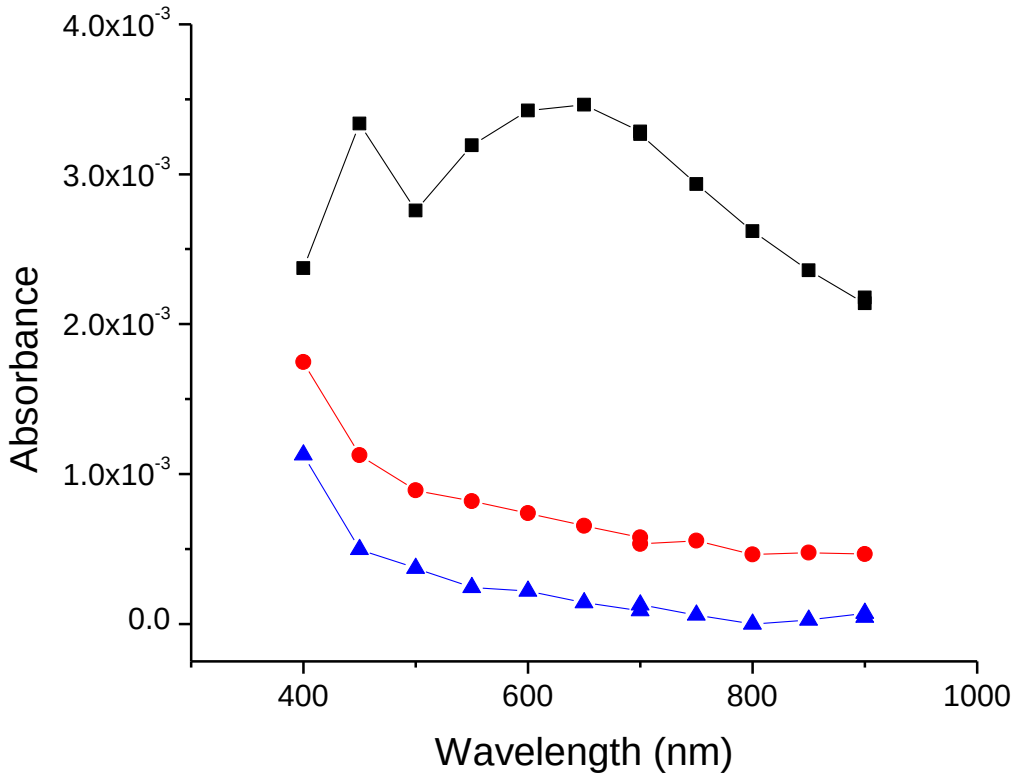

Figure 7.11 Transient spectra obtained from a water/amide-IL system after 2 d of contact time; ■ 1 ns, ● 10 ns, and ▲ 200 ns after a radiation pulse.

The absorption bands with their maxima at 450 nm and at 650 nm in the amide-IL spectra overlap considerably. Since the absorbance at 450 nm appears to be strongly influenced by an absorption band centered at shorter wavelengths, only the decay profile of the absorbance at 650 nm was analyzed in detail. Again a good fit to the data required two decay constants (see Figure 7.12 and Table 7.2).

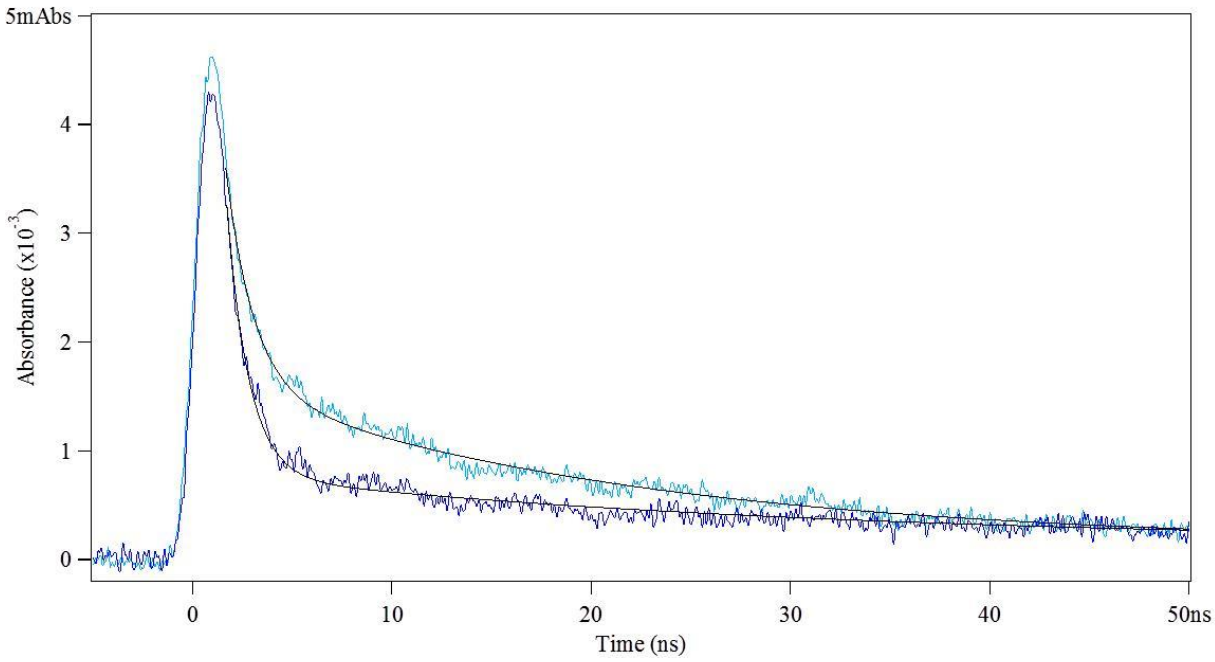

Figure 7.12 The decay curves at 650 nm for pure amide-IL (dark blue) and water/amide-IL (light blue). The black lines are the fitted lines.

Table 7.2 Decay constants determined from the absorbance profiles at 650 nm for amide-IL and water/amide-IL.

pure amide-IL		**water/amide-IL**	
k_1 (s^{-1})	k_2 (s^{-1})	k_1 (s^{-1})	k_2 (s^{-1})
9×10^8 s^{-1}	3.4×10^7 s^{-1}	5.7×10^8 s^{-1}	4.5×10^7 s^{-1}

The decay constants obtained from the absorbance at 650 nm for the amide-IL (with and without water present) are significantly higher than those observed for the water/dicyanamide IL system. The 1st decay constant is larger than the second. The fast

decay (lifetime of ~ 1 ns) is attributed to the radiative decay of an electronically excited IL species which absorbs light at shorter wavelengths. The 2nd decay rate constant (lifetime of 20 to 30 ns) is still faster than normally seen for a chemical reaction rate, even for a reactive radical such as the hydrated electron. Hence, the 2nd decay is also attributed to the radiative decay of a different electronically excited IL species with a maximum absorption at 650 nm.

Due to data limitations the decay constants that we have obtained from the amide-IL experiments have relatively large uncertainties. Within those uncertainties, the decay constants obtained for pure amide-IL are the same as those for water/amide-IL and this suggests that water molecules do not interact appreciably with the electronically excited IL species. The low absorbance at 650 nm (where we would expect to observe hydrated electron absorbance) in the water/amide-IL samples suggests that the production of hydrated electrons is very low in this system.

7.5 SUMMARY

We have initiated a study to examine the dynamic behaviour of hydrated and IL-solvated electrons in water/IL systems. Experiments were designed to examine the production and decay of the electrons as a function of time during emulsification. To date we were only able to study the pure IL and the IL in contact with water for 2 days. Transient species generated by pulse radiolysis in pure IL or water/IL samples and their decays were followed by transient absorption spectroscopy. The preliminary results from these experiments suggest the presence of both electronically excited IL species as well as IL-solvated electrons. However, at this stage, our data is too limited to make strong

connections between the measurements and specific processes in the water/IL system. More extensive, careful examination of the decay profiles in water/IL systems over a wider range of wavelengths and as a function of the time evolution of the mixed water/IL system in the future should provide better information on the nature and decay pathways of the transient species produced by irradiation of water/IL systems.

7.6 ACKNOWLEDGMENTS

Travel funding for this research was provided by the ASPIRE award from the Western University Department of Chemistry. Thanks to Dr. James Wishart and his research group for their assistance and guidance in the experimental process and many helpful discussions.

7.7 REFERENCES

1. J.F. Wishart, P. Neta, J. Phys. Chem. B, 107 (2003) 7261-7267.
2. J.F. Wishart, A.M. Funston, T. Szreder, A.R. Cook, M. Gohdo, Faraday Discuss., 154 (2012) 353-363.
3. Radiation Chemistry: From Basics to Applications in Material and Life Sciences, M. Spotheim-Maurizot, M. Mostafavi, T. Douki, J. Belloni (Eds.) EDP Sciences, France (2008).
4. A.O. Allen, The Radiation Chemistry of Water and Aqueous Solutions, Van Nostrand, New York, NY (1961).
5. A.E. Bragg, J.R.R. Verlet, A. Kammrath, O. Cheshnovsky, D.M. Neumark, Science, 306 (2004) 669-671.
6. P.K. Walhout, P.F. Barbara, Ultrafast Processes in Chemistry and Photobiology, M.A. El-Sayad, I. Tanaka, Y. Molin, (Eds.), Blackwell Scientific, Cambridge, MA (1995).
7. J.F. Yang, T. Kondog, K. Norizawa, R. Nagaishi, M. Taguchi, K. Takahashi, R. Katoh, S.V. Anishchik, Y. Yoshida, S. Tagawa, Radiat. Phys. Chem., 77 (2008) 1233-1238.
8. E.W. Castner, J.F. Wishart, H. Shirota, Acc. Chem. Res., 40 (2007) 1217-1227.
9. S. Arzhantsev, N. Ito, M. Heitz, M. Maroncelli, Chem. Phys. Lett., 381 (2003) 278-286.

10. J.F. Wishart, I.A. Shkrob, The Radiation Chemistry of Ionic Liquids and its Implications for their Use in Nuclear Fuel Processing in Ionic Liquids: From Knowledge to Application, N.V. Plechkova, R.D. Rogers, K.R. Seddon (Eds.), ACS Symposium Series, Oxford University Press, Washington, DC (2009) pp. 119-134.
11. R. Katoh, Y. Yoshida, Y. Katsumura, K. Takahashi, J. Phys. Chem. B, 111 (2007) 4770-4774.
12. A. Asano, J.F. Yang, T. Kondoh, K. Norizawa, R. Nagaishi, K. Takahashi, Y. Yoshida, Radiat. Phys. Chem., 77 (2008) 1244-1247.
13. V. De Waele, I. Lampre, M. Mostafavi, Time Resolved Study on Nonhomogeneous Chemistry Induced by Ioizing Radiation with Low Linear Energy Transfer in Water and Polar Solvents at Toom Temperature in Charged Particle and Photon Interactions with Matter: Recent Advances, Applications and Interfaces, Y. Hatano, Y. Katsumura, and A. Mozumder (Eds.) CRC Press, Boca Raton, FL (2011) pp. 290-318.
14. K.D. Jordan, Science, 306 (2004) 618-619.
15. B. Abel, U. Buck, A.L. Sobolewski, W. Domcke, Phys. Chem. Chem. Phys., 14 (2012) 22-34.
16. C. Silva, P.K. Walhout, K. Yokoyama, P.F. Barbara, Phys. Rev. Lett., 80 (1998) 1086-1089.
17. Photochemistry and Radiation Chemistry: Complimentary Methods for the Study of Electron Transfer, J.F. Wishart, D.G. Nocera, (Eds.), ACS Symposium Series, Oxford University Press, Washington, DC (1998).
18. F.Y. Jou, G.R. Freeman, J. Phys. Chem., 83 (1979) 2383-2387.
19. J. Herbert, Structure and Dynamics of Solvated Radicals, http://chemistry.osu.edu/~herbert/projects/solvated_radicals.html.
20. J.C. Alfano, P.K. Walhout, Y. Kimura, P.F. Barbara, J. Chem. Phys., 98 (1993) 5996-5998.
21. G.V. Buxton, C.L. Greenstock, W.P. Helman, A.B. Ross, J. Phys. Chem. Ref. Data, 17 (1988) 513-886.
22. I.A. Shkrob, S.D. Chemerisov, J.F. Wishart, J. Phys. Chem. B, 111 (2007) 11786-11793.
23. I.A. Shkrob, J.F. Wishart, J. Phys. Chem. B, 113 (2009) 5582-5592.

Chapter 8. Characterization of Ionic Liquid Emulsions and Micelles by Neutron Scattering

8.1 INTRODUCTION

Previous chapters examined the effects of gamma radiation on the gas/IL and water/IL systems and described micelle and emulsion layer formation in some water/IL systems. Analyses as a function of contact time showed that ion exchange and transfer between the IL and aqueous phases occurred, and that the exchange is accelerated by gamma irradiation. The exchange led to micelle and emulsion formation. The presence of micelles was confirmed using dynamic light scattering (DLS) and transmission electron microscopy (TEM).

Though the presence of micelles in the biphasic systems is clear, it is important to characterize the structure and nature of the micelles formed. Small angle neutron scattering (SANS) is a technique useful for the determination of the structure and interactions of micelle systems. The technique can yield information on the number, size and shape of aggregates within a sample, and the location of different molecules or molecular components within the micelles [1-4]. This noninvasive technique can use light and heavy water mixtures in contrast matching experiments to extract these parameters [2, 5].

This chapter studies the formation and characterization of micelles in the amide-IL and the bromide-IL using SANS. Since the water/amide-IL system has led to the easiest micelle identification, the studies were mostly confined to the water/amide-IL system.

All SANS experiments were performed at the National Research Council Canadian Neutron Beam Centre at the Chalk River Laboratories of Atomic Energy of Canada Limited. The N5 neutron beam of the National Research Universal (NRU) reactor provides a means of measuring structures between ~ 2 – 110 nm, and this size range corresponds with our micelle size range as determined by light scattering and TEM in chapter 5 [6, 7].

8.2 EXPERIMENTAL

8.2.1 Sample Preparation

The ionic liquids trihexyltetradecylphosphonium bis(trifluoromethylsulfonyl)amide (amide-IL) and trihexyltetradecylphosphonium bromide (bromide-IL) were purchased from Sigma Aldrich. Quartz cuvettes of 2 mm sample path-length, with caps, were used as test vials in the neutron beam.

Biphasic water/IL samples were prepared in an aerated atmosphere and exposed to gamma radiation at Western University to accelerate the ion transfer and formation of the emulsion layer. Test samples were irradiated for 24 h and then allowed to sit in contact for 48 h. For neutron scattering experiments biphasic water/IL samples were prepared by: (a) extracting a portion of the emulsified and already irradiated IL phase and depositing it in the cuvette, and (b) extracting a portion of the already irradiated water phase and depositing it on top of the IL phase in the quartz cuvette.

Fresh biphasic amide-IL and bromide-IL samples were also prepared with heavy water (deuterium oxide, D_2O, 99.9 % isotopic purity) or water directly in quartz cuvettes. Fresh samples were prepared by: (a) depositing a portion of the chosen IL at the bottom

of the quartz cuvette, followed by (b) depositing the heavy water or water on top of the IL phase using a syringe. The sample was then capped. Some of these samples were run immediately, while others were allowed to sit in contact for an extended period of time to allow for emulsion formation.

8.2.2 Sample Analysis

The quartz cuvettes were placed in a sample holder specially designed for our experiments. The zirconium holder had five cuvette locations around an electronically controlled rotating axis. This allowed for switching of cuvettes in and out of the neutron beam remotely using a computer control. The sample holder was temperature controlled. Measurements in the neutron beam were calibrated by measuring the neutron scattering background of the empty holder and cuvettes with pure-ILs, pure light water, and pure heavy water.

As discussed in Chapter 3, the resulting measurements of neutron flux as a function of scattering angle were analyzed using methods developed and customized by researchers at the Canadian Neutron Beam Centre. These methods will not be discussed in detail.

8.3 RESULTS

When studying IL systems using SANS, the object of the experiment was to measure the q value of a sample, or the differential cross section per unit of volume. Data reduction from the q value results in a SANS curve, which can be analyzed for full system information and characterization (chapter 3). Thus, initial experiments involved

the collection of data from an empty sample holder and from pure-IL and water samples to obtain a background signal. Following the collection of the background signal in each cuvette size, biphasic sample cuvettes were placed in the automated neutron scattering apparatus and scattering data were accumulated over a period of 24 h. Over this duration, the neutron beam was tuned through a range of wavelengths.

The biphasic water/amide-IL sample that was previously irradiated in the gamma cell at Western University contained a clear water layer and a cloudy amide-IL emulsion layer. Following lengthy data collection in the neutron beam, no difference was observed between the scattering signal from this sample and background samples. Tests of this sample were repeated over a period of two weeks and there was no change in this result. A sample of the water/bromide-IL system was prepared in the same manner and this also gave no changes in the scattering curve from background scattering data.

Biphasic samples containing fresh heavy water/IL were placed in the neutron beam and data collection continued for 16 h to 36 h to determine any differentiation in the sample or any scattering. The longer time period allows for the greater data collection required for analysis at low q values [6]. Again the results showed no difference between the test sample and the background scattering data. Even with long contact times between the two phases and the visually apparent emulsion layer, SANS appeared unable to detect structures in the emulsion.

One possible explanation for the failure to see micelles using SANS was rapid aggregation of the micelles in the samples into large structures that were outside of the range of detection of the N5 instrument (i.e., > 110 nm). In an effort to reduce the aggregation time for micelles in the IL phase, the time required to transport the samples

from Western University to Chalk River was eliminated. Emulsified water/IL samples were prepared by staff of the Reactor Chemistry and Corrosion Branch at AECL using a 2.5 MeV Van de Graaff accelerator (High Voltage Engineering Inc.). The Van de Graaff was operated at 2.25 MeV in repetitive pulse mode (maximum rate of 2 μs pulses at 5 pulses per second). Each pulse provided approximately 50 Gy in deposited energy as determined by chemical dosimetry using a "Super Fricke" dosimeter. Running the initial samples at the maximum pulse rate resulted in the sample overheating. After some testing, irradiation was carried out with 2 μs pulses at 1 pulse·s^{-1} without overheating.

Due to time constraints, only the amide-IL was studied in this manner. Samples of amide-IL and heavy water were irradiated using the Van de Graaff for various periods of time from 2 minutes (6 kGy total deposited energy) to 20 minutes (60 kGy deposited). Visual examination of the samples after irradiation confirmed various stages of emulsion development, with the IL layer varying between clear and cloudy depending on the irradiation time.

These samples were then quickly placed in the neutron scattering instrument and scattering data were collected for extended periods of time (minimum 16 h). The N5 instrument was also pushed to the lowest and highest limits of q that it could provide. Unfortunately, the results were the same; no differences were observed between the collected SANS data and the background signal.

8.4 DISCUSSION

Despite repeated efforts and experimental adaptations, we were unable to detect any structures in our test samples using SANS. This is not a unique experience, as other

studies have had difficulty characterizing micelles in ILs using SANS techniques. When examining the formation of micelles using imidazolium cation based ionic liquids, Anderson *et al.* [8] found that the aggregates formed resulted in no usable SANS signal, whether using deuterated surfactants or not. Measureable signals were only obtained when the sample conditions were below the critical micelle concentration (CMC) and they contained very low numbers of aggregates. In other work to determine critical aggregation concentrations (CACs), Bowers *et al.* [9] used surface tension measurements in conjunction with conductivity measurements to determine CAC values, as the bizarre scattering patterns provided by SANS data could not be fit and did not allow for a CAC determination. Sastry *et al.* [10] found no measurable differences in SANS peaks from the background because the aggregates of ILs were simply too small. The work of other researchers, as well as this study, illustrate that using SANS to collect information and characterize micelles can be very difficult. The system must contain micelles that meet limited size and concentration criteria to allow for data collection.

The work of others above shows that SANS can be used to characterize IL micelles (if at all) in the period prior to the critical aggregation concentration or the critical micelle concentration [8-10]. It is unknown at exactly which point this occurs in the water/amide-IL system (irradiated or otherwise) and there may only be a miniscule window of opportunity for effective SANS analysis, which evaded us. A further complication arises in trying to use neutron scattering as an analysis technique when it is so sensitive to the state of micelle formation. A neutron flux provides a source of ionizing radiation and, as determined previously, radiation accelerates the transfer of ions across a biphasic sample [11] and accelerates micelle formation. During the long times

required to collect neutron scattering data, the radiation may cause the system to rapidly transit through the period during which CMC occurs and greater aggregation of micelles begins. This could make SANS analysis extremely challenging.

The lack of a cold neutron source at the NRU facility is also a detriment. A cold neutron source is normally used in dedicated SANS facilities to produce a focused neutron beam with low energies (longer wavelength). At the NRU facilities, the N5 beam was adapted for use in SANS measurements but the adaptation may not have been adequate for this study [6]. A consequence of this adaptation is that data collection takes a long time. As well, counting statistics at the N5 SANS facility tested weakly in comparison to dedicated facilities, due to a smaller detector area and greater interference from air scattering [6]. These factors may have impacted our experiments heavily.

8.5 CONCLUSIONS

The water/amide-IL and water/bromide-IL systems were studied using small angle neutron scattering in an attempt to characterize the micelle formation in biphasic samples. Despite numerous attempts, experimental adaptations, and alterations in data collection, no signals that differed from background scattering were observed. This occurred despite the fact that an emulsion was clearly visible in the tested samples. Although surprising, this is not the first study to encounter difficulties using SANS techniques for the determination of micelle and aggregate formation in ILs [8-10]. Large aggregations, small micelle sizes, and SANS curves that cannot be fit have all hindered the study of IL micelles and their characterization using a neutron beam. Although, at this point it is uncertain why the samples studied here did not provide useful scattering

data, a couple of factors could have been important. The aggregate size may have been outside of the size range of the N5 instrument, and the neutron source was not ideal. Such limitations could be overcome by performing experiments at a different dedicated SANS facility. However, a more complete understanding of micelle formation in the water/IL systems, including knowledge about the critical micelle concentration would aid with troubleshooting and adapting SANS experiments in order to obtain useful results.

8.6 ACKNOWLEDGEMENTS

Travel funding for these experiments was provided by the Canadian Institute for Neutron Scattering. Thanks to Dr. Norbert Kucerka and Dr. Zin Tun at the Canadian Neutron Beam Centre for their helpful discussion and assistance in performing the experiments. We would also like to thank Dr. Craig Stuart and Dr. Patrick Causey for their assistance in using the Van de Graaff accelerator.

8.7 REFERENCES

1. C. Hardacre, J.D. Holbrey, C.L. Mullan, T.G.A. Youngs, D.T. Bowron, J. Chem. Phys., 133 (2010) 074510-1 - 074510-7.
2. P.S. Goyal, V.K. Aswal, Curr. Sci., 80 (2001) 972-979.
3. J.B. Hayter, J. Penfold, Colloid Polym. Sci., 261 (1983) 1022-1030.
4. Z Modern Techniques for Characterizing Magnetic Materials, Y. Zhu (Ed.), Kluwer Academic Publishers, Boston, MA (2005).
5. S.H. Chen, Annu. Rev. Phys. Chem., 37 (1986) 351-399.
6. M.P. Nieh, Z. Yamani, N. Kucerka, J. Katsaras, D. Burgess, H. Breton, Rev. Sci. Instrum., 79 (2008) 095102-1 - 095102-6.
7. M.P. Nieh, Z. Yamani, N. Kucerka, J. Katsaras, J. Phys.: Conf. Ser., 251 (2010) 012061-1 - 012061-4.
8. J.L. Anderson, V. Pino, E.C. Hagberg, V.V Sheares, D.W. Armstrong, Chem. Commun., 19 (2003) 2444-2445.
9. J. Bowers, C.P. Butts, P.J. Martin, M.C. Vergara-Gutierrez, R.K. Heenan, Langmuir, 20 (2004) 2191-2198.

10. N.V. Sastry, N.M Vaghela, P.M. Macwan, S.S Soni, V.K. Aswal, A. Gibaud, J. Colloid Interface Sci., 371 (2012) 52-61.
11. S.E. Howett, J.M. Joseph, J.J. Noël, J.C. Wren, J. Colloid Interface Sci., 361 (2011) 338-350.

Chapter 9. Summary and Future Work

9.1 SUMMARY

The effects of ionizing radiation on phosphonium-based ionic liquids have been explored. Phosphonium-based ILs are relatively radiation resistant in a gamma radiation field. From electrochemical impedance spectra and Raman spectra, it can be seen that the ILs experienced negligible radiolytic degradation. Those products that were detected in a cover gas were attributed to the degradation of the ILs. The absence of oxygenated species in the gas phase (with air present) shows that radiation-induced reactions of organic radicals with O_2 at the gas/IL interface are negligible.

The behaviour of water/phosphonium-based IL systems is more complex. Even for ILs considered to be immiscible with water, biphasic mixing occurs during extended periods of contact between the two phases. Ions are transferred from the IL phase to the water phase and, when the concentration of these ions reaches the critical micelle concentration in the water phase, micelles and reverse micelles are formed at or near the interface. Migration of the micelle species into the two phases induces mixing between the two phases and the interfacial region expands, further accelerating micelle and reverse micelle formation. With time, reverse micelles in the IL phase swell and aggregate to eventually form a distinct emulsion layer. Gamma radiation acts to accelerate the process of micelle and emulsion formation. This is thought to occur through the production of radiolytic decomposition products that act as loci for micelle formation at the interface.

The differing behaviours of an amide-IL and a dicyanamide-IL illustrate the fact that ILs can be tailored to have desired properties. While both of these ILs are relatively radiation resistant, their interactions with water are quite different. Gamma-radiation acted to accelerate the formation of the emulsion layer in a water/amide-IL system. However, no such process was evident for a water/dicyanamide-IL under steady-state radiation; a visible emulsion layer was only apparent under pulse radiolysis. We cannot rule out the presence of a nanoemulsion in the water/dicyanamide system under steady state radiation that forms following the input of high amounts of energy. Evidence for the formation of a transient nanoemulsion is a fine precipitate in the aqueous layer found after a test vial was removed from the γ-cell chamber. Currently, this precipitate has not been fully characterized, though it does appear to incorporate the dicyanamide anion of the IL.

Pulse radiolysis experiments were performed to study the behaviour of hydrated and IL-solvated electrons in water/IL systems. Transient absorption spectroscopy was used to follow the decay of transient species generated by pulse radiolysis. Results were preliminary, but suggested the presence of hydrated and IL-solvated electrons, as well as electronically excited IL species.

Using neutron scattering techniques, characterization of the micelle structures present in the systems was attempted. Unfortunately, due to micelle size and distribution, to limitations in the available neutron scattering equipment (neutron scattering angle and the lack of cold source), experiments were not successful. Thus, although the structure of the micelles and reverse micelles in our water/IL systems can be postulated from other spectroscopic methods, unambiguous characterization cannot be confirmed at this time.

9.2 FUTURE WORK

This research has added to our knowledge of the effects of steady-state ionizing radiation on ILs. A more complete understanding of the physical and chemical nature of the water/IL system can be achieved with some additional experiments. As noted above, characterization of the micelles and reverse micelles formed should be improved. This would require access to a dedicated neutron scattering facility with the requisite small angle neutron scattering instrument and narrow neutron energy spectrum (a cold source).

There is scope for additional study of the nature of the micelles formed in the water/IL systems and particularly the chemistry within the micelle structures. Research in radiation-induced chemistry normally looks at bulk phases. Solvent properties in such systems have a strong effect on the primary chemical yields per unit absorbed radiation energy. The solvent molecules act to stabilize transient species such as the solvated electron. In micelles or emulsions, we have no distinct bulk aqueous or IL phase and no solvent with extended interactions. How the radiation interacts with micro-phases, such as the aqueous interior of a reverse micelle, has not been studied. Such work would be of particular interest, not only for insights into the effect of ionizing radiation on the structure of the micelle, but also with regards to the potential formation of particulates within micelles, as was observed in the case of the water/dicyanamide-IL system.

Further experimental analysis could be performed on the products formed in the liquid phase, particularly the IL phase. Chemical analysis was limited to the gas phase in this thesis, but research should be extended to determine the extent of degradation in the IL phase using chromatographic techniques.

Research performed for this thesis focused on smaller sample sizes and used radiation sources available at the University of Western Ontario. For the intended real world applications the liquid will be exposed to a far greater amount of radiation. Thus, it is important to expose the pure IL and the biphasic water/IL systems to a large amount of radiation to determine the stability under a high dose of radiation.

Radiolytic degradation of the large organic components of IL ions produces smaller fragment molecules. These become impurities in the IL phase, but can also migrate to the water phase in a biphasic system. In both phases, these small molecules can act as loci in the formation of micelles and reverse micelles. We have only examined the effect of impurities in the water/IL system indirectly, relying on irradiation to produce them. Alternatively the effect of organic impurities in the water/IL systems could be studied by deliberated introducing known quantities of different species. Studying the effect of organic impurities in such systems would be of both academic and practical value, as any application of ILs in a separation process will doubtlessly include considerable levels of uncontrolled additives. The effects of such additives should be studied in depth, with and without irradiation, to understand how they would affect phase mixing in water/IL systems.

The study of ILs is of particular interest for evaluation of their utility in heavy metal and waste stream separations processes. However, in order to apply ILs to this purpose, we must understand the partitioning of metal species between the IL and the aqueous phases. The oxidation state of metal ions can strongly influence the metal solubility in water and the ability of the ions to complex with other compounds. Since ionizing radiation produces highly reducing ($\bullet e_{aq}^-$, $\bullet H$, $\bullet O_2^-$) and oxidizing ($\bullet OH$, H_2O_2)

species in water, it can change the stable oxidation state of the metal species dissolved in water. If the complexation of metal ion to an IL ligand depends on its oxidation state irradiation could alter biphasic separation efficiency.

While we have shown that phosphonium-based ILs have sufficient radiation stability for use in a radioactive waste separation process, work is required to determine the partitioning of metal species between the water and IL phases for a candidate IL. In doing such studies, both thermodynamic and kinetic factors of the phase partitioning must be considered. Ultimately, a metal/water/IL system should be studied as a function of contact and irradiation time to determine the acceptability of such a system for metal ion separation.

There is an extremely large number of possible ILs, even if this is restricted to the phosphonium class. Finding candidates for targeted separation of selected metal ions, and particularly trans-uranics is a challenge. Work has shown that density functional theory and molecular dynamics modeling can help us to understand the microscopic chemistry and physical properties of the phosphonium-based ILs. It may be that such calculational techniques can help to identify candidate ILs. Molecular dynamics studies can give an understanding of the interaction energies and reactions that can occur at a microscopic level and this may be useful in extrapolating to reactions and complexation in bulk systems.

Susan E. Howett

EDUCATION

Ph.D. in Physical Chemistry, the University of Western Ontario 09/2008 – 09/2013

B.Sc., Specialization in Chemistry, the University of Western Ontario 09/2004 – 05/2008

RESEARCH EXPERIENCE

Graduate Student 09/2008 – 09/2013

- Material analysis of phosphonium ionic liquids in contact with aqueous and gas phases; experiments conducted with and without the presence of a γ-radiation field.
- Training and experience in the use of a γ-cell for radiolytic chemistry studies
- Experience with electrochemical techniques, including
    - cyclic voltammetry
    - electrochemical impedance spectroscopy
- Experience in the use of surface and materials analysis techniques, and chromatography techniques, including
    - Fourier transform infrared spectroscopy
    - ultraviolet-visible spectroscopy
    - Raman spectroscopy
    - Gas chromatography with a mass selective detector
    - transmission electron microscopy

Visiting Researcher at Brookhaven National Laboratory 01/08/2012 – 01/21/2012

- International research experience at the Center for Radiation Chemistry Research at the Linear-Electron Accelerator Facility.
- Conducted experiments in an effort to observe electron kinetics in phosphonium ionic liquids and aqueous micelles.
- Gain experience with pulse-radiolysis hardware and software (including WaveMetrics Igor Pro and LabVIEW).

TEACHING & MENTORING

Mentor to Undergraduate Students 09/2008 – 09/2013

- Assisted in the training of 4th year thesis project undergraduate students and summer students in analysis techniques, sample preparation, and presentation.

Teaching Assistant – Introductory Analytical Chemistry 09/2008 – 04/2013

- Teaching and training students in basic analytical techniques and laboratory practices

Teaching Assistant – Instrumental Analytical Chemistry 09/2008 – 04/2013

- Teaching and training student instrumental preparation, operation, and practices

AWARDS & ACHEIVEMENTS

- 2013: Faculty of Science Graduate Student Teaching Award
- 2012: Outstanding Poster Awards at the Gordon Research Conference on Radiation Driven Processes in Physics, Chemistry, Biology, and Industry
- 2011: ASPIRE Award for an international research experience
- 2010: Young Investigator Talk at the Gordon Research Conference: Radiation Driven Processes in Physics, Chemistry, and Biology

SELECTED POSTERS, PRESENTATIONS & PUBLICATIONS

1. S.E. Howett, J.J. Noel and J.C. Wren. The Radiation Stability of Organic Ionic Liquids in Biphasic Systems. Proceedings of the 34th Annual Conference of the Canadian Nuclear Society, Toronto, June 9-12, 2013.
2. S.E. Howett, J.M. Joseph, J. Noël, and J. C. Wren. The Biphasic Stability of Phosphonium Ionic Liquids in Radiation Environments. Gordon Research Conferences: Radiation Driven Processes in Physics, Chemistry, and Biology, Proctor Academy, Andover, NH, July 28-August 3, 2012. (Poster Presentation)
3. S.E. Howett, J.M. Joseph, J.J. Noël, and J. C. Wren. Effect of Gamma Irradiation on Gas-Ionic Liquid and Water-Ionic Liquid Interfacial Stability. *J. Colloid Interface Sci*, 2011. 361(1): p. 338-350.
4. S.E. Howett, J.M. Joseph, J.J. Noël, and J.C. Wren, The Effect of Gamma Radiation on Biphasic Stability in Gas-Ionic Liquid and Water-Ionic Liquid Systems. 14th International Congress of Radiation Research, Warsaw, Poland, August 28-September 1, 2011. (Poster Presentation)
5. S.E. Howett, J.M. Joseph, J.J. Noël, and J.C. Wren, The Phase Transport and Reactions of Gamma-Irradiated Aqueous-Ionic Liquids, Proceedings of the International Conference on Water Chemistry of Nuclear Reactor Systems. Nuclear Plant Chemistry 2010 Conference, Quebec City, Quebec, October 3-7 2010.
6. S.E. Howett, J.M. Joseph, S. Peiris, J.J. Noël, Z. Ding, and J.C. Wren, Aqueous-Ionic Liquid Interfacial Reactions and Transport Under Gamma-Irradiation. Gordon Research Conference on Radiation Chemistry and Radiation Driver Processes in Physics, Chemistry, and Biology, Proctor Academy, Andover, NH, July 18-23, 2010. (Oral Presentation)